1979

The interaction and reactivity of nitric oxide and carbon monoxide on ruthenium surfaces

Edward Edwards Quick
Iowa State University

Recommended Citation

Quick, Edward Edwards, "The interaction and reactivity of nitric oxide and carbon monoxide on ruthenium surfaces " (1979). *Retrospective Theses and Dissertations*. 7305.
https://lib.dr.iastate.edu/rtd/7305

INFORMATION TO USERS

This was produced from a copy of a document sent to us for microfilming. While the most advanced technological means to photograph and reproduce this document have been used, the quality is heavily dependent upon the quality of the material submitted.

The following explanation of techniques is provided to help you understand markings or notations which may appear on this reproduction.

1. The sign or "target" for pages apparently lacking from the document photographed is "Missing Page(s)". If it was possible to obtain the missing page(s) or section, they are spliced into the film along with adjacent pages. This may have necessitated cutting through an image and duplicating adjacent pages to assure you of complete continuity.

2. When an image on the film is obliterated with a round black mark it is an indication that the film inspector noticed either blurred copy because of movement during exposure, or duplicate copy. Unless we meant to delete copyrighted materials that should not have been filmed, you will find a good image of the page in the adjacent frame.

3. When a map, drawing or chart, etc., is part of the material being photographed the photographer has followed a definite method in "sectioning" the material. It is customary to begin filming at the upper left hand corner of a large sheet and to continue from left to right in equal sections with small overlaps. If necessary, sectioning is continued again—beginning below the first row and continuing on until complete.

4. For any illustrations that cannot be reproduced satisfactorily by xerography, photographic prints can be purchased at additional cost and tipped into your xerographic copy. Requests can be made to our Dissertations Customer Services Department.

5. Some pages in any document may have indistinct print. In all cases we have filmed the best available copy.

University
Microfilms
International

300 N. ZEEB ROAD, ANN ARBOR, MI 48106
18 BEDFORD ROW, LONDON WC1R 4EJ, ENGLAND

8010256

QUICK, EDWARD EDWARDS

THE INTERACTION AND REACTIVITY OF NITRIC-OXIDE AND CARBON-MONOXIDE ON RUTHENIUM SURFACES

Iowa State University PH.D. 1979

University
Microfilms
International 300 N. Zeeb Road, Ann Arbor, MI 48106 18 Bedford Row, London WC1R 4EJ, England

The interaction and reactivity of nitric oxide and carbon monoxide on ruthenium surfaces

by

Edward Edwards Quick

A Dissertation Submitted to the
Graduate Faculty in Partial Fulfillment of the
Requirements for the Degree of
DOCTOR OF PHILOSOPHY

Department: Chemistry
Major: Physical Chemistry

Approved:

Signature was redacted for privacy.

In Charge of Major Work

Signature was redacted for privacy.

For the Major Department

Signature was redacted for privacy.

For the Graduate College

Iowa State University
Ames, Iowa

1979

TABLE OF CONTENTS

INTRODUCTION

During the past ten years an extensive effort has been made in the field of catalytic chemistry to describe the nitric oxide reduction system. This interest was precipitated by the 1970 Clean Air Act calling for the diminution of nitric oxide emission from automobile exhaust. Since then literally thousands of conceivable catalysts have been tested but it is safe to say that transition metal oxides and noble metal catalysts have shown the most promise. A difficulty arising in these studies is that no given catalytic material will promote the reduction at the required rate and lead to a specified product distribution. The problem is multiplied by the fact that the exhaust composition usually consists of not just nitric oxide and carbon monoxide but also hydrocarbons, oxygen, water and hydrogen (1) as well as a number of inert components. This leads to up to eleven different thermodynamically possible reactions occurring in a given catalyst bed.

The hydrogen-CO oxidation catalysts that were rapidly developed during the early 1970's can be attributed solely to the wealth of fundamental studies conducted over previous years in defining the mechanisms of the possible reactions and the characterization of the catalysts investigated. Major research thrusts in this area led to a decreased priority in the area of NO research and thus contributed to the less advanced development of NO_x reduction catalysts at the present time. Without the necessary kinetic and mechanistic information available, suitable catalysts that would reduce NO_x emissions to meet Federal standards have not resulted. This has, therefore, brought forth a new significance to the pursuance of fundamental studies between the active components comprising motor vehicle exhausts. Since it is difficult to obtain meaningful kinetic data that can be related to a specific mechanism from a system where many reactions are possible, only one reductant was chosen for investigation, namely carbon monoxide. The reaction between nitric oxide and carbon monoxide can lead to two possible nitrogen-containing products: nitrous oxide and molecular nitrogen as depicted in the following reactions:

$$2NO + CO \rightleftharpoons CO_2 + N_2O \qquad (1)$$

$$2NO + 2CO \rightleftharpoons 2CO_2 + N_2 \qquad (2)$$

Of the catalysts that have been investigated, metallic ruthenium is of considerable interest. It is favored not only for its high activity but also because under exhaust conditions it has been shown to be more selective to the formation of N_2 over ammonia (2-8) than platinum or rhodium.

Due to these reasons as well as to the interesting surface chemistry involving ruthenium, a study has been undertaken utilizing a single crystal ruthenium disc of the

(102) orientation. This thesis will describe a multi-faceted investigation incorporating not only kinetic and isotopic studies, but also employing the low energy electron diffraction (LEED), Auger electron spectroscopy (AES), x-ray photoelectron spectroscopy (XPS) and thermal desorption spectroscopy (TDS) techniques. From the spectroscopies utilized, the surface characteristics of the ruthenium catalyst have been probed both before and following interaction with the reactants so as to discern the nature of the adsorbed intermediates as a function of temperature and pressure. By incorporating kinetic and isotopic studies into this investigation, a mechanism consistent with the surface characterization data will be developed. Previous kinetic work has led to only a qualitative understanding of the nitric oxide reduction system.

The conditions under which this work has been performed are from 10^{-9} to 10 Torr reactant partial pressures with substrate temperatures ranging from room temperature to 1000°C. The kinetic reaction conditions are of a more limited nature as the partial pressures studied were in the 10^{-3} to 10 Torr range using a catalyst temperature of 475°C.

This dissertation will be divided into three sections comprising a survey of literature relevant to the nitric oxide reduction reactions on ruthenium, an experimental procedures section and finally a presentation and discussion of the results.

LITERATURE SURVEY

This survey will be divided into two main areas. The first area will consist of a literature review of the reaction kinetics that are pertinent to this study. The second section will deal with a review of the research concerning the interaction of nitric oxide and carbon monoxide with ruthenium surfaces and the interactions between the adspecies. These will be discussed in light of their relationship to the elementary reactions in the NO reduction mechanism.

Reaction Kinetics

The nitric oxide reduction reactions, although studied for up to ten years, are not at all completely understood. This is especially true of kinetic investigations. A difficulty that immediately arises is that in most previously reported investigations the temperature range of study has been from 25°C to 350°C, whereas a typical exhaust stream temperature ranges from 320°C to 800°C (1) with the average temperature being about 500°C. Thus, inferences drawn from previous experimental results are unlikely to be relevant to the practical application.

With regard to former kinetic work, only two studies exist that are concerned solely with the reaction of NO and

CO over ruthenium catalysts. One study by R. Schleppy and Y. Shah (9), using ruthenium supported on fiberglass, investigated the reaction between 100-350°C. Using a differential tubular reactor and operating at a total pressure of one atmosphere, they fit their kinetic results to a power rate law of the form:

$$\text{rate} = k_o \exp(-E/RT)\, P_{NO}^{a}\, P_{CO}^{b}. \tag{3}$$

The reactant partial pressures were varied from 4-38 Torr with the remaining gas constituent being helium. The best fit of the data was obtained using the parameters in Table 1.

Table 1. Power law correlations

Fitting Parameters	Reaction (Reactants/Products) $NO-CO/N_2O-CO_2$	$NO-CO/N_2-CO_2$
Rate Constant, $k_o \times 10^{-3}$ mole·min^{-1}·g of catalyst^{-1}	5.56	154.0
Activation Energy, E kcal·mole^{-1}	18.8	23.0
NO order, a	-0.31	-0.62
CO order, b	0.59	0.81

It is obvious from the parameters that a significant amount of NO will be converted to nitrous oxide below 300°C. A study involving the total conversion of NO as a function of catalyst bed temperature was included and the production of N_2O peaked at about 260°C with its maximum production being approximately 30%. Above 260°C, the rate of nitrous oxide production sharply decreased so that by 300°C N_2 is the dominant product (>95%).

A similar result was observed by Shelef and Otto (10) using supported transition metal oxides. Assuming that N_2O is the intermediate in a two step consecutive reaction scheme, they postulated that the reaction:

$$N_2O + CO \longrightarrow N_2 + CO_2 \qquad (4)$$

has a high potential energy barrier and is rate limiting at lower temperatures. Schleppy and Shah attempted to incorporate this result into their quantitative analysis but found that at total conversions of greater than 50% a nondefined three step mechanism had to be utilized. They concluded that the N_2O intermediate mechanism may be valid in the narrow pressure range they studied below 300°C, but it is doubtful that this is accurate under different and more relevant reaction conditions.

The second investigation by J. Butler and D. Davis (11) studied the reaction between 250-350°C using an alumina supported 0.5% w/w ruthenium catalyst. They also fit their data to a power rate law of the following form:

$$\text{Rate}_{CO_2} = 6.6 \times 10^{8} \exp(-19.7 \pm 3.6 \text{ kcal/mole/RT})\ P_{NO}^{0}\ P_{CO}^{0} \quad (5)$$

Their reaction chamber was a closed system and the gas composition was monitored mass spectrometrically after passing through a capillary-type leak. It is interesting that while they reported zero order in both CO and NO their log-log plot for nitric oxide indicated an order dependent on P_{NO}. At low NO pressures the order was ≈+1 and decreased to zero as the partial pressure was increased to 30 Torr. The total pressure in this work ranged from 38-75 Torr. Their study, unlike the work of Schleppy and Shah, did not indicate the presence of N_2O in the reaction chamber so that equation (5) pertains only to reaction (2). Two mechanisms were proposed for the reaction with NO either adsorbing associatively and adsorbed carbon monoxide inducing N-O bond rupture, or with dissociation of the nitric oxide following adsorption. The two reaction mechanisms are:

$$S + NO_{(g)} \overset{K_1}{\rightleftharpoons} \underset{S}{\overset{NO}{|}} \quad (6)$$

$$S + CO_{(g)} \overset{K_2}{\rightleftharpoons} \underset{S}{\overset{CO}{|}} \quad (7)$$

$$\underset{S}{\overset{NO}{|}} + \underset{S}{\overset{CO}{|}} \xrightarrow{k_3} \underset{S}{\overset{N}{|}} + CO_{2(g)} + S \quad (8)$$

or

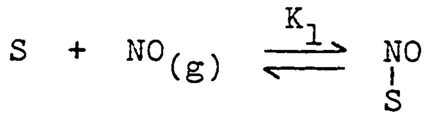

$$S + NO_{(g)} \overset{K_1}{\rightleftharpoons} \underset{\underset{S}{|}}{NO} \qquad (9)$$

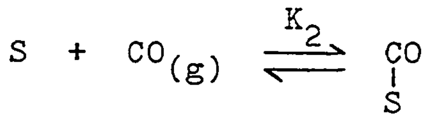

$$S + CO_{(g)} \overset{K_2}{\rightleftharpoons} \underset{\underset{S}{|}}{CO} \qquad (10)$$

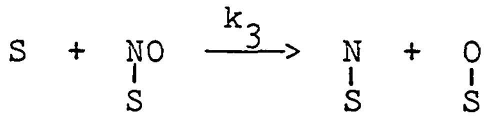

$$S + \underset{\underset{S}{|}}{NO} \xrightarrow{k_3} \underset{\underset{S}{|}}{N} + \underset{\underset{S}{|}}{O} \qquad (11)$$

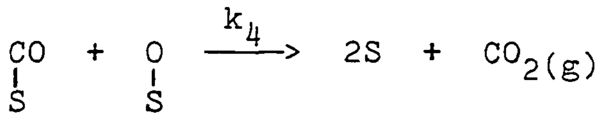

$$\underset{\underset{S}{|}}{CO} + \underset{\underset{S}{|}}{O} \xrightarrow{k_4} 2S + CO_{2(g)} \qquad (12)$$

where S designates a vacant surface site. Taking the first proposed mechanism and assuming rapid equilibria establishment, the rate of carbon dioxide production would be:

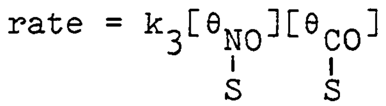

$$\text{rate} = k_3[\theta_{\underset{\underset{S}{|}}{NO}}][\theta_{\underset{\underset{S}{|}}{CO}}] \qquad (13)$$

where the θ indicates the fractional surface coverage of the designated adspecies.

Substituting the equilibrium expressions from equations (6) and (7):

$$\text{rate} = k_3K_1K_2P_{NO}P_{CO}[\theta_S]^2 \qquad (14)$$

and incorporating a conservation of surface sites relationship:

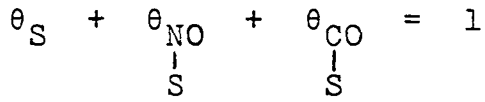

$$\theta_S + \theta_{\underset{\underset{S}{|}}{NO}} + \theta_{\underset{\underset{S}{|}}{CO}} = 1 \qquad (15)$$

with the appropriate equilibria substitution will result in the following rate law:

$$\text{rate} = \frac{k_3 K_1 K_2 P_{NO} P_{CO}}{[1 + K_1 P_{NO} + K_2 P_{CO}]^2} \qquad (16)$$

If the second mechanism was chosen and the association of nitrogen adatoms was again assumed to be rapid, then only the $\underset{S}{\underset{|}{O}}$ species would require the use of the steady state approximation:

$$\frac{d[\theta_{\underset{S}{\underset{|}{O}}}]}{dt} = 0 = k_3[\theta_{\underset{S}{\underset{|}{NO}}}][\theta_S] - k_4[\theta_{\underset{S}{\underset{|}{CO}}}][\theta_{\underset{S}{\underset{|}{O}}}] \qquad (17)$$

The derived rate law would be:

$$\text{rate} = \frac{k_3 K_1 K_2 P_{NO}}{[1 + K_1 P_{NO} + K_2 P_{CO} + k_3/k_4 (P_{NO}/P_{CO})]^2} \, . \qquad (18)$$

Using the rate expressions equations (16) and (18), it can be shown that neither will explain the zero order in carbon monoxide or in nitric oxide over a large pressure range. Consequently, at this time no reaction mechanism has been postulated that is consistent with observed kinetic data.

It is interesting to compare the two kinetic studies presented. Schleppy and Shah found that N_2O is an intermediate in the reaction leading to N_2 and CO_2 and that the orders with respect to carbon monoxide and nitric oxide are +0.81 and -0.62, respectively. In contrast, Butler and Davis reported that N_2O was not involved in any significant role in the NO-CO reaction system and that the order with respect to NO is +1 to 0 and is 0 for CO. Considering the similarities in reaction conditions, the differences in the results are striking; this is an illustration of an apparent weakness in both studies demonstrating the need for surface characterization of the catalyst. Neither study investigated the state of the supported ruthenium outside of determining the surface area. A possible reason for the variance in the results could be the dual state nature of ruthenium.

Several studies of a more general nature have been published involving a mixture of NO, CO, H_2, CO_2 and H_2O. Initiated by the General Motors Research Laboratories, these studies demonstrated that ruthenium can exist in two catalytic states (3). Using a 0.1% ruthenium catalyst supported on alumina and a gas mixture containing 1% CO, 0.3% H_2, 0.1% NO, 10% H_2O and 10% CO_2 in a nitrogen atmosphere, Taylor and Klimisch determined that ruthenium exists in an "oxidized" and "reduced" state. The reduced state was the state of the catalyst following treatment in hydrogen at 400°C for two hours. The oxidized state could be obtained by calcination in air at 500°C or by passing a feedstream containing 10% excess oxygen for 200 seconds at temperatures greater than 200°C. The product distribution was different depending on the state of the catalyst and this suggested different mechanisms occurring on the two surfaces. The oxidized state was found to be more effective toward ammonia decomposition and the water gas shift reaction was promoted only by the oxidized state. Conversion between the two states was reversible as the reduced catalyst resulted from heating an oxidized catalyst to 700°C in a reducing atmosphere.

In an effort to characterize each state, Taylor, Sinkevitch and Klimisch (5) undertook an effort to distinguish the features of both by investigating the activities of ammonia decomposition, nitric oxide reduction and the CO-H_2 and water-gas shift reactions. They found that the oxidized state was more active for each except for the overall removal rate of NO where both were equally effective. The oxidized state was more selective for nitrogen formation. Since such dramatic behavior was noted, they suspected that the oxide catalyst was either RuO_2 or a reconstructed state of the reduced catalyst. By oxygen titration it was determined that at 100°C the same amount of oxygen could be removed from the reduced catalyst as from the oxidized catalyst. This ruled out the possibility that the oxidized catalyst was RuO_2;

consequently Klimisch et al. concluded that the oxygen caused surface reconstruction by the oxygen atoms becoming "buried" in the ruthenium crystallites. This reconstructed state was then more active as deactivating metal-support interactions, which were postulated to occur in the reduced state, would be diminished. From this author's viewpoint, the decision to eliminate ruthenium dioxide as the catalytically active surface was a bit hasty since it was based on oxygen titration data at 100°C. Previous results indicated that a temperature of 650°C was required for the transition from the oxidized to the reduced state to occur in the presence of hydrogen. By performing the titration at 100°C, no transition would transpire so the conclusion they presented was possibly erroneous.

With regard to the reaction study over the two catalysts using the reactant gas mixture described above, Taylor and Klimisch (4) found that for the reduced case, which is the condition of the ruthenium under typical engine exhaust conditions, the reaction mechanism appears to differ from that under oxidizing conditions (7). Under reducing conditions, the formation or decomposition of ammonia was found not to be a major pathway from NO to N_2 and that if the CO concentration was reduced, the concentration of NH_3 in the exhaust stream decreased in spite of the presence of hydrogen. This suggests that the carbon monoxide is involved in either one of two roles. According to Shelef and Gandhi (2) increasing the NO concentration will increase the number of surface N species and the probability of nitrogen adatoms pairing, thus leading to the formation of N_2. If carbon monoxide is considered to adsorb and compete for the same type of sites, then less nitrogen atoms would occupy adjacent sites. Increased production of ammonia would result due to the interaction of N atoms with hydrogen. An alternate mechanism could be the formation of an isocyanate (-NCO) intermediate that would favor ammonia formation.

$$(-NCO) + 2H_2O \longrightarrow NH_3 + CO_2 + (-OH) \tag{19}$$

$$(-OH) + (-H) \longrightarrow H_2O. \tag{20}$$

With the oxidized catalyst (7), an increase in the space velocity in a flow reactor led to an increase in the ammonia concentration. This lends credence to the suggestion that NH_3 is an intermediate formed in the NO to N_2 pathway. Since the water-gas shift and the NH_3 decomposition reactions are promoted on the oxygen treated catalyst, this conveys the following (12) reaction sequence:

$$CO + H_2O \longrightarrow CO_2 + H_2 \tag{21}$$

$$5H_2 + 2NO \longrightarrow 2NH_3 + 2H_2O \tag{22}$$

$$2NH_3 \longrightarrow N_2 + 3H_2. \tag{23}$$

While an ammonia intermediary is a possible route from NO to N_2, it was Klimisch and Taylor's hypothesis that it played a minor role in the catalysis of the NO reduction system since the ammonia concentration had only a weak dependence on space velocity. The actual reaction pathway leading to nitrogen formation is hence not established on either ruthenium state. The reaction pathway given in reactions (22) and (23) has been investigated by ternary kinetic studies involving H_2, NO and NH_3 (2,8,13,14) on noble metals and metal oxides but due to its lack of significance to this study or to the nitric oxide reduction system, these studies will not be discussed further. The predominant pathway from NO to N_2 was probably _via_ an oxidation reduction sequence (3):

$$NO + M \longrightarrow \tfrac{1}{2}N_2 + M\text{-}O \qquad (24)$$

$$CO + M\text{-}O \longrightarrow CO_2 + M \qquad (25)$$

where M is a metal site and M-O represents oxygen adsorbed on a metal site.

Several ternary kinetic studies involving nitric oxide, carbon monoxide and hydrogen have been undertaken by researchers outside of the automotive industry (6,15-17). A study by Kobylinski and Taylor (6), which essentially duplicated the work by Klimisch _et al._, compared the activities of Pd, Pt, Rh and Ru. They found that ruthenium was the least active of the four noble metals for the NO/H_2 reactions but the most active for the NO/CO reaction and that the rate of removal of NO by CO was greater than by H_2. They also confirmed that as a catalyst Ru had a high selectivity for the formation of N_2 over ammonia. Mechanistically, they reported the pathway of nitrogen production to be:

$$2NO + 2H_2 \longrightarrow 2H_2O + N_2 \qquad (26)$$

$$2NO + 5H_2 \longrightarrow 2NH_3 + 2H_2O \qquad (27)$$

$$6NO + 4NH_3 \longrightarrow 5N_2 + 6H_2O \qquad (28)$$

with the rate of reaction (28) faster than reaction (27). Their conclusion left the role of carbon monoxide undefined especially in light of the high rate of NO/CO reaction.

A study by R. Voorhoeve and L. Trimble (15) compared the reactivity of bulk ruthenium metal with that of γ-alumina supported Ru of different crystallite sizes. They found that the dispersion of the metal made little difference with regard to the occurrence of an oxidized ruthenium state, but they observed a significant difference between the reduced state of the supported ruthenium and bulk ruthenium which had been reduced by hydrogen. Similar behavior could only be observed if the bulk Ru was treated with H_2 and then a CO-NO-H_2 mixture at 520°C. It was claimed that the reduced state was a consequence of surface contamination by a nitrogen overlayer, possibly a ruthenium nitride layer (18). The oxidized state was then a state where the nitrogen had reacted with oxygen to form NO or NO_2. The oxygen treated surface would then actually be, by their line of reasoning, metallic ruthenium. The proposed RuN surface would explain the low decomposition rate of NH_3 as metal nitrides have a low activity for ammonia decomposition (19).

This model proposed by Voorhoeve and Trimble hinges on the formation of ruthenium nitride or a nitrogen covered surface existing at temperatures greater than 250°C. The actual formation of the nitride from nitrogen on ruthenium is questionable under the reaction conditions (P_{total} = 1 atmosphere, <500°C) studied; indeed as a general rule hcp and fcc type metals do not form any type of bulk nitrides (20). The proposal of a nitrogen covered Ru surface at 500°C will be dealt with later in this dissertation.

An extension of the earlier work by R. Schleppy and Y. Shah (9) considered the $NO/CO/H_2$ system (16). It confirmed the earlier results of Kobylinski and Taylor (6) and Voorhoeve and Trimble (15) with regard to the reducing nature of carbon monoxide. Simply on the basis of kinetic data, they put forth the hypothesis that the bond strength of NO was greater than CO.

Even though a reasonable amount of research has been performed on the NO reduction system from a kinetic viewpoint, a good qualitative understanding of the nature of the reactions involved is not available. It is agreed that ruthenium can exist in two catalytically active forms but the exact nature of these states is ill-defined. The reaction order with regard to nitric oxide has not been established as there is a conflict as to whether it is 0 or -0.62. A recent study by Ohara, Yokota and Fujitani (17) ascertained a value of +1.0 in the 400-600°C temperature range. The role of carbon monoxide under reducing conditions is also unclear. Chemisorption has been proposed to occur on both the metal atoms and adsorbed nitrogen atoms resulting in isocyanate formation.

Reactant Surface Interactions

From a kinetic viewpoint, a reaction mechanism consisting of a series of elementary steps is generally conceivable, but it should also have a foundation based on the specific interactions of adsorbates with the catalytic surface. Most of the research in this area, under catalytic reaction conditions, has involved surface analysis by infrared spectroscopy.

Soon after Klimisch and Taylor reported their preliminary findings on the use of a ruthenium catalyst, Unland published two accounts (21,22) of an infrared study on the reaction of nitric oxide and carbon monoxide on noble metal catalysts. This work was the first of a number of articles on NO-CO interactions with ruthenium in either one of its dual catalytic states. Before discussing these interactions, which result in the formation of an isocyanate complex, work on the adsorption of the individual reactants as followed by infrared spectroscopy will first be summarized.

In 1964 L. Lynds (23) reported the first study of the adsorption of CO on alumina or silica supported ruthenium. Two adsorption bands were observed at 2125 and 2060 cm^{-1} on Ru/Al_2O_3 and 2151 and 2083 cm^{-1} on Ru/SiO_2. Three years later C. R. Guerra and J. H. Schulman (24) cited two broad bands upon carbon monoxide adsorption on unsupported Ru metal in the frequency ranges 2010-1990 cm^{-1} and 1910-1870 cm^{-1}. They tentatively assigned them to RuCO and Ru_2CO, respectively. Additional band heads were observed which were attributed to surface heterogeneity (25) or multiple CO adsorption on a Ru site.

It was not until 1973 when M. Kobayaski and T. Shirasaki (26) again looked at CO adsorption on Ru at 150°C that another description was available. Two carbon monoxide bands were observed at approximately 1990 and 2080 cm^{-1} on a Ru/SiO_2 catalyst which was suspended in Nujol. Based on adsorption data in which the CO/Ru ratio was greater than unity, it was suggested that Ru-$(CO)_2$ and Ru-$(CO)_3$ are the adsorption modes of CO. This was substantiated by reporting that $Ru_3(CO)_{12}$ also exhibited two bands at 2100-1990 cm^{-1}.

Later an EPR study by Kobayaski and Shirasaki (27) confirmed the presence of $Ru(CO)_3$ and $Ru(CO)_4$ at 150°C. They presumed the existence of $Ru(CO)_2$ as it was diamagnetic and could not be detected.

In a detailed investigation A. A. Davydov and A. T. Bell (28) incorporated the dual state hypothesis of Klimisch et al. resulting in a more specific description of CO adsorption. Using a reduced sample at 25°C, they detected three bands at 2145, 2080 and 2040 cm^{-1}. The 2040 cm^{-1} band frequency was coverage dependent as it decreased to 2010 cm^{-1} upon desorption and heating to 100°C while the bands at 2145 and 2080 cm^{-1} shifted to 2130 and 2070 cm^{-1}, respectively. Based on the CO vibrational frequencies of ruthenium carbonyls, the 2040 cm^{-1} band was assigned to Ru-C≡O. The shift from 2040 to 2010 cm^{-1} with decreasing coverage was ascribed to an increase in the availability of d electrons as the coverage diminished. These could then be used for back bonding which would strengthen the Ru-C bond and correspondingly weaken the C-O bond, causing the observed vibrational frequency decrease.

The remaining two bands were found to change in intensity in a parallel manner upon carbon monoxide adsorption or desorption thus suggesting that they are linked by a common form of adsorption. The results of R. Dalla Betta (29) and M. Brown and R. Gonzalez (30) differ from this observation but the significance of their results is in question, as they were based on either weak spectra (29) or spectra having poor resolution between the 2080 and 2040 cm^{-1} bands. Since the vibrational frequencies are in close correspondence to those of halocarbonyls, this implies the following structure:

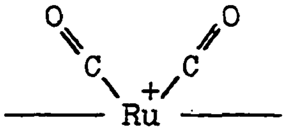

where the adsorption site is partially ionized. This structure would produce two infrared bands -- the symmetric and asymmetric stretches. The decrease in CO desorption temperature on surface oxidation is also consistent as the oxidized surface will have fewer d electrons available. The degree of back bonding will then decrease thereby increasing the CO stretching frequency as is also consistent with the observed results on the oxygen treated surface.

Brown and Gonzalez (30) in a similar fashion assigned the 2030-2010 cm^{-1} band to Ru-CO but the two high frequency bands were modeled differently. The 2080 cm^{-1} peak was, in their opinion, due to CO adsorption on an oxygen perturbed Ru site and the 2150-2135 cm^{-1} band was due to CO adsorbed on a ruthenium oxide site.

Dalla Betta (29), likewise, saw three bands; the low frequency band was due to adsorption on a metal site with a coordination number of 8 or 9 while the two higher frequency bands, 2084 and 2144 cm^{-1}, were due to adsorption on sites of lower coordination such as edges or corners. Multiple adsorption was not ruled out on the corner or edge sites. Considering the results of Davydov and Bell and those of Brown and Gonzalez, the two high frequency bands seem improperly assigned and should be associated with an oxidized surface.

A similar discordance exists in the interpretation of NO adsorption as followed by infrared spectroscopy. On oxidized ruthenium Brown and Gonzalez (31) observed a peak at 1880 cm^{-1} which was independent of coverage. On a reduced surface two bands at low coverages were observed at 1800 and 1630 cm^{-1}. As the coverage was increased with the sample at 25°C, the 1800 cm^{-1} shifted to 1820 cm^{-1} and a peak at 1860 cm^{-1} appeared. On heating in vacuum to 200°C for two hours, the 1820 and 1860 cm^{-1} bands merged and a band at 1880 cm^{-1} resulted. This suggests that nitric oxide at 200°C is capable of oxidizing ruthenium to the same extent as O_2. The 1820 cm^{-1} and 1630 cm^{-1} bands appeared to be related to a single adsorbed species as both increased or decreased in a parallel manner. Anionic nitrosyl ligands ($-NO^-$) absorb in the 1600 cm^{-1} region and cationic nitrosyl ligands (-NO^+) absorb in the 1800 cm^{-1} region. Consequently since Ru forms stable complexes with NO^+ and NO^- ligands (32), the 1820 cm^{-1} band was assigned as $Ru^{\delta-}$-$NO^{\delta+}$ and the 1630 cm^{-1} band as $Ru^{\delta+}$-$NO^{\delta-}$. They are related as they will be weakly coupled via the activation of an adjacent site for an oppositely charged NO group. The 1860-1880 cm^{-1} band head was assigned as NO adsorption on an oxygen perturbed Ru site. The shift of the frequency from 1860 to 1880 cm^{-1} with increase in oxygen coverage is due to the oxygen decreasing the electron density around the Ru atom. This would allow a more complete transfer of the π^* antibonding electron in NO to the Ru site thus resulting in a higher NO wavenumber.

Davydov and Bell (28) undertook a similar investigation and though the results were in agreement, the interpretation was quite different. They argued against a $Ru^{\delta+}$-$NO^{\delta-}$ species on the basis that on adsorption a metal d electron would be transferred into the $2\pi^*$ orbital (33,34), thus weakening the N-O bond. Since they did not identify any band at 1630 cm^{-1}, NO adsorption was modeled in terms of NO^+ species.

According to Davydov and Bell upon introduction of nitric oxide onto the ruthenium surface dissociation of the N-O bond occurred resulting in site oxidation:

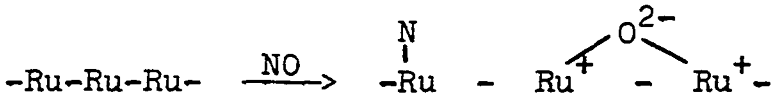

$$\text{-Ru-Ru-Ru-} \xrightarrow{\text{NO}} \overset{\text{N}}{\text{-Ru}} - \overset{\text{O}^{2-}}{\text{Ru}^{+} - \text{Ru}^{+}}\text{-} \qquad (29)$$

in agreement with the previous observation that NO oxidizes ruthenium. Upon NO adsorption on the oxidized site, the N-O vibrational frequency at 1810 cm^{-1} results:

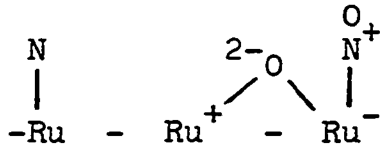

and π* electron transfer into an empty d orbital occurs. Further oxidation would produce an intermediate absorbing in the 1860-1880 cm^{-1} region:

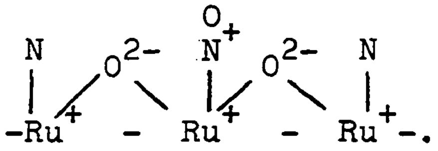

The shift from 1810 to 1860 cm^{-1} results because fewer d electrons are available which increases transfer of the π* electron to the ruthenium. Following this line of reasoning, it might be expected that upon initial adsorption both bands would be present, but upon an increase in the nitric oxide pressure the high frequency band would predominate as increased oxidation would ensue. This was not experimentally observed.

Upon the adsorption of CO on a NO predosed surface at 25°C (35), a new band at 2180 cm^{-1} appeared. Isotopic studies using ^{13}CO and ^{15}NO confirmed the presence of nitrogen and carbon atoms in the complex. Using the assignments of Brown and Gonzalez (36), this was assigned to an isocyanate species of the form $Ru^{\delta+}$-$NCO^{\delta-}$. If the adsorption sequences were reversed, the nitric oxide would displace the carbon monoxide, in agreement with the results of Schleppy and Shah (16), and no isocyanate bands would appear.

This isocyanate complex would appear to play a significant role in NO/CO reaction kinetics at room temperature, but above 100°C its surface concentration seems to diminish according to Davydov and Bell (35). F. Solymosi and J. Raskó (37) did a detailed study of this matter using a 5% NO, 10% CO and 85% N_2 mixture at 100 Torr and found for a reduced Ru sample the maximum in intensity occurred at ≈ 250°C; above 400°C none appeared. This indicates that any reaction studies above 400°C need not consider the -NCO intermediate.

Since no isocyanate complex forms according to Davydov and Bell, upon displacement of a CO adlayer, a probable mechanism of formation is by a Rideal-Eley process:

$$\text{Ru-N} + CO_{(g)} \longrightarrow \text{RuNCO}. \qquad (30)$$

The isocyanate could then react *via* three possible reaction pathways:

$$\text{RuNCO} \longrightarrow \text{RuN} + CO_{(g)}, \qquad (31)$$

$$\text{RuNCO} + NO_{(g)} \longrightarrow \text{Ru} + N_{2(g)} + CO_{2(g)} \qquad (32)$$

or

$$\text{RuNCO} + \text{RuNO} \longrightarrow 2\text{Ru} + N_{2(g)} + CO_{2(g)} \qquad (33)$$

Brown and Gonzalez (36) did observe a weak band at 2180 cm^{-1} upon adsorption of NO on a CO predosed surface. Isotopic shifts for the band of 60 cm^{-1} using ^{13}CO and 17 cm^{-1} using ^{15}NO were observed. Since the greater frequency shift was observed for the C, this suggests CO bonding to the ruthenium through the N atom. The band head frequency could, therefore, be assigned as RuNCO or Ru-N≡C, but since no terminal isonitriles have been prepared for ruthenium, the 2180 cm^{-1} band was interpreted as an ionically bound isocyanate similar to K^{+}-NCO^{-} (38). This led Brown and Gonzalez to postulate the following mechanism for Ru$^{\delta+}$-NCO$^{\delta-}$ formation:

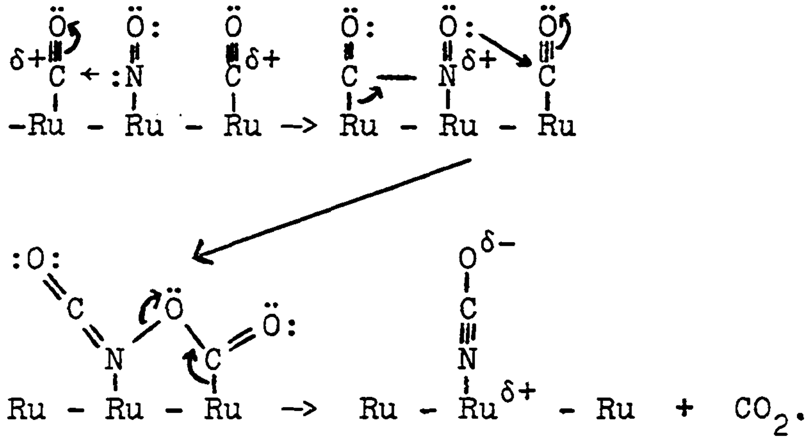

(34)

The isocyanate could then react via reactions (31-33).

Unland (21,22) had previously detected the isocyanate species on ruthenium and noted that of the noble metals Pt, Pd, Rh, Ir and Ru, the latter gave the weakest isocyanate band. Also using an alumina support, the band appeared in the 2260-2270 cm^{-1} region which would suggest a covalently bound isocyanate, Ru-NCO. Unland saw only a weak band which was probably due to using a sintered support as the Ru/Al_2O_3 samples were heated to 400°C before dosing. The wave number for isocyanate absorption varied appreciably with support; it was 2259 cm^{-1} on alumina supported ruthenium and 2180 cm^{-1} on silica supported ruthenium. Obviously the support is playing a major role in the -NCO formation and a question arises concerning the site of -NCO adsorption. If the site were a metal atom, the support would be expected to have a minor effect but a shift of approximately 80 wavenumbers supports possible adsorption on the support. This idea has been pursued by R. A. Dalla Betta and M. Shelef (39) and by F. Solymosi, J. Kiss and J. Sárkány (40) on alumina supported platinum catalysts. In the former work using two different platinum loadings, 2 wt. % and 10 wt. % Pt/Al_2O_3, resulted in an order of magnitude difference in platinum surface concentration. The infrared spectra of the two catalysts showed equal intensities of the isocyanate bands while the bands due to adsorbed carbon monoxide differed by a factor of $\sim$10, indicating adsorption on the alumina support.

Solymosi, Kiss and Sárkány performed a similar study but in addition looked at the decomposition of the isocyanate complex. Relating their H_2-O_2 adsorption data and the partial pressure increases of CO, N_2 and CO_2 that resulted from -NCO decomposition with the assumption of one isocyanate group per Pt atom, they ascertained that the number of isocyanate groups on the catalyst greatly outnumbered the number of surface platinum atoms. Furthermore, the decomposition reaction occurred in three stages; first the isocyanate reacted with any chemisorbed oxygen:

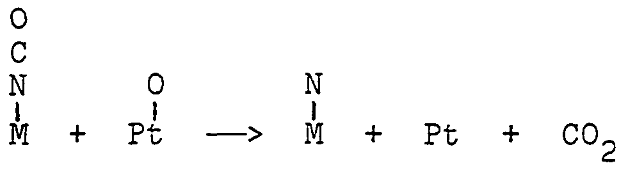

$$\overset{\substack{O\\C\\N\\|}}{M} + \overset{\substack{O\\|}}{Pt} \longrightarrow \overset{\substack{N\\|}}{M} + Pt + CO_2 \qquad (35)$$

where M designates either Pt, Si or Al depending on the support. Following removal of the surface oxygen, the next stage is postulated to involve N-C bond dissociation:

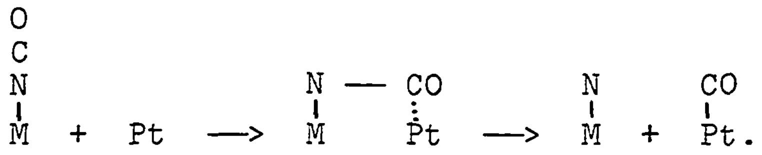

$$\overset{\substack{O\\C\\N\\|}}{M} + Pt \longrightarrow \overset{\substack{N \,-\, CO\\ | \qquad \vdots}}{M \qquad Pt} \longrightarrow \overset{\substack{N\\|}}{M} + \overset{\substack{CO\\|}}{Pt}. \qquad (36)$$

The final stage involves a decomposition similar to reaction (36) except that only the support atoms act as surface sites.

The significance of this study is that though most of the isocyanate may reside on the support, a reasonable fraction is adsorbed on the metal and is involved in catalysis. Davydov and Bell (35) concur as their attempt to form the isocyanate on just the silica support was unsuccessful. One possible pathway leading to support adsorption could involve surface diffusion from the metal to a support site.

To briefly summarize the infrared work, a mechanism leading to the formation of N_2 and CO_2 from the reactants nitric oxide and carbon monoxide has been developed. The mechanism, which is valid probably only below 300°C, involves the formation of an isocyanate intermediate. This complex can decompose or react via several pathways, as given above, and is formed either through the interaction of gas phase carbon monoxide with surface nitrogen (Rideal-Eley type mechanism) or via the interaction of adsorbed CO and NO (Langmuir-Hinshelwood type mechanism) with the resultant formation of carbon dioxide.

A wide variety of spectroscopies have been utilized to characterize the adsorption of nitric oxide and carbon monoxide on ruthenium single crystals. Though no specific studies have been performed over the (102) ruthenium crystal face there seems to be a consensus that nitric oxide will adsorb associatively with a sticking coefficient of approximately one, then dissociate via a reaction similar to equation (11). According to an ultraviolet photoemission study (UPS) by H. P. Bonzel and T. E. Fischer (41) over a ruthenium (100) crystal, both dissociated and molecular nitric oxide will coexist on the surface and be available for reaction. At temperatures of <350°C it was postulated that the molecular nitric oxide in the presence of hydrogen might form NH_3 and the dissociated NO would form N_2.

Carbon monoxide is generally considered to adsorb associatively, at least at pressures $<10^{-4}$ Torr. At higher pressures several kinetic studies indicate that dissociation of CO may occur, as evidenced by the formation of a carbon overlayer; however, the sufficiency of that evidence is debatable. An exchange study (42) of $^{13}C^{16}O$ and $^{12}C^{18}O$ suggests that above 350K reversible dissociation occurs.

While considerable effort has been involved in characterizing the NO-CO reaction system, a clear consensus as to the elementary reactions, the adsorption sites or even the character of the ruthenium surface in either one of its dual states is not available. This has, as stated earlier, contributed to the slow development of effective catalysts to aid in the reduction of nitric oxide emissions. It is from this basis that a study has been initiated. The role of the isocyanate complex is also in need of definition at temperatures >350°C. By using a characterizable single crystal of ruthenium, kinetic data will be used in conjunction with various electron spectroscopies to derive a consistent description of the NO-CO/Ru reaction system.

EXPERIMENTAL

The reaction between nitric oxide and carbon monoxide using a ruthenium single crystal catalyst of the (102) orientation was studied by a variety of experimental techniques. Utilizing a reactor system capable of attaining an ultra-high vacuum, the reaction kinetics were examined over a pressure range greater than three magnitudes and up to reactant partial pressures of 10 Torr. Thermal desorption spectroscopy (TDS) and isotopic studies using labeled carbon monoxides and oxygen were likewise conducted in the system. Surface characterization *via* low energy electron diffraction (LEED) and Auger electron spectroscopy (AES) were performed in a commercial surface analysis system constructed by Varian Associates/Vacuum Division (Palo Alto, California) to obtain an elemental analysis of surface constituents and the overlayer structure of adsorbates. Both chemical and elemental analyses of the ruthenium disc were accomplished *via* x-ray photoelectron spectroscopy (XPS or ESCA) employing instrumentation available through AEI Scientific Apparatus, Inc. (Elmsford, New York). Ultra-high vacuum techniques were utilized extensively in this study and several satisfactory general reviews concerning both theoretical and experimental aspects (43,44) are available; consequently, no résumé will be made of this area.

Reactor System Design

The reactor system used in this work was constructed primarily of Corning 7740 borosilicate glass (Pyrex) and 304 stainless steel. It incorporated a mercury diffusion pumping system capable of obtaining minimum background pressures in the 10^{-10} Torr range. The ambient pressure within the system was monitored by thermocouple and Bayard-Albert ionization guages, a differential capacitance manometer and a quadrupole mass spectrometer. A schematic representation of the system is illustrated in Figure 1. The reactor was conveniently designed in two sections, an ultra-high vacuum section including the quadrupole mass spectrometer and a high pressure side (shaded area, Figure 1) incorporating the reaction cell, capacitance manometer and the gas manifold. The cell could be isolated from the high pressure section by closing valve C2 and opening valve L1 which had a high conductance of up to 10 liters/second. The ruthenium crystal, which was mounted in the reaction cell, see Figure 2, could then be heated by electron bombardment. The entire reactor was bakable to 400°C excepting for the pumping section.

The ultra-high vacuum pumping system consisted of a liquid nitrogen (LN_2) trapped roughing pump glass blown to two series connected two stage mercury diffusion pumps. The diffusion pumps were LN_2 trapped to prevent mercury contamination of the system. The pumps, positioned on the gas

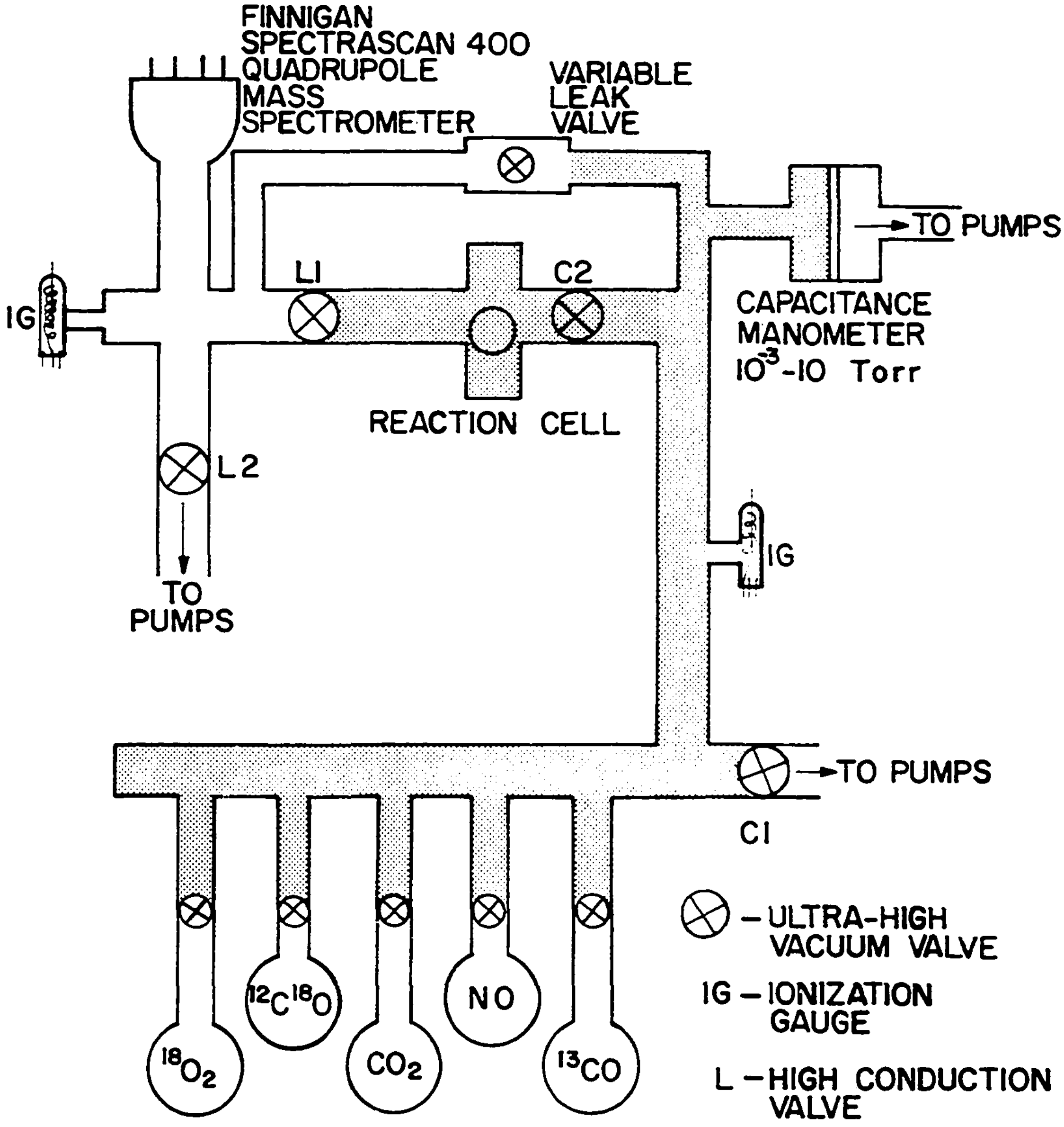

Figure 1. Schematic drawing of ultra-high vacuum system used in kinetic and flash desorption experiments

(Shaded area = reaction volume ≈ 1.6 liters)

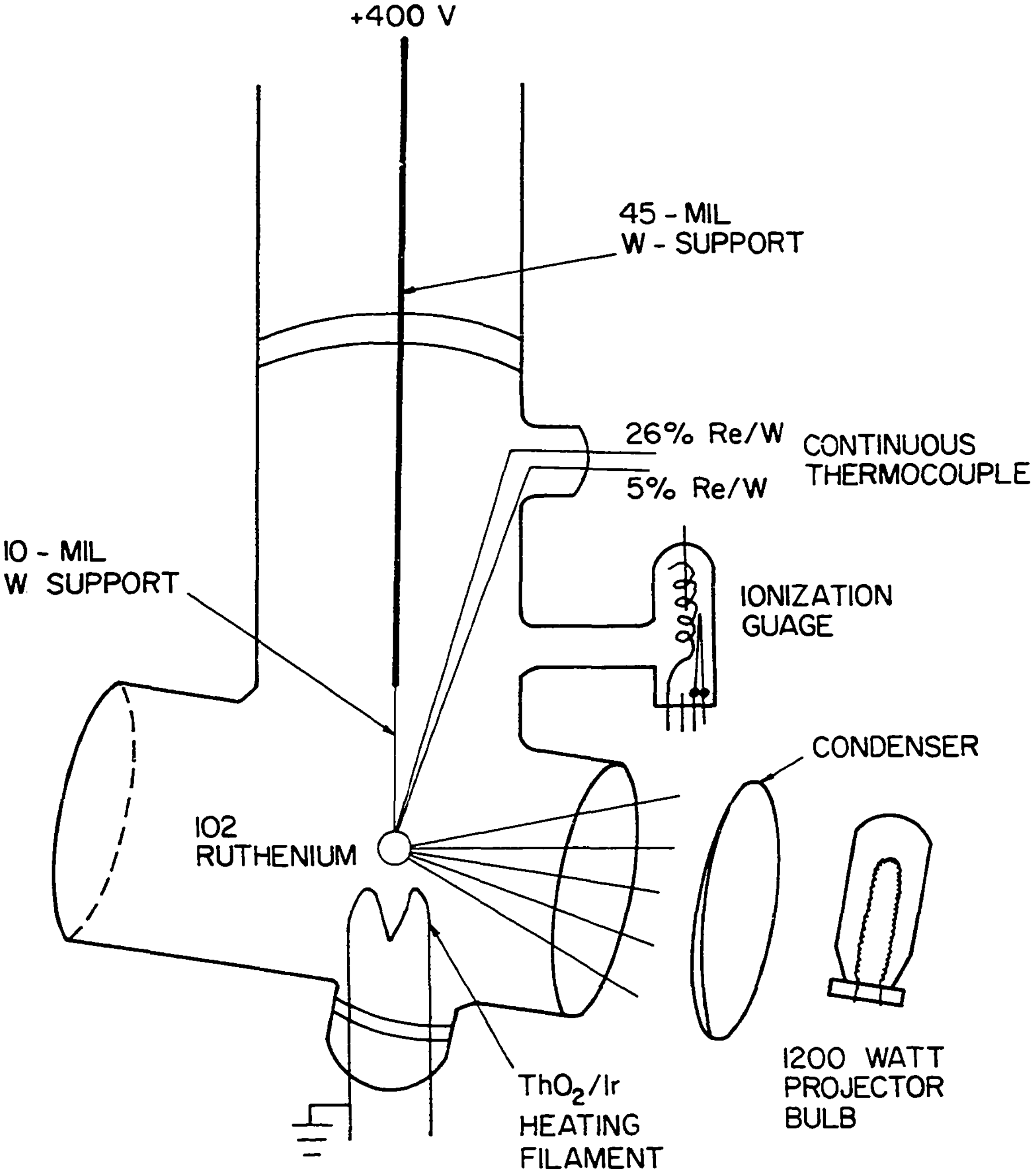

Figure 2. Reactor cell design illustrating the two crystal heating arrangements, either by electron bombardment or by a well-focused beam of light

manifold side, which in addition maintained a vacuum in the reference chamber of the capacitance manometer, were similarly designed.

A capacitance manometer (Granville Phillips, Series 212, Boulder, Colorado) was utilized to measure reactant partial pressures upon their initial introduction into the manifold volume. The manometer was capable of accurately measuring partial pressures between 1 μm and 10 Torr. Since the sensing head has a temperature coefficient of about 0.01 Torr per degree, it was found necessary to thermostatically control the head temperature using a water jacket to prevent manometer zero drift due to changes in ambient temperature.

The sensing head consists of two chambers separated by a thin metal diaphragm. One chamber, A, is connected directly to the reactor system. The reference chamber, B, is continually pumped by the gas manifold pumping system to a pressure of $\sim 10^{-7}$ Torr. When both chambers are evacuated so that the pressure in chamber A is $<10^{-4}$ Torr, the diaphragm rests at its equilibrium (zero) position. Upon introduction of a gas into the gas manifold with valve C1 and either L1 or C2 closed, the diaphragm will be displaced relative to a fixed probe in chamber B. As the diaphragm shifts, the capacitance between the diaphragm and probe changes. This results in a capacitance bridge imbalance producing an a.c. electrical signal which, following amplification and phase detection, is displayed on a meter in the manometer control unit.

The manometer was calibrated using argon against a McLeod guage (Consolidated Vacuum Corporation, Type GM-100A, Rochester, New York) capable of measuring gas pressures greater than 0.01 μm with an uncertainty of ±0.005 μm. Each of the five pressure scales with a maximum range of approximately 100 μm, 300 μm, 1 Torr, 3 Torr and 10 Torr was calibrated and least squares fit to a linear equation of the form:

$$\text{Pressure } (\mu\text{m}) = A(\text{scale deflection}) + B \tag{37}$$

or a power curve of the form:

$$\text{Pressure } (\mu\text{m}) = A(\text{scale deflection})^{B}. \tag{38}$$

The fits were in error by less than 2%. The calibration was checked periodically and found to deviate by less than 10% from the initial calibration.

The variable leak valve (Granville-Phillips, series 203, Boulder, Colorado) can effectively be viewed as a capillary of variable bore size. The valve was employed to regulate the flow of reactants and products from the reaction cell, which served as a static reactor, to the mass spectrometer chamber. By adjusting the leak valve the conductance could be varied from 0.4 to 10^{-11} liters per second and the pressure between the cell and the ultra-high vacuum chamber could readily be reduced by a factor of 10^8. The mass spectrometer filament would then be protected from a high oxidizer concentration and more importantly, the pressure drop due to the leak would be negligible for the duration of an experiment (up to 7 minutes).

The quadrupole mass spectrometer used was a Spectrascan 400 built by the Finnigan Corporation (Sunnyvale, California). The instrument had a mass range of 0-400 u and utilized a Channeltron electron multiplier (Galileo Electro-Optics Corporation, Model 4750, Sturbridge, Massachusetts). The mass range scanned for gas composition analysis during reaction was 0 to 50 u. Above that range no peaks were detected except for a quadruplet of peaks centered at 186, 202, 218 and 234 ± 1 u. These peaks were due to ionized oxides of rhenium (45) resulting from oxidation of the tungsten-3% rhenium mass spectrometer filament by the nitric oxide. The spectrometer head was operated only at pressures of 10^{-5} Torr and below to prevent filament "burn out" and repeated saturation of the electron multiplier. The mass spectrum was scanned every 5 seconds and displayed on either a two-channel strip chart oscillographic recorder (Hewlett-Packard, model 7402A, Palo Alto, California) or an oscilloscope (Tektronix, Inc., type 545A, Portland, Oregon).

The volume of the system was determined by argon expansion from a standard volume connected to a gas inlet; it was calculated to be 1612.2 cm^3.

The valves denoted by C and L were ultra-high vacuum valves (Granville-Phillips Co., series 202, series 204, Boulder, Colorado), as was the leak valve; all were bakable in an open position to 400°C.

Ruthenium Crystal Preparation

The ruthenium crystal was cut from a zone refined quarter-inch single crystal rod obtained from Materials Research Corporation (Orangeburg, New York). The purity level of the ruthenium was 99.99%. Initial attempts to obtain a back reflectance Laue x-ray diffraction pattern were unsuccessful, possibly due to spark-cutting damage on the rod ends. After several endeavors to remove the disordered layer, a faint pattern could be observed. An electropolishing technique was then employed using 80 cc of saturated NaCl with 20 cc of concentrated hydrochloric acid to etch the ruthenium rod ends. Using a variable a.c. power supply, 34 volts was applied between the rod and a platinum electrode with the solution temperature between 0 and -10°C to reduce oxidation. A ruthenium chloride was formed in solution and the resultant rod gave a clear, undistorted Laue pattern. Following orientation, the (102) ruthenium disc was spark cut and mechanically polished using 0.03 μm particle size Linde B alumina. The final orientation was found to be within 0.5° of the (102) pole. The total geometric surface area of the disc was 0.98 cm^2 with the area of the (102) crystal faces being 0.86 cm^2. The edge area was only 12% of the total surface area. An idealized representation of the (102) crystal is depicted in Figure 3. The unit cell dimension along the (010) direction is 6.35 Å and along the $(\bar{2}\bar{1}1)$ direction is 2.71 Å. The surface is an open structure (5.84×10^{14} atoms/cm^2) with a trough that runs parallel to the $(\bar{2}\bar{1}1)$ direction. These troughs may play a significant role in adsorption and surface diffusion processes.

The crystal was mounted within the reaction cell (Figure 2) by spotwelding the disc to a 10-mil (0.254 mm) tungsten support wire. The wire was then spotted to a 45-mil (1.14 mm) tungsten support rod incorporated into a 4-lead glass press seal-dewar assembly. The 10-mil wire was used to reduce conductive heat transfer from the crystal. A continuous thermocouple, which was welded to the crystal face, was used to monitor crystal temperature. The thermocouple wire (Hoskins Manufacturing Co., Detroit, Michigan) used was 3 mil (0.08 mm) Tungsten/26% Rhenium, Tungsten/5% Rhenium.

Under vacuum conditions ($<10^{-6}$ Torr) it was possible to heat the crystal _via_ electron bombardment. A current (∿4a)

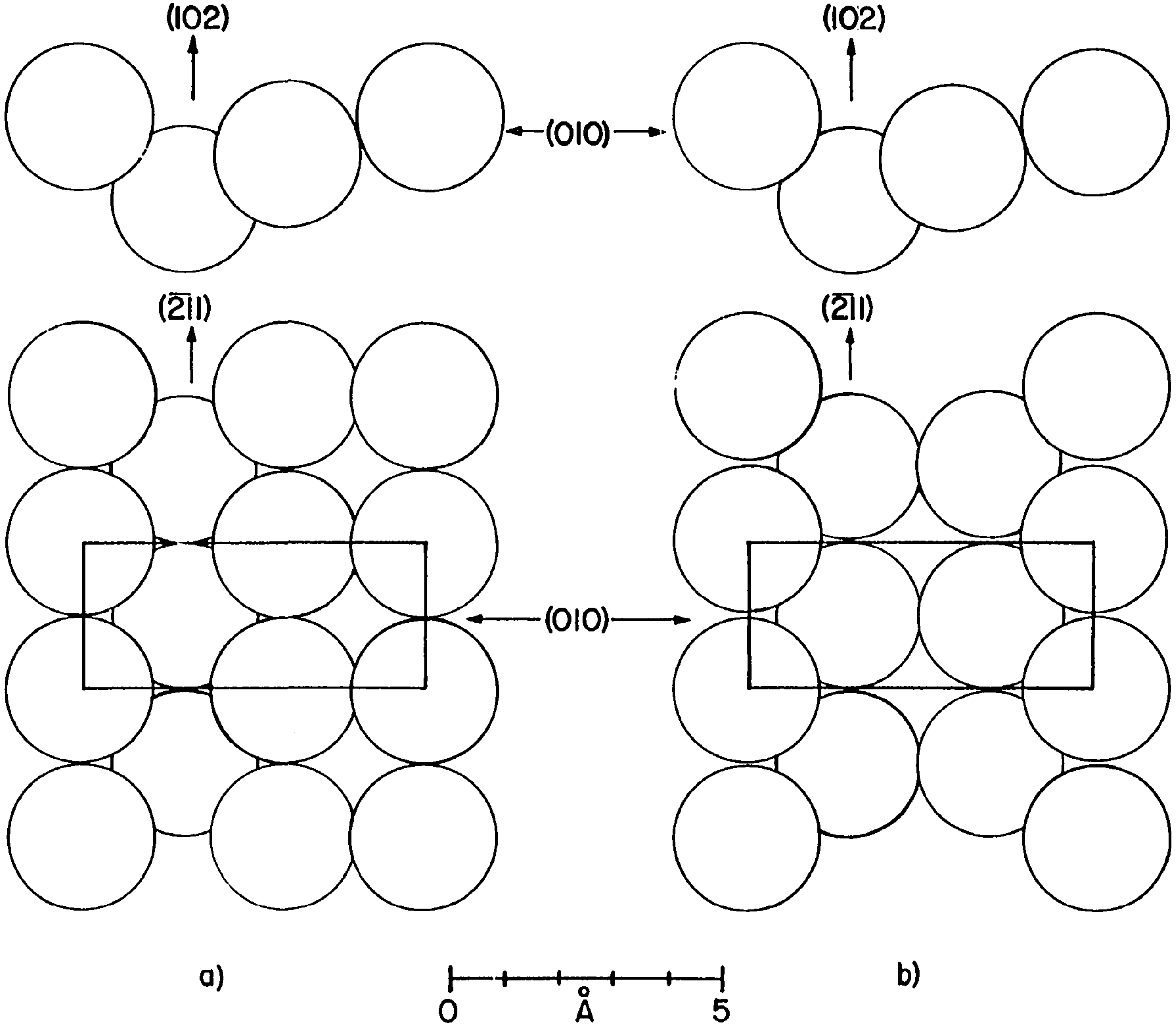

Figure 3. Surface lattice arrangement of ruthenium (102) orientations, models a) and b) illustrate the two possible unit cells for the hexagonal crystal

was passed through the thoria coated iridium filament from a modified d.c. power supply (Hewlett-Packard, model 6286A, Palo Alto, California). This sufficed to maintain a constant electron emission current between the filament and the crystal. The filament was grounded and a positive 400 volt potential was applied to the crystal by a regulated high voltage d.c. power supply (Heath Company, model SP-17A, Benton Harbor). The emitted electrons would then impact the ruthenium disc and cause it to heat. Under vacuum the sample could be heated up to 1500K. Considerable precaution was taken to insure the heating filament temperature did not rise about 1400°C lest vaporization of the thoria would occur and contaminate the ruthenium surface.

The crystal was routinely maintained at a temperature of ∿600°C, which was high enough to prevent most background gas adsorption and yet low enough to kinetically limit diffusion of impurities to the surface. While the surface cleaning procedure developed will be discussed in the following section, it was determined that employing the reproduction of a standard kinetic rate under a given set of reaction conditions was a reasonable criterion for surface cleanliness. To observe reasonably reproducible rates, it was found necessary only to heat the sample to 1000°C for an extended period of time (several days) until the outgassing rate dropped so that the system pressure was $<10^{-8}$ Torr. A series of argon bombardment-oxygen cleaning cycles was attempted to increase the standard reaction rate but it was ineffectual. This cycled cleaning procedure, found to be compulsory on the (100) face of ruthenium (46), was not essential to obtain a clean surface on the Ru(102) face. The reason for this difference will be discussed in the LEED/Auger section of the Results and Discussion.

Kinetic Procedure

The procedure used to obtain a reaction rate measurement, commonly denoted a "run", initially involved flashing the crystal to 1000° from 600°C *in vacuo* to remove any chemisorbed oxygen. This could be accomplished either by electron bombardment or by focusing the light from a 1200 watt projector bulb onto the crystal using a series of condensor lenses (Figure 2). The focused light was the heating method used during kinetic studies as the high total pressure in the reaction cell prevented the use of electron bombardment. The maximum crystal temperature attainable by this method was a function of the ambient gas pressure in the cell; under vacuum conditions it was approximately 900°C.

The temperature of the crystal was regulated by a solid state temperature controller (Ames Laboratory electronic service group) to within ±2° under reaction conditions. The controller monitored the thermocouple e.m.f. which was compared to a preset internal voltage. The projector bulb voltage was then adjusted to eliminate voltage differences and thereby maintain a constant temperature.

The reactions of nitric oxide and carbon monoxide can possibly lead to three reaction products: N_2, N_2O and CO_2. As a mass spectrometer is being used to analyze product distribution the difficulty of separation of nitrous oxide and carbon dioxide is apparent, since they both have a $(m/z) = 44$. Even though Schleppy and Shah (9) indicate that production of N_2O is insignificant above 300°C, it seemed reasonable to at least consider the possibility of its formation on an unsupported ruthenium catalyst at reaction temperatures of 475°C where most kinetic data were collected. This difficulty was circumvented by using high-purity carbon-13 monoxide (^{13}CO) as a reductant. The reaction product $^{13}CO_2$ could then be monitored by the $(m/z) = 45$ peak. Nitrogen was not considered as the product to follow the reaction as nitric oxide will decompose on stainless steel (47,48) to form either nitrous oxide or nitrogen dioxide.

A typical kinetic experiment was initiated with valves L1 and C1 closed (Figure 1) and valves L2 and C2 open to incorporate the reaction cell into the gas manifold volume and to allow differential pumping of the mass spectrometer. The variable leak was then "set" by dosing a known quantity of carbon dioxide (∿200 μm) into the manifold and adjusting the leak valve opening until the pressure within the mass spectrometer chamber was in the 10^{-7} Torr range. The gas was then evacuated through valve C1, redosed with all ionization guage filaments turned off, and the mass spectrometer sensitivity of the carbon dioxide, in μm CO_2 in cell/mv (m/z) = 44, determined. The sensitivity of the product gas was found to vary by less than 10% with increase in carbon dioxide pressure or background reactant gas pressure. Equilibration of the carbon dioxide across the leak usually occurred in five seconds or less. The sensitivity calibration was made previous to each set of kinetic data collected.

The rate measurements were made by dosing the desired partial pressures of the reactants from the gas manifold into the reactor volume using the capacitance manometer. The production of carbon dioxide was monitored with the mass spectrometer. Experimental rates (μm CO_2/sec) could then be determined using the CO_2 sensitivity; incorporating the system volume and assuming an average overall reactor temperature the rate could be determined in molecules CO_2/sec. The reactor temperature used was 303K. The plots of the CO_2 pressure in the reactor cell versus time were linear as only initial rates were measured. In most cases the fraction of the limiting reagent which had undergone conversion during a run was less than 5%. After making the rate measurement, the gases were evacuated through the gas manifold until the pressure dropped below 5 x 10^{-5} Torr and the capacitance manometer rezeroed before redosing.

The reaction system chosen placed several limitations on the kinetic studies. For a practical investigation to be undertaken using catalysts with surface areas on the order of 1 cm^2 the turnover number (TON), molecules produced$\cdot$site$^{-1}\cdot$sec^{-1}, must be greater than approximately 0.1. For this system the minimum temperature satisfying this condition was 400°C.

The maximum temperature can be dictated by two factors. Though not a difficulty with the NO-CO system, the increased reactivity at higher temperatures could lead to high conversions before the product could equilibrate across the leak. This results in nonlinear rate plots. The chief limitation in the present work stemmed from the increase in thermal conductivity with increased gas pressure which reduced the temperature of the catalyst for a given heat input rate. In the system used, it was found that the maximum temperature that could be maintained with 10 Torr of gas in the reaction cell was approximately 550°C.

Since a high intensity light source was used to heat the crystal, consideration was given to the possibility that a photoreaction was occurring in the gas phase and to the possibility that the reaction was actually promoted by a photo-induced process on the ruthenium and not thermally-induced. The possibility of the first effect was eliminated by focusing the light beam directly into the reaction cell without heating the crystal; no reaction products were detected. The second concern was dealt with by heating the ruthenium to reaction temperature and then turning off the lamp. If the reaction was photo-induced, the reaction would immediately stop; instead the rate decreased as a function of catalyst temperature indicating a thermally-activated reaction.

The catalytic activity of the tungsten support rods and the thoria-coated iridium filament were also examined by allowing the light to illuminate them directly, they were found to be virtually inactive.

Thermal Desorption Techniques

A limited number of thermal desorption (flash desorption) studies was undertaken to elucidate the bonding of carbon monoxide and nitric oxide on the ruthenium surface and to develop models for the reaction intermediates involved in the reaction mechanism. Two types of flash studies were undertaken on the Ru(102) face. One involved the adsorption of NO and CO at pressures of less than 10^{-6} Torr. A known quantity of gas would be dosed and measured in langmuirs

(1 langmuir (L) = 1 x 10^{-6} Torr•s). The other study comprised flashing the crystal following a kinetic run.

The first investigation required an initial cleaning of the surface and reduction of the background ambient pressure into the 10^{-10} Torr range. Since doses on the order of one langmuir usually involve adsorbate coverages of less than one monolayer, it is critical that the adsorption rate of background gases be kept to a minimum. After cleaning, the sample was then cooled to <50°C, assisted by filling the cell dewar, which incorporates the 4-lead press seal, with liquid nitrogen or a dry ice-acetone slurry. The reactant gas would then be dosed and a pressure *versus* time plot would be recorded by monitoring the ionization guage controller output on an X-Y recorder (Hewlett-Packard, model 7044A, Palo Alto, California) with a time base drive. The area under the curve could then be converted to langmuirs. Next, the crystal would be heated at a constant heating rate using the focused light beam; the rate was dependent on the voltage applied to the bulb.

The heating rate using 120 V was constant at ∿11K/s from room temperature to 600°C. The desorption pressure would then be monitored by the ionization gauge and the product distribution followed by the mass spectrometer. Even though the total pressure in the reaction cell never exceeded 10^{-6} Torr during this type of study, the crystal was not heated by electron bombardment. This was to eliminate the possibility of electron-adsorbate interactions which could lead to alternate desorption products.

The desorption study following a kinetic run involved dosing pressures on the order of one Torr of both nitric oxide and carbon monoxide into the reaction cell with the crystal at temperatures of 400 to 550°C. Following reaction for 5-10 minutes, the crystal was cooled to <50°C; the cell was then evacuated to 10^{-5} Torr. The valve, L1, between the mass spectrometer and the reaction cell was opened and the crystal was flashed while the desorption products were monitored. The crystal temperature and system pressure were simultaneously recorded to measure the temperature of the maximum desorption rate.

LEED/Auger Procedure

The techniques of low energy electron diffraction (LEED) and Auger electron spectroscopy (AES) were used to characterize the ruthenium surface before and after the NO-CO reduction reaction was made. LEED provides information concerning the symmetry of an ordered adlayer and its relationship to the symmetry of the ruthenium substrate. The diffraction pattern can also be used as a measure of the adlayer surface coverage if the surface is saturated. AES furnishes an elemental analysis of the adsorbates and the first 2-3 atomic layers of the ruthenium. By utilizing both techniques, a semiquantitative representation of the condition of the surface under reactive conditions can be obtained. Several excellent reviews on the theory and application of LEED (49,50) and Auger (50,51) are available.

The LEED/Auger experiments were performed in a Varian 981-2000 vacuum system equipped with 4-grid LEED optics and an Auger cylindrical mirror analyzer. The system, which was capable of obtaining a base pressure of 2×10^{-10} Torr, was evacuated by ion pumps and bakable to 623K. The crystal was mounted in an offset manipulator with X, Y and Z translation and 360° rotary motion so that the disc could be positioned in front of either the Auger spectrometer or LEED optics without breaking the vacuum. It could be heated to 1500K conductively <u>via</u> an indirect heater block positioned behind the sample. A tungsten/26%Re, tungsten/5%Re continuous thermocouple was spotwelded to the face of the disc to allow for temperature measurement. The sample could be argon bombarded for cleaning purposes using an ion gun when the sample was located at the cylindrical mirror focal point.

The Auger spectra were recorded using a 10 μA filament emission current and a beam energy of 2000 eV so as to reduce electron disruption of the overlayer. A scan width of 50-550 eV was generally recorded (3.3 eV/s) using a peak to peak voltage of 10 V. LEED patterns were obtained utilizing beam voltages of 50-100 eV.

The system was modified to include a gas handling system similar to the gas manifold incorporated in the reactor system. Gases were dosed into the 304 stainless steel bell jar housing the LEED unit and the mirror analyzer using a Granville-Phillips variable leak valve.

Studies included both high (∿1 Torr range) and low ($<10^{-5}$ Torr) pressure dosing. The low range investigation included studies of the adsorption of nitric oxide and oxygen and determination of resulting LEED patterns. The electron guns in both units were operated briefly and only for the time of analysis so as to eliminate any electron induced effects such as enhanced adsorption or molecular decomposition.

The high pressure range studies involved dosing NO and CO into the gas handling system using a mercury manometer which was isolable when not in use. The poppet valve, a high conductance valve within the LEED/Auger unit which separates the ion pumps from the upper half of the bell jar housing the instrumentation, was then closed and the gas mixture was introduced into the system. Following a specified reaction time with the crystal heated to ∿650K, the bell jar was evacuated with VacSorb pumps. These would reduce the pressure to approximately 10^{-4} Torr within 2 minutes after which limited analysis could be undertaken. The poppet valve could then be opened resulting in a pressure drop from 10^{-4} to 10^{-8} Torr. The total pumping time to evacuate the system from 1 to 10^{-8} Torr was three minutes.

X-Ray Photoelectron Spectroscopy Experiments

XPS was used to establish the chemical state of the catalyst following the reduction reaction. An AEI model ES 100B XPS/UPS spectrometer was employed for the analysis of the binding energies of the ruthenium ($3d_{5/2,3/2}$) and oxygen (1s) electrons. The Al K_α line (1486.6 eV) served as the initial energy source of x-ray photons. Most of the XPS studies entailed using a ruthenium sample which previously had been used as a catalyst for the NO reduction reaction in the reactor system. It was necessary to transfer the sample in air to the XPS spectrometer, thus subjecting it to atmospheric contamination but probably not to a change in chemical state. An *in situ* study was also attempted within the XPS spectrometer.

Materials

Most of the gases utilized in this study were of ultra-high purity. The oxygen (99.995%), argon (99.9995%) and carbon dioxide (99.998%) were acquired from the Linde Division of Union Carbide (Chicago, Illinois) in 1 liter Pyrex bulbs with breakable seals. These were used without further purification. The nitric oxide (at least 99.0%) was obtained from Air Products and Chemicals, Inc. (Tamaqua, Pennsylvania). Since it was only available in lecture bottles, it was transferred into a 1-liter Pyrex bulb with a breakable seal after the gas was vacuum distilled several times in an ultra-high vacuum system to remove contaminants. A mass spectral analysis indicated no detectable impurities after distillation. The carbon-13 monoxide that was obtained from Monsanto Chemical Company (Mound Laboratory, Miamisburg, Ohio) had an enrichment of 99%. The purity level was unknown but no impurities were detected upon mass analysis. The $^{12}C^{18}O$, which was used in an exchange study, was 99% enriched; it was obtained from Prochem/Isotopes (Summit, New Jersey). A small impurity of argon (<0.5%) was detected but the gas was used without purification. For the LEED/Auger experiments some hydrogen, used for cleaning purposes, was purified by a Pd/25% Ag diffusion.

The Materials Research Corporation was the source of the ruthenium; atomic emission analysis confirmed the purity level of 99.99%.

RESULTS AND DISCUSSION

An oft-stated concern in the field of catalytic chemistry is the seeming lack of relationship between surface kinetic studies and investigations in the field of surface physics dealing with adsorbate-substrate interactions of specific chemical species. Investigations in surface physics are prevailingly accomplished under ultrahigh vacuum conditions (10^{-8} to 10^{-10} Torr) whereas kinetic studies generally involve minimum total pressures of one Torr. This study covers both pressure ranges; the relationship between the two fields will be manifested in the rationalization of a consistent description of the NO-CO reaction.

Kinetics Introduction

The kinetic studies undertaken involved the variation of reactant pressures from 6 μm to 10 Torr, a variation of over three orders of magnitude. This is significant as the studies of Schleppy and Shah (9) and those of Butler and Davis (11) were accomplished only over a range of approximately one magnitude. Often this will lead to the reporting of reactant orders that are not pressure dependent, whereas most general theories of surface kinetics (52) indicate that such a result is erroneous. Summaries of the two most commonly encountered general kinetic mechanisms, Rideal-Eley and Langmuir-Hinshelwood mechanisms, are given in Appendix I. In keeping with the desired relevance of this study and its relation to practical application, the characteristic nitric oxide and carbon monoxide partial pressures in an automotive exhaust are on the order of 10 µm and 5 Torr, respectively, both of which are in the range of study. Most of the kinetics to be reported were determined at 475°C, which is a typical exhaust temperature at 30-40 mph (1).

The kinetic data will be presented as a ln rate (R) *versus* ln pressure (P_x) plot (order plot). The slope of the curve at any pressure represents the kinetic order of the reaction with respect to the reactant, x, at that pressure. The rates are plotted in units of $10^{15} \cdot \text{molecules} \cdot \text{cm}^{-2} \cdot \text{s}^{-1}$ which gives an approximate value of reaction turnover number assuming 10^{15} reaction sites per cm^2.

A carbon monoxide order plot, determined using a constant nitric oxide pressure of 255 µm, is shown in Figure 4. The scatter within the data is less than ±10% and can be attributed to instrumental noise. According to the plot, the order with respect to CO varies from +1 to -1. This, at least initially, indicates that a Langmuir-Hinshelwood (LH) type mechanism is operative. The sharpness of the maximum presents a slight problem as LH mechanisms are generally more broad if the limiting orders are +1 and -1. Data could not be obtained at higher pressures due to manometer

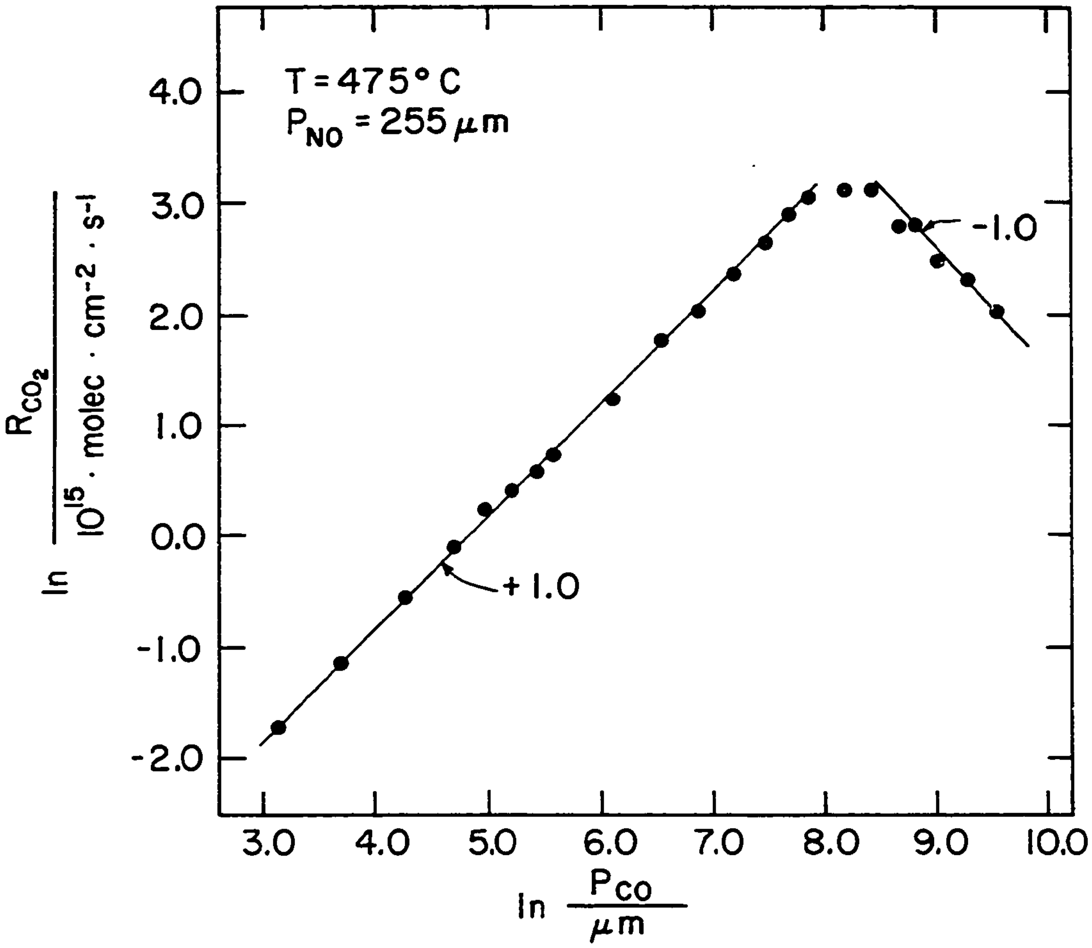

Figure 4. Carbon monoxide order plot determined using a constant nitric oxide pressure of 255 μm. The slope of the lines drawn indicate the reactant order and sharpness of the peak maximum

limitations but the sharpness of the peak may possibly indicate a more negative order. Comparing this result with previous work, it is difficult to rationalize the zero order in carbon monoxide over a one order of magnitude pressure change as reported by Butler and Davis (11). The order value of Schleppy and Shah (9) of 0.81 does seem reasonable in light of these results.

The order plot at 475°C of nitric oxide using a constant pressure of carbon monoxide of 540 µm is illustrated in Figure 5. The plot is clearly not simple. At low nitric oxide pressures a positive order is indicated which may be +1 at lower reactant pressures. As the pressure was increased the order decreased to zero and became negative ($\sim$-0.3) and remained at that value as the pressure was increased from 40 µm to 650 µm, over one order of magnitude. The reactant order then abruptly increases to approximately +1. At nitric oxide pressures greater than 2.5 Torr the slope rapidly decreases to zero and finally becomes negative with a slope of less than -2. Such order behavior is not predictable from a simple LH mechanism. Since the curve maxima in the plot vary greatly in sharpness and the limiting reactant orders appear to be different for each curve, $\sim$+1 at low NO pressures (region I) and >+1 for the curve in region III and -0.3 in region II as compared to -2 to -4 in region IV, the results

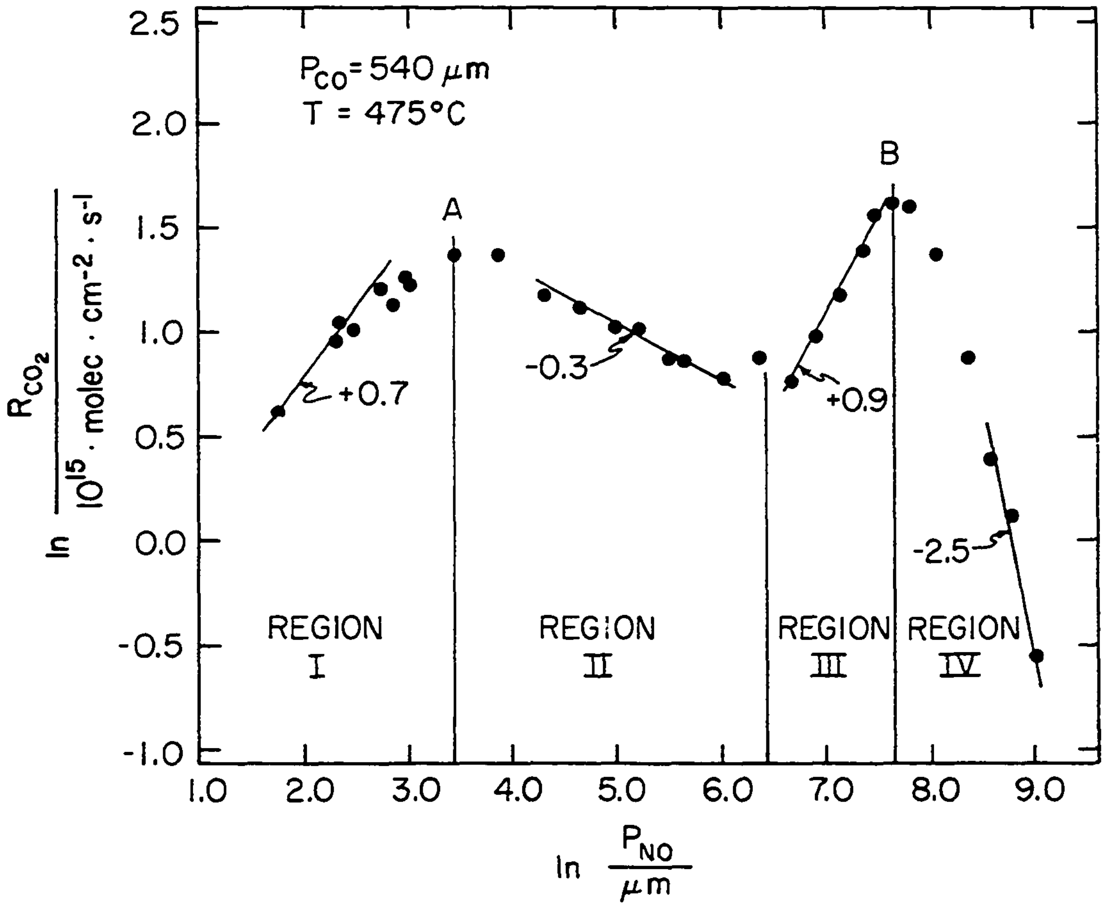

Figure 5. Nitric oxide order plot determined using a constant carbon monoxide pressure of 540 μm. The reactant order was determined from the slopes of the lines drawn

suggest that there may be two reaction mechanisms operative in different pressure regions.

Two mechanisms of this character could result if one surface species was formed at low NO pressures, while at higher pressures another type of species were formed which displaces the former species. It could also be due to a change in the catalytic surface which also would lead to the formation of different reaction intermediates.

As the NO/CO ratio is less than one at the first maximum, A, it seems reasonable to consider that the catalyst would be in a reduced state relative to the catalyst condition at the second maximum, B, where the NO/CO ratio is greater than one. This could contribute to an oxidized state of the ruthenium. This evidence would support the hypothesis put forth by General Motors researchers that different mechanisms may occur on the two states, reduced and oxidized, of the catalyst.

A visual observation was made of the catalyst in the process of making the rate measurements. It was noted that when kinetic data were collected under reducing conditions using a newly polished cyrstal with a mirror finish, the crystal maintained its high reflectivity. If the ruthenium disc was used under oxidizing conditions, the reflectivity decreased due to the formation of a dark blue overlayer on the sample. Upon reducing the tarnished catalyst with carbon monoxide, the overlayer was removed but the reflectivity could not be restored even after heating to 1000°C overnight.

The hypothesis is therefore set forth that the NO-CO reaction can occur by two reaction mechanisms depending on the oxidation-reduction characteristics of the reaction gas mixture used. One mechanism could occur on a reduced state of ruthenium, possibly ruthenium metal, and the other on an oxidized state, possibly ruthenium dioxide. For the sake of discussion the reaction mechanism under reduced conditions will be labelled "Mechanism A" and that under oxidizing conditions "Mechanism B".

Previous kinetic work yielded nitric oxide orders of -0.62 and 0. While the zero order of Butler and Davis seems difficult to rationalize, the -0.62 is comparable to the -0.3 value reported in region II of Figure 5. Under all conditions no nitrous oxide was detected at 475°C which is in accord with previously published results.

Chemisorption of carbon dioxide and the formation of carbonates have been detected <u>via</u> infrared spectroscopy over ruthenium surfaces (22,35,36). Since a significant coverage of either species would alter the curvature of the reactant order plot and dictate the inclusion of a CO_2 desorption process:

$$\mathrm{Ru} - \mathrm{O} \overset{\cdots}{\text{—}} \mathrm{C} \overset{\cdots}{\text{—}} \mathrm{O} \rightleftharpoons \mathrm{Ru} + \mathrm{CO_2(g)} \qquad (39)$$

or

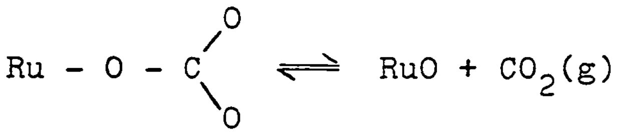

$$\mathrm{Ru} - \mathrm{O} - \mathrm{C}\!\begin{smallmatrix} \diagup \mathrm{O} \\ \diagdown \mathrm{O} \end{smallmatrix} \rightleftharpoons \mathrm{RuO} + \mathrm{CO_2(g)} \qquad (40)$$

a carbon dioxide order plot was made to see if either of the reactions would need consideration. Under both reducing and oxidizing conditions an order plot was measured and found to have a slope of zero. The results under oxidizing conditions are exhibited in Figure 6. Due to the large carbon dioxide pressure range studied, the order will be considered to be zero in carbon dioxide for this investigation. From this result it can be concluded that the rate of desorption of carbon dioxide is rapid and that as a carbon dioxide molecule is produced it desorbs. If the rate limiting step were therefore to be the formation of CO_2 then it would not be necessary to consider it as the forward step in an equilibrium.

Apparent activation energy plots for the oxidized and the reduced mechanisms, A and B, are presented in Figure 7. The slope of the curve at any point is -E/R where E is the apparent activation energy. While the plot is useful in comparing rates of reaction at different temperatures, the calculated activation energy has no direct relationship to the actual activation energy of an elementary step. The

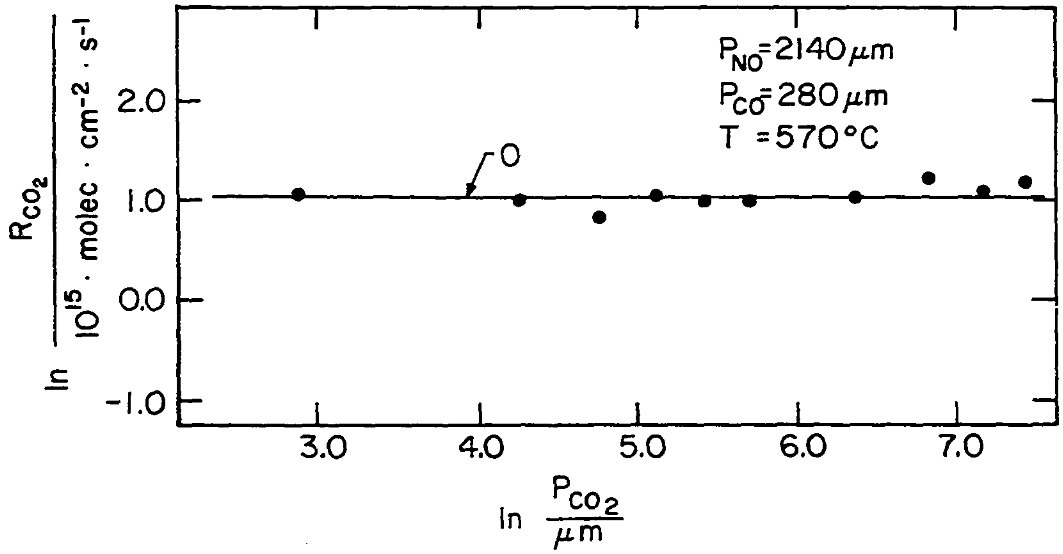

Figure 6. Order plot indicating that the reaction is zero order in carbon dioxide

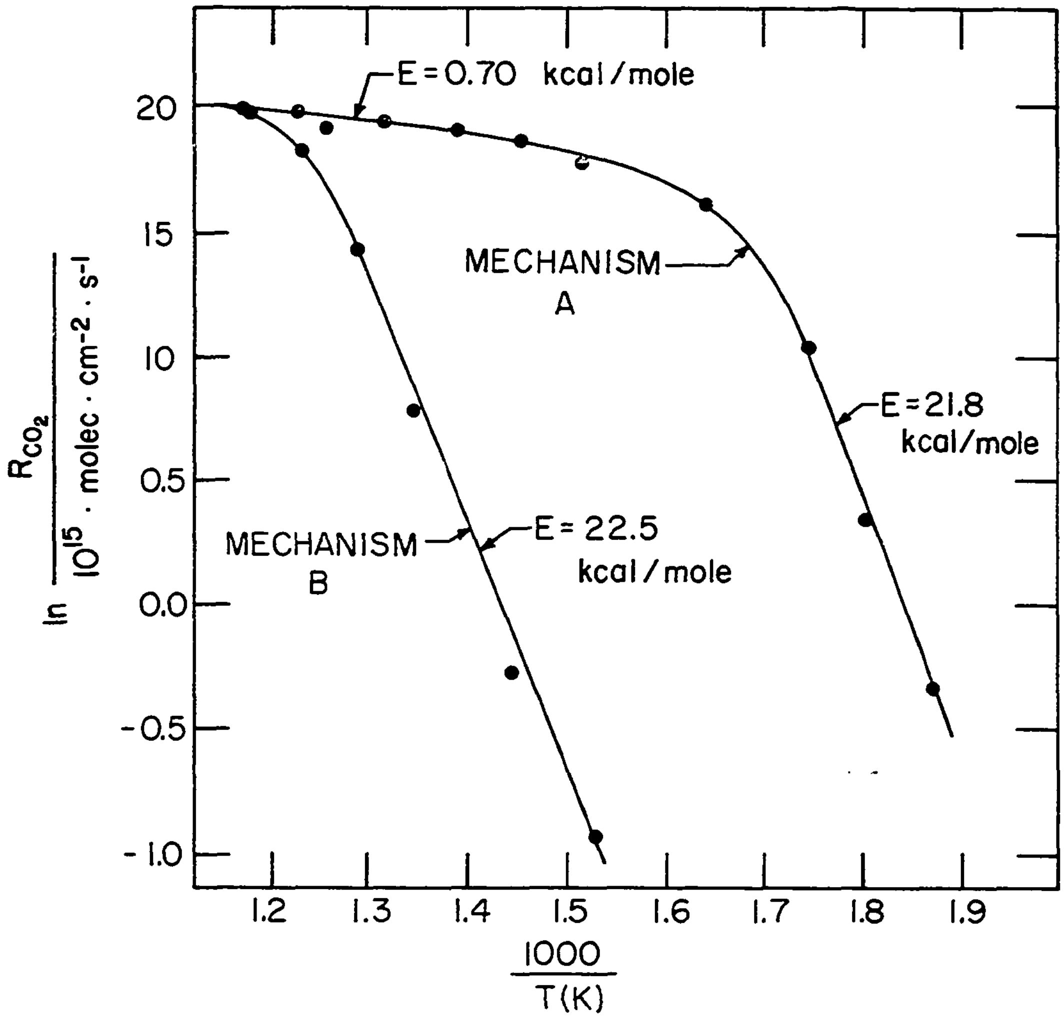

Figure 7. Temperature dependence of the two reaction mechanisms A and B which are functional under reducing and oxidizing conditions, respectively. The reducing gas mixture used was 225 μm NO and 890 μm CO and the oxidizing mixture was 1890 μm NC and 320 μm CO

calculated E value is the result of the overall temperature dependence of the rate law which contains summations of products and quotients of actual rate constants. This often will lead to nonlinear Arrenhius type plots as evidenced in Figure 7. For mechanisms A and B, the apparent activation energies calculated were 21.8 and 22.5 Kcal/mole, respectively, in the linear region. At higher temperatures the activation energy decreases to approximately zero. In the low temperature range of 250-350°C, the activation energies compare quite well with those reported previously. Schleppy and Shah (9) cited a value of 23.0 Kcal/mole while the value determined by Butler and Davis (11) was 19.7 ± 4.5 Kcal/mole. From the plot it is seen that mechanism B will not be as significant at lower temperatures as mechanism A. This would be expected if at higher NO pressures the surface was reconstructed or oxidized thus favoring a different reaction mechanism. Since both processes are thermally activated, both will be considered as possible explanations of this effect.

Surface Characterization

LEED/Auger characterization

In an effort to understand the condition of the catalytic surface during the NO-CO reaction, a series of LEED/Auger experiments was performed. For the Auger analysis the elemental concentrations of ruthenium, nitrogen, carbon and oxygen were determined. For ruthenium the principal Auger electron energies occur at 150, 198, 228 and 273 eV and for oxygen a triplet exists at 475, 490 and 510 eV with the 510 eV peak being the most intense. Nitrogen and carbon peaks are at 380 and 271 eV, respectively. Since the carbon and ruthenium Auger energies differ by 2 eV, quantitative coverages of carbon were not directly obtainable. With the oxygen or nitrogen, no difficulty should be encountered in determining the surface coverages.

A relative measurement of the carbon coverage was obtained by determination of the degree of asymmetry of the Ru(273) peak. Clean ruthenium will give an almost symmetric Auger peak spectrum with the distance from the baseline to the peak maximum divided by the baseline to peak minimum being approximately 0.92. The carbon Auger spectrum is asymmetric, having a greater distance to the minimum than maximum. Upon spectrum overlap, a carbon covered ruthenium surface spectrum will exhibit a greater asymmetry, and as the carbon coverage increases, the asymmetry ratio, F', will decrease. For reportedly clean ruthenium surfaces, this ratio has a literature value of between 0.75 and 0.80 as derived from published Auger spectra. The value of 0.92 which was observed in this laboratory seems high, but this could be due to differences in spectrometer characteristics or due to unsuspected contamination of the reported spectra. The F' value cannot be simply related to an actual carbon coverage without incorporation of the elemental sensitivities of the ruthenium and carbon which relate to the Auger transition probabilities, the actual asymmetry of the carbon Auger 271 eV peak relative to the ruthenium 273 peak and the attenuation of the ruthenium contribution due to the carbon overlayer. Since these factors are not accurately known, the F' value will be considered sufficient for this investigation.

After the ruthenium disc was mounted in the manipulator, the system was baked at 250°C for 18 hours. The sample was then outgassed at 1050°C for 45 minutes to remove any chemisorbed gases resulting from atmospheric transfer or bakeout. The resulting Auger spectrum is presented in Figure 8a. The sample was not clean at this point as silicon (89 eV) and phosphorus (118 eV) Auger transitions were detected. The carbon coverage was considered to be small since $F' = 0.82$, which was toward the high end of the range $0.44 < F' < 0.92$ encountered in this study. No oxygen was detected but several small peaks in the 300 to 500 eV range were observed. These peaks were persistently found throughout this work and have been the topic of a great amount of discussion in the literature. While the possibility does exist that the small peaks at ∿400 and ∿420 eV are due to a small Ti impurity, it is generally believed that these are attributable to a

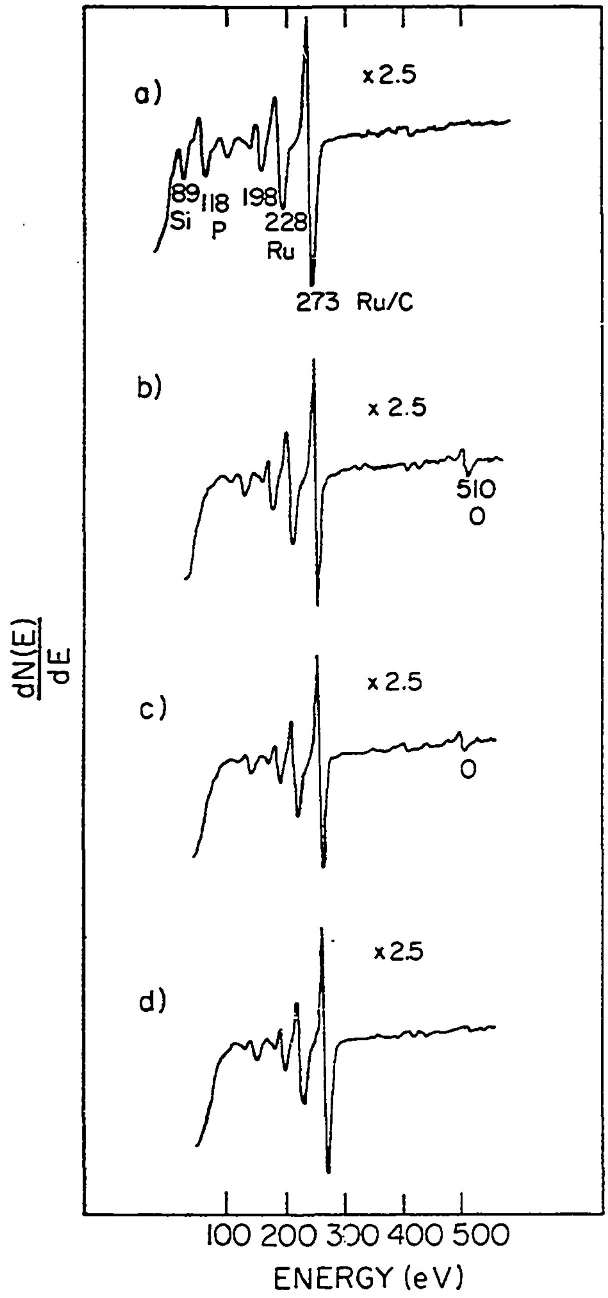

Figure 8. The sequential cleaning procedure of the ruthenium crystal: (a) Auger spectrum after heating at 1050°C for 45 minutes, F' = 0.82, (b) after oxygen cleaning using 5×10^{-6} Torr O_2 at 1000°C for 1000 seconds, F' = 0.91, (c) after flashing to 1000°C, F' = 0.87, (d) after heating at 925°C for 45 minutes, F' = 0.83

diffraction process (53-55) involving secondary electrons. This was confirmed by Orent and Hansen (56) in a study of the temperature dependence of the Auger intensities resulting in their characterization with an accompanying Debye-Waller factor. Several other peaks in the 300-500 eV range are due to MNV or MVV ruthenium Auger transitions (53). Depending on the cleanliness and the condition of the surface, these peaks were noticed to vary in intensity, possibly due to valence band changes (57).

In order to further clean the surface an oxygen treatment was undertaken dosing 5×10^{-6} Torr of O_2 for 1000 seconds with the catalyst at 1000°C. Figure 8b indicates that the silicon and phosphorus are removed and the F' value increased from 0.82 to 0.91, indicating carbon removal. Upon flashing the crystal to 1000°C, only a small decrease in the oxygen was detected (Figure 8c). It was only after the crystal was heated at 925°C for 45 minutes that a clean spectrum could be recorded as in Figure 8d. This Auger spectrum is qualitatively the same as those reported in recent studies (47,53,56,58,59) on ruthenium.

It was observed during the initial phases of study upon high temperature flashing or heating that carbon segregated to the surface as exemplified by the F' decrease in Figures 8c and 8d. Following a series of oxygen treatments this carbon contamination difficulty was eliminated.

The procedure used to clean the crystal demonstrates that under kinetic reaction conditions the surface would be "clean" as the carbon, phosphorus or silicon would be removed by reaction with nitric oxide.

The effect of oxygen cleaning at 1000°C led to an interesting result that was a foreshadowing of a conclusion concerning nitric oxide adsorption. Upon attempting to thermally desorb the surface oxygen, the coverage underwent only a slight decrease. This result is somewhat contrary to that expected for chemisorbed oxygen. Ku, Gjostein and Bonzel (47) had noted that once oxygen was adsorbed on the Ru(100) face it could be desorbed by flashing with the onset occurring at 800°C and reaching a maximum desorption rate at 1000°C. Madey, Engelhardt and Menzel (53) saw desorption on a Ru(001) face at ∿1000°C as did Reed, Comrie and Lambert (60) on a (101) face, thus indicating that the oxygen, if in a chemisorbed state, would have desorbed. It was only until the disc was maintained for an extended time, *e.g.*, 45 minutes, at a high temperature (>900°C) that the coverage on the (102) face was reduced. This behavior may result from the high (1000°C) dosing temperature in the present work leading to oxygen diffusion into the bulk. This conclusion is consistent with the known endothermicity of oxygen dissolution into ruthenium (61). It is also consistent with the finding that upon increase in the surface temperature the work function, $\Delta\phi$, of an oxygen covered ruthenium surface becomes increasingly more negative without the simultaneous decrease in coverage due to oxygen desorption (62).

The LEED pattern resulting from the cleaning procedure was a (1 x 1). The ratio of the lattice constants from the pattern was 2.34 ± 0.03, which is identical to the ideal unreconstructed surface unit cell for the (102) crystal face. The surface unit cell therefore appears to be the same as the bulk unit cell structure for the (102) crystal plane. Verification of this is impossible without LEED spot intensity analysis to determine the surface structure.

Since the purpose of the LEED/Auger study is to develop a model for the reaction surface, it was imperative to calibrate the Auger spectrometer so as to determine adsorbate coverages. It was found that subsequent to a NO-CO reaction, the only adsorbate of significant concentration was oxygen. An effective means to determine the relationship between Auger intensities and surface coverage is to relate the LEED diffraction pattern coverage to a surface saturated Auger intensity.

Oxygen readily forms ordered LEED patterns on ruthenium. On a (100) face adsorption at temperatures below 400°C will form a c(2x4) which, upon increase in coverage, forms a (2x1) with $\theta_0 = 0.5$ (47,56). The (001) ruthenium crystal at 300K produces a "2x2" structure which has been interpreted as 3 degenerate domains having (1x2) symmetry (53,58); the (101) orientation generated three phases (60) which were |11,30|, |21,50| and |41,90| using condensed matrix notation (59). Condensed matrix notation utilizes the unit mesh vectors a and b of the substrate unit cell to describe the surface unit vectors of the overlayer. As an example, a (2x2) can be rewritten in matrix notation as |20,02| where $x = 2 \cdot a + 0 \cdot b$ and $y = 0 \cdot a + 2 \cdot b$. Oxygen likewise produced an ordered pattern of c(2x2) symmetry on ruthenium (102) which corresponds to a coverage of 0.5.

At 380°C an oxygen adsorption isotherm was recorded using oxygen peak to peak values, O_{pp}, as a measure of surface oxygen concentration. A c(2x2) pattern formed after a 5 langmuir dose. Following surface saturation in a c(2x2) structured adlayer an increase in the total amount of oxygen dosed resulted in the formation of a c(2x4) pattern which saturated at a coverage of 0.75. The isotherm corresponding to this experiment is shown in Figure 9. LEED patterns are here indexed with the first lattice vector along the (010) direction and the second parallel to the $(\bar{2}\bar{1}1)$ direction. The oxygen phase transitions on a ruthenium (102) surface are:

$$(1x1) - Ru \longrightarrow c(2x2) - O \longrightarrow c(2x4) - O. \qquad (41)$$

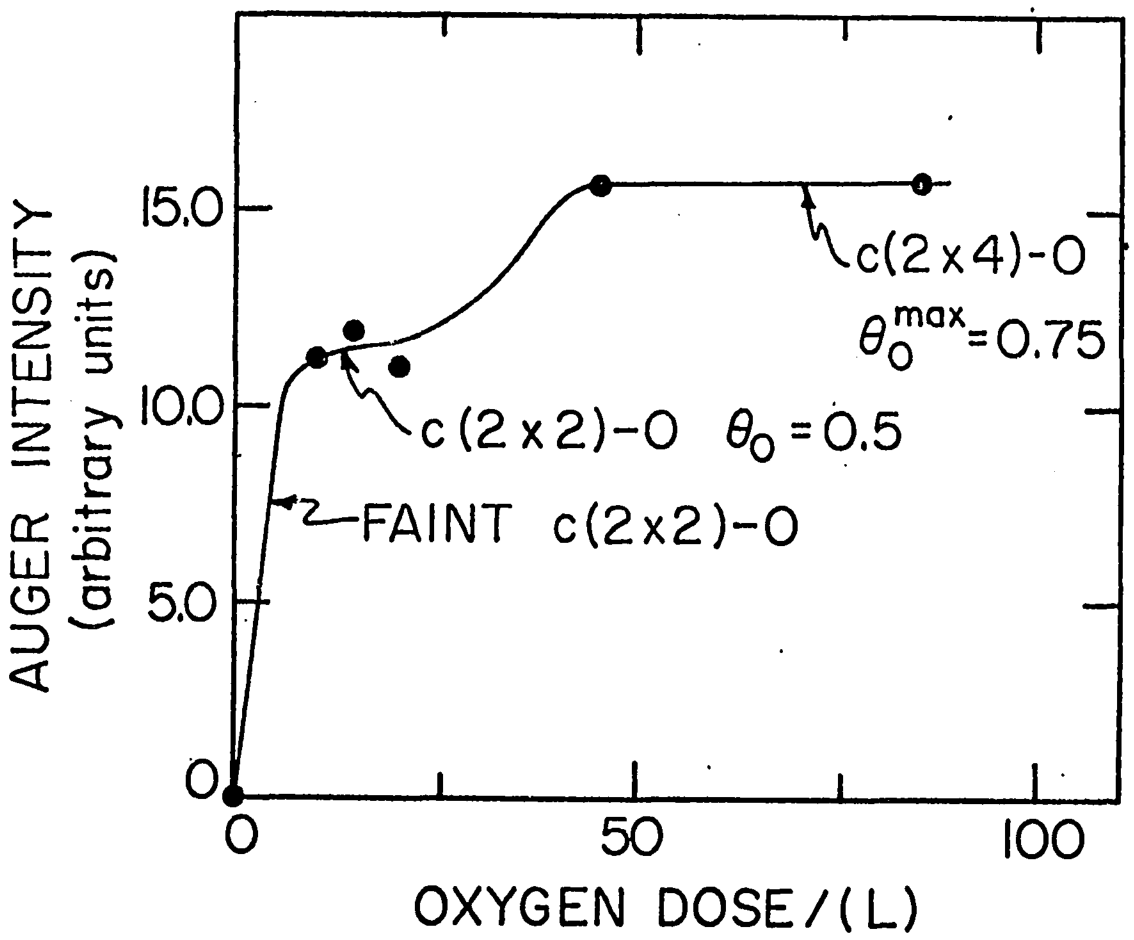

Figure 9. Oxygen Auger intensity *versus* oxygen dose correlation diagram. As the oxygen dose was increased, the symmetry of the surface structures underwent a (1x1) - Ru —> c(2x2) - 0 —> c(2x4) - 0 transition. The oxygen adsorption temperature was 380°C

Oxygen coverages were assumed proportional to O_{pp}, and the proportionality constant was established using the first plateau in the oxygen adsorption isotherm to indicate surface saturation of the c(2x2) pattern with $\theta = 0.50$. On this basis O_{pp} values for the two points in the second plateau correspond to coverages of $\theta_0 = 0.68$ and 0.73. Since it was undesirable to calibrate the analyzer every day, a standard calibration curve was drawn. The values of O_{pp}/Ru_{pp} at =0.50, 0.68 and 0.73 were plotted versus coverage and found to be strictly proportional to it. The equation which relates the peak to peak ratio to oxygen coverage is:

$$\text{Oxygen coverage, } \theta_0 = 8.50\ (O_{pp}/Ru_{pp}). \qquad (42)$$

The change in surface coverage could then be calculated by comparing calculated θ_0 values before and after dosing. This calibration was found to deviate by less than 10% upon periodic checking. The O_{pp}/Ru_{pp} method was employed, instead of a direct relationship between oxygen peak to peak values and coverage, because oxygen would reduce the electron multiplier gain over a period of time. This affected both the ruthenium and oxygen peaks while the ratio was found to be independent of the gain. The attenuation of the ruthenium due to oxygen adsorption is inherently incorporated into equation 42. Electron mean free path attenuation due to increases in total system pressure are also compensated for in equation 42. This is significant as some Auger spectra were recorded at 10^{-4} Torr and not under ultra-high vacuum conditions.

The expected saturation coverage of a simple c(2x4) pattern is 0.25; since the maximum coverage was calculated to be 0.75, this is indicative of a coincidence type lattice. For the case of a noncoincidence lattice, the overlayer (oxygen) unit vector is an integral multiple of the substrate (ruthenium) unit vector, but in a coincident lattice a periodicity is adopted regardless of the substrate. The overlayer and substrate lattice would coincide at certain points forming an apparent superstructure or coincidence lattice. Since the incident electrons are capable of penetrating the overlayer, the diffraction pattern obtained is not due just to the overlayer structure but also to the adatoms which are in coincidence with the ruthenium lattice surface structure. A more exacting discussion of coincidence lattices has been made by Roberts and McKee (63). This indicates that oxygen atoms reside in a pattern on the ruthenium surface which will lead to the direct formation of a simple c(2x4) as well as in nonlattice point positions.

A (1x1)-Ru LEED pattern and a representative model of the ruthenium (102) surface are presented in Figure 10. In Figures 11 and 12 the corresponding LEED patterns of the c(2x2) and c(2x4) overlayer structures and their nonprimitive cells are depicted. The surface structures represented in

(a)

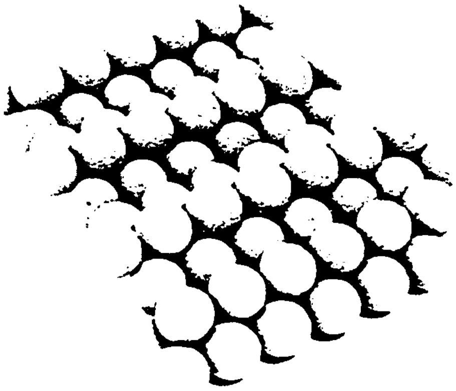

(b)

Figure 10. Clean ruthenium (102) a) LEED pattern using a beam energy of 74 eV, (1x1)-Ru; b) ball model of the surface using lattice arrangement (b) from Figure 3

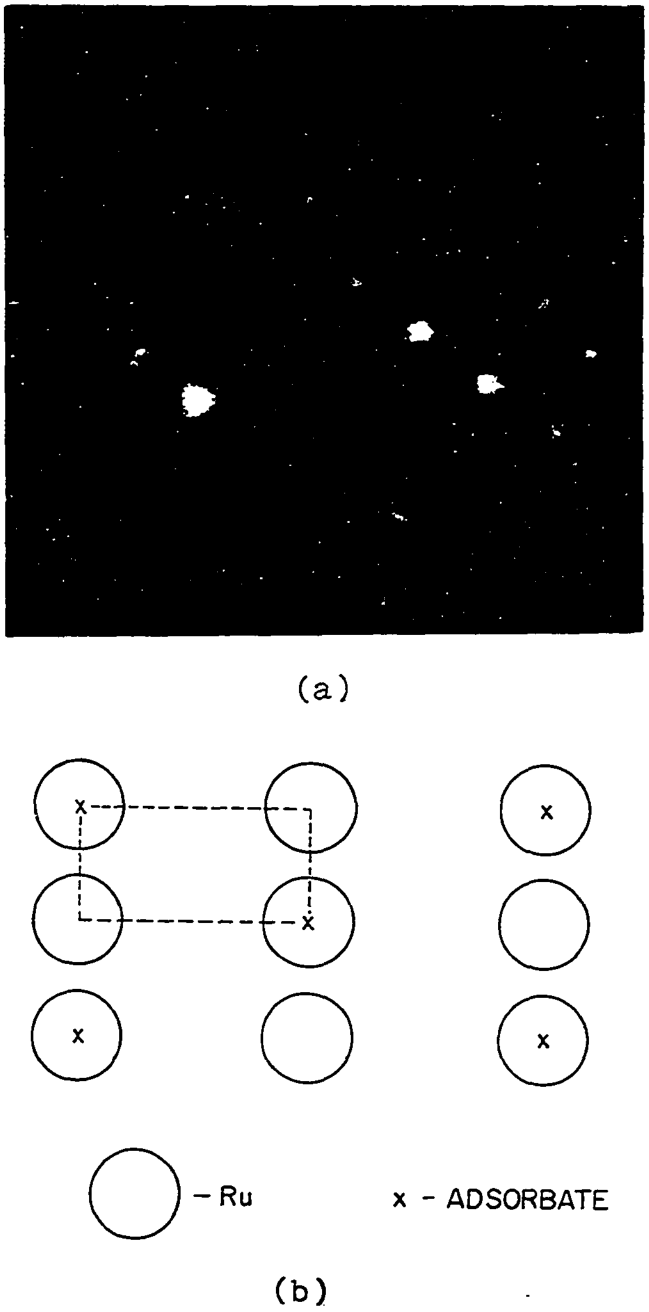

Figure 11. LEED pattern (a) and representation of the oxygen overlayer (b) following an O_2 dose: a) c(2x2)-O diffraction pattern using a beam energy of 75 eV; b) configuration of adsorbed oxygen based on the LEED pattern where x represents the oxygen adsorbate. The rectangle defines the (102) unit cell

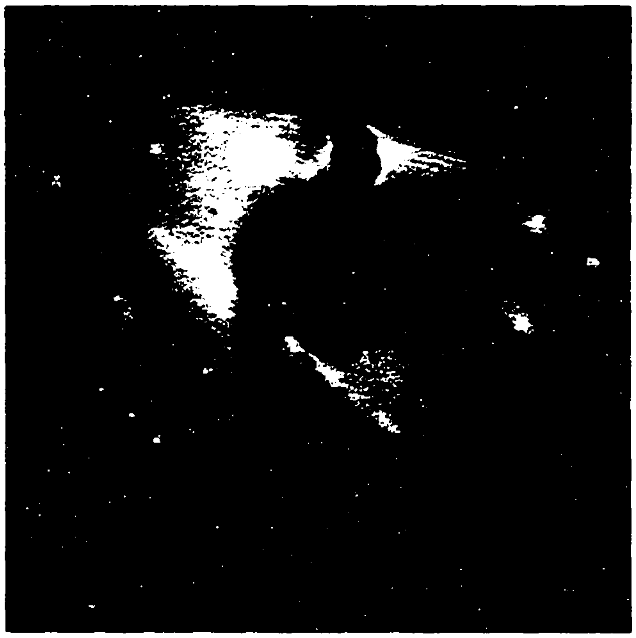

(a)

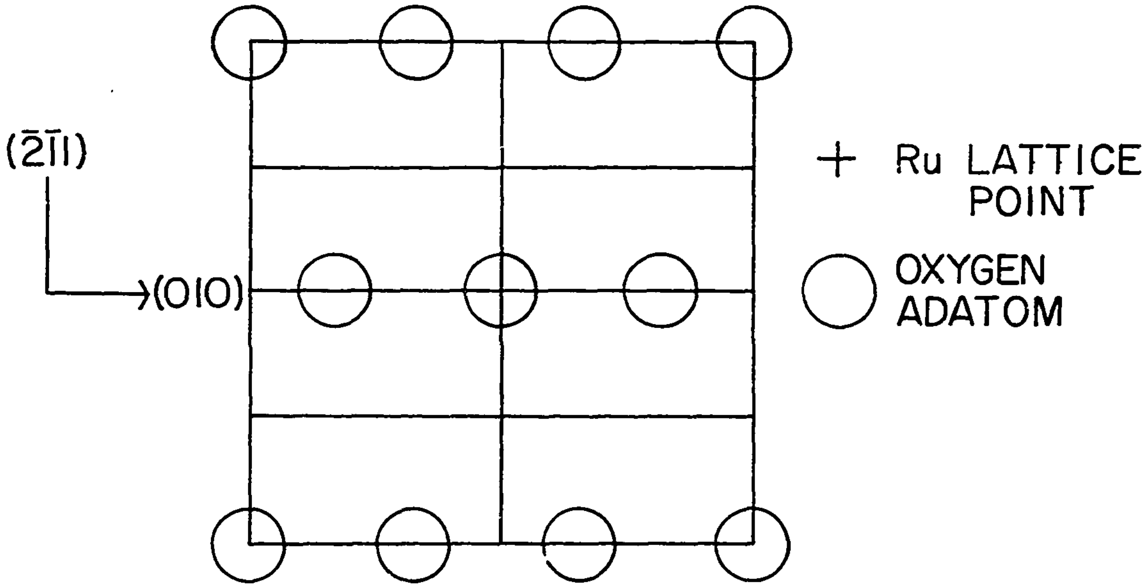

(b)

Figure 12. LEED pattern (a) and oxygen overlayer representation (b) following an O_2 dose: a) c(2x4)-O coincident lattice diffraction pattern using a beam energy of 94 eV; b) nonprimitive centered-rectangular unit cell of c(2x4)-O overlayer

these figures have the oxygen atoms bonded to ruthenium lattice sites but the same LEED pattern would be obtained if all oxygen atoms were displaced by a constant vector.

Following the oxygen study, the crystal was flashed to 1000°C and the chemisorbed oxygen was removed. It was consistently found that if the oxygen were adsorbed at temperatures of less than 700°C, it could conveniently be thermally desorbed below 1000°C as illustrated by Figure 13. The chemisorbed oxygen was also found to be reactive to 10^{-6} Torr hydrogen at 600°C. Figure 14 illustrates this as following a 25.5 L O_2 dose at 490°C the adlayer could be completely removed by hydrogen.

Since the oxygen had a high reactivity, it is believed that the oxygen is dissociatively adsorbed and probably is not bonded in the form of any surface oxide. In two recent articles using high resolution electron energy loss spectroscopy (HREELS), Thomas and Weinberg (64,65) confirmed this as they detected only low intensity inelastically scattered electrons following oxygen adsorption. The intensity was only $\sim 2\%$ of that expected from an ionic metal oxide (66,67). The oxygen was believed to adsorb in a bridge-position or three-fold site as the frequency of the metal-oxygen bond did not correspond to an on-top site position.

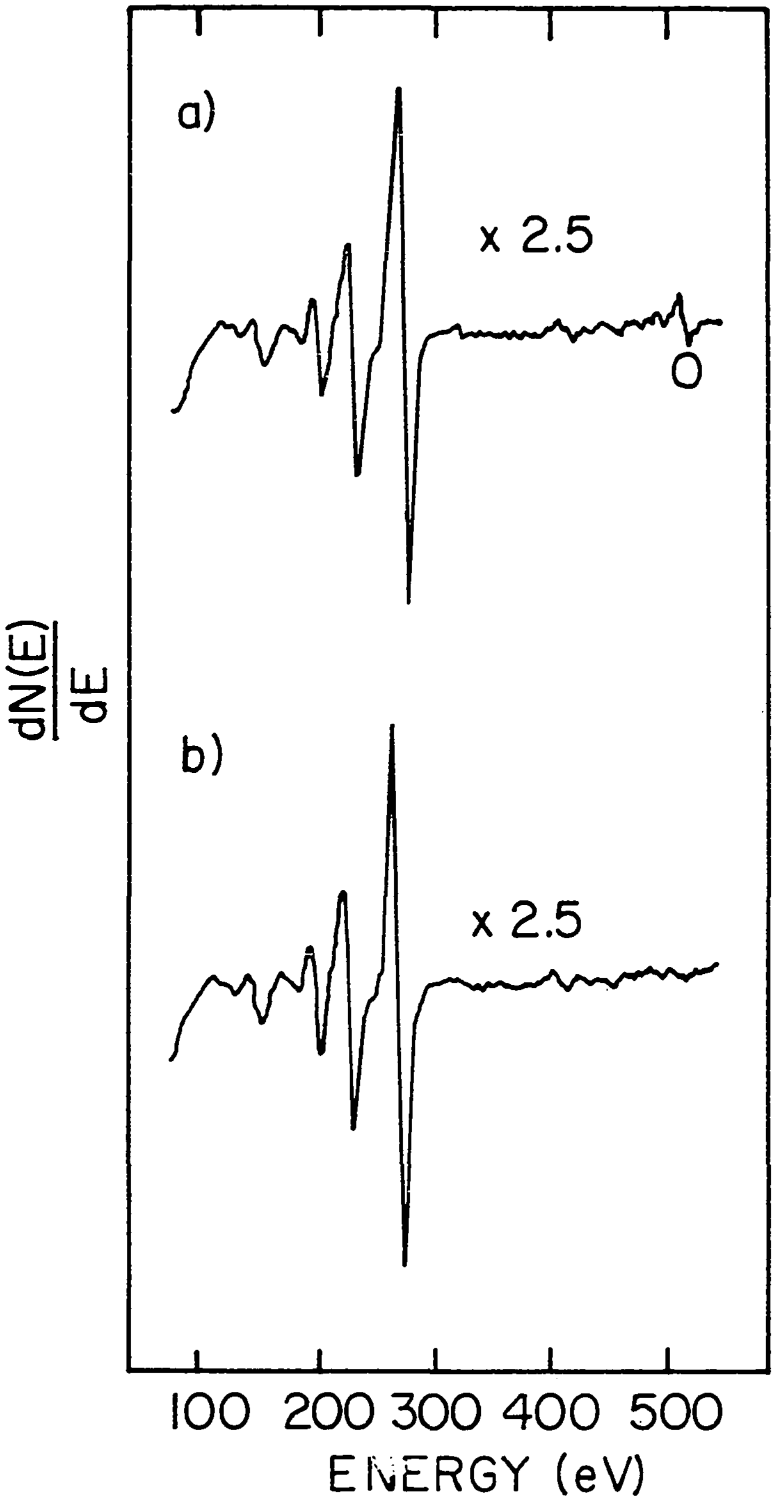

Figure 13. Oxygen adsorption study on ruthenium: a) Auger spectrum following a 10^{-5} Torr O_2 dose at 700°C for 500 seconds; b) after flashing the crystal to 1000°C

Figure 14. Study demonstrating reactivity of chemisorbed oxygen: a) clean ruthenium (102) Auger spectrum, b) after 25.5 L O_2 dose at 490°C; c) after hydrogen cleaning using 10^{-6} Torr H_2 at 590°C for 1100 seconds

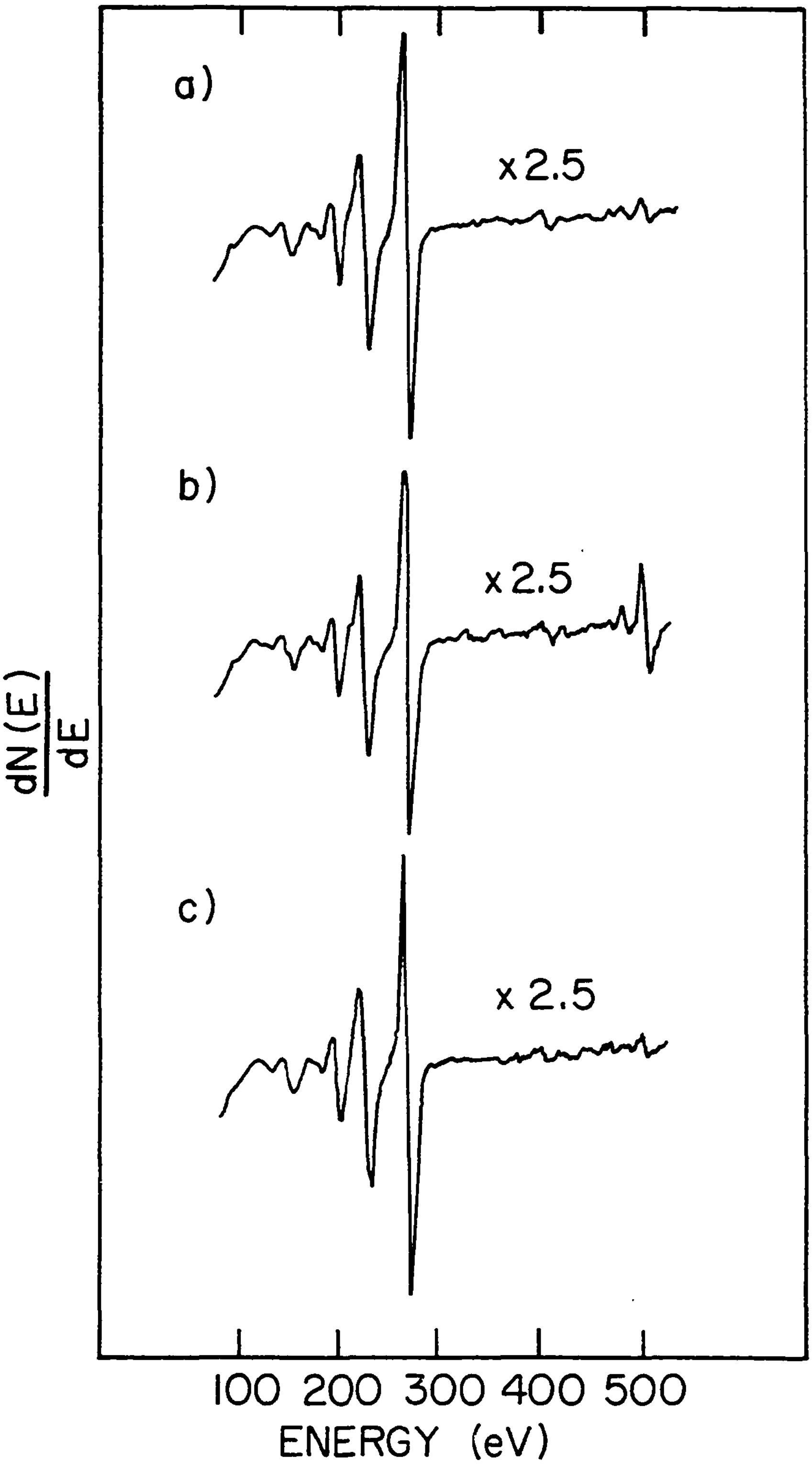
a)
x2.5
b)
x2.5
c)
x 2.5
dN(E)/dE
100
200
300
400
500
ENERGY (eV)

The adsorption of nitric oxide provides a contrast to oxygen adsorption. Taking a clean ruthenium surface, 400 μm of NO was dosed into the bell jar with the crystal at 490°C. Following evacuation, a diffraction pattern was obtained that indexed as (1x3)-O; no nitrogen or carbon was detected on the surface. Under catalytic reaction conditions, this implies nitric oxide adsorption into a precursor state which dissociates into nitrogen and oxygen adatoms.

$$\mathrm{Ru} + \mathrm{NO}_{(g)} \longrightarrow \mathrm{RuNO} \tag{43}$$

$$\mathrm{Ru} + \mathrm{RuNO} \longrightarrow \mathrm{RuN} + \mathrm{RuO} \tag{44}$$

The data do not establish whether or not these reactions are in equilibrium. The nitrogen adatoms at 490°C are then sufficiently mobile to allow association and desorption.

The oxygen differed in type from that resulting from oxygen gas chemisorption. This is evidenced by two observations, first the oxygen coverage was greater than the 0.75 as reported for the c(2x4) structure; it was calculated to be $\theta_O = 1.22$ as shown in Figure 15b. Also, this species is unreactive to hydrogen and resistive to thermal desorption. Upon flashing the crystal to 1000°C (Figure 15c) the coverage decreased to 1.08 and the LEED pattern became a (1x1) without an increase in background intensity. The coverage remained substantially unchanged by hydrogen treatment at 600°C (Figure 15d). Heating the crystal to 1000°C did reduce the

Figure 15. Nitric oxide adsorption study: a) clean ruthenium Auger spectrum; b) after 400 μm NO dose at 490°C for 300 seconds, $\theta_O = 1.22$, LEED pattern is a (1x3)-O; c) after flash to 1000°C, $\theta_O = 1.08$

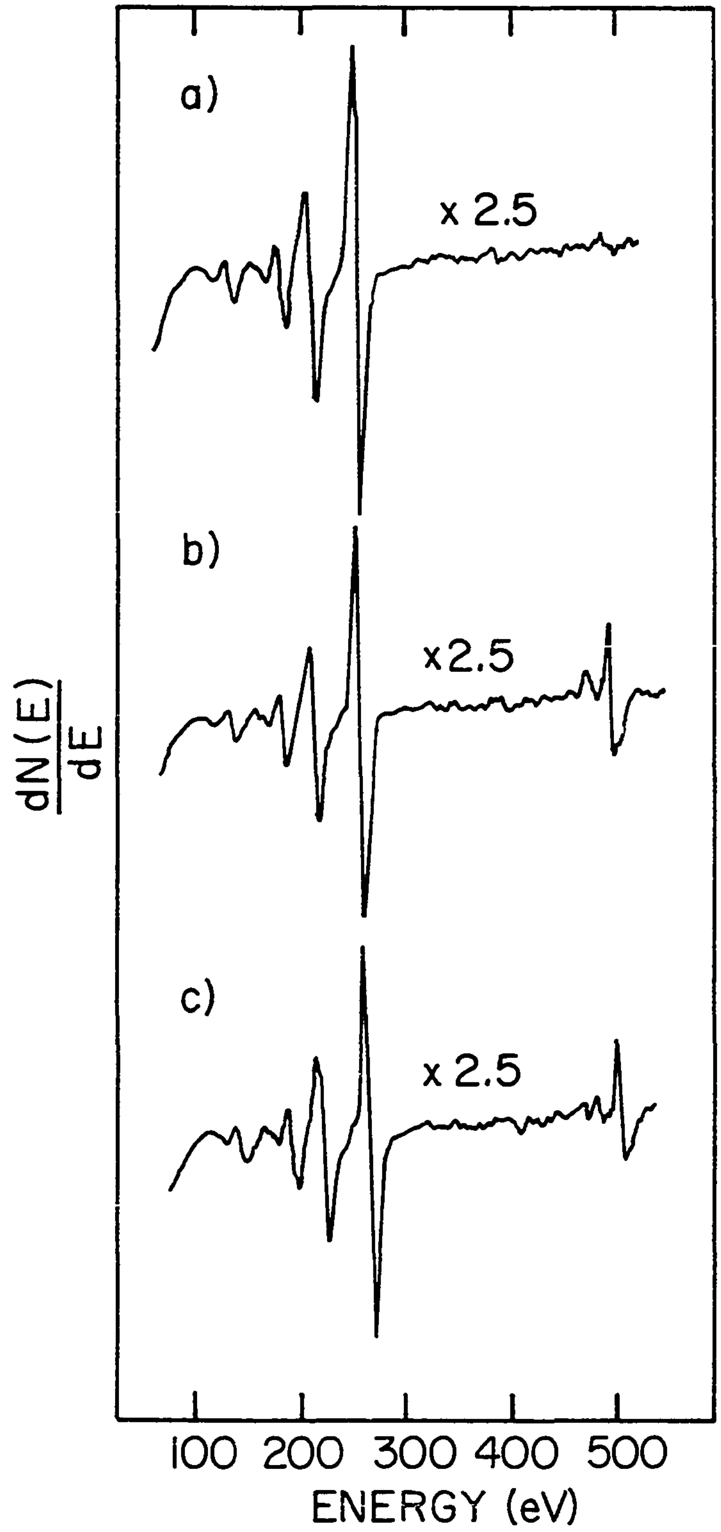
a)
x 2.5
b)
x2.5
c)
x 2.5
dN(E)/dE
100
200
300
400
500
ENERGY (eV)

Figure 15. (Continued)

Nitric oxide adsorption study: d) Auger spectrum after 10^{-6} Torr H_2 dose at 600°C for 500 seconds, $\theta_0 = 1.06$; e) after 45 minute treatment at 1000°C, $\theta_0 = 0.87$; f) after Ar^+ bombardment (1000 eV, 1 μa, 100 seconds), $\theta_0 = 0$

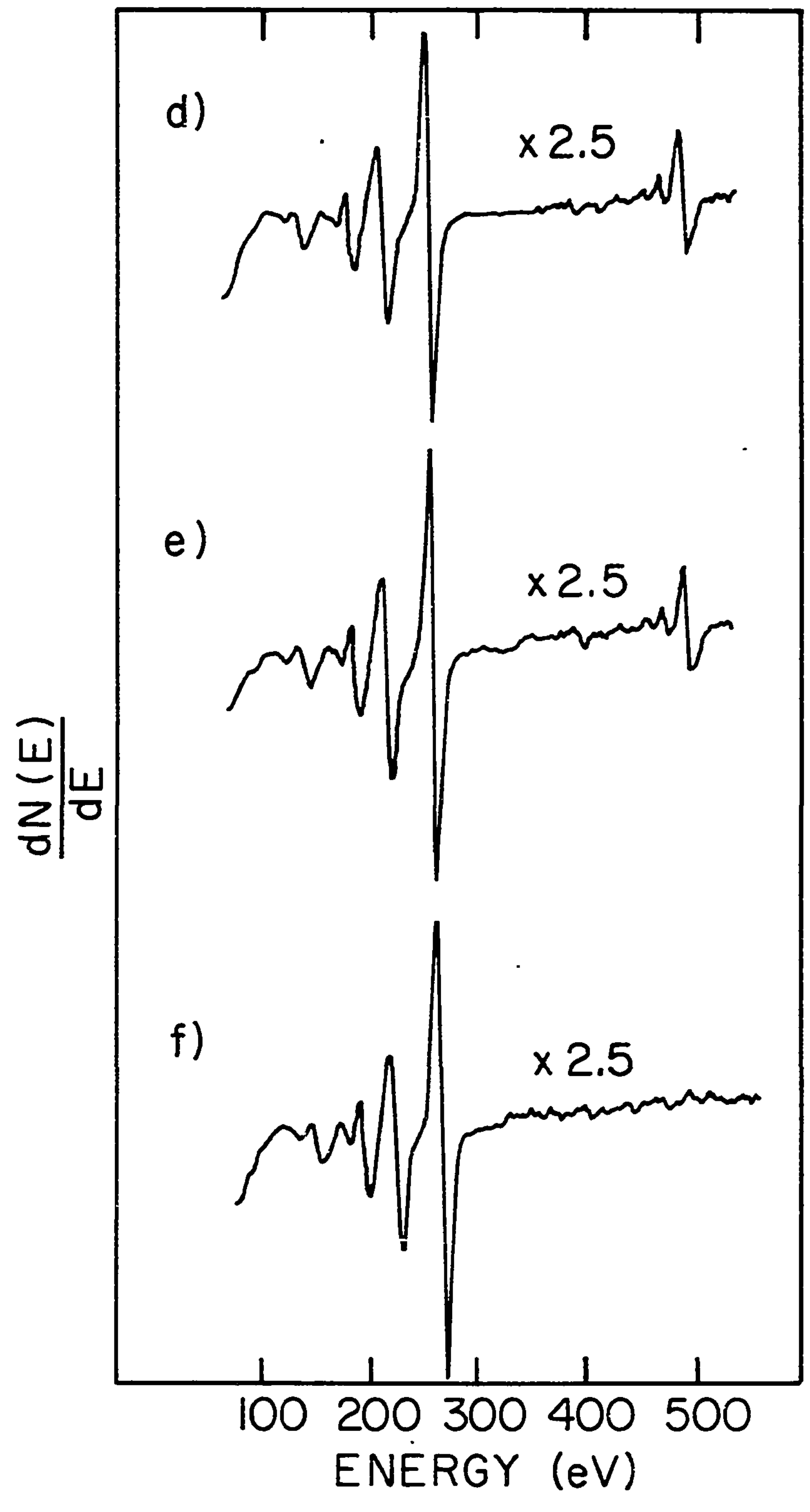
d)
x 2.5
e)
x 2.5
f)
x 2.5
dN(E)/dE
100
200
300
400
500
ENERGY (eV)

apparent coverage to 0.87 but the most effective means of removal found was argon bombardment, which reduced the coverage to zero. Since the oxygen does not undergo desorption up to 1000°C, it seems reasonable that the species is more strongly bound and could possibly be a surface oxide.

In an effort to characterize the oxygen species more fully, a dynamic equilibrium of nitric oxide was established within the LEED/Auger chamber of 10^{-6} Torr with the catalyst initially at 65°C. The temperature was then raised by 25 to 70°C intervals with the surface concentrations of nitrogen and oxygen recorded following the increase. The result is plotted in Figure 16. The figure can be divided into three temperature regions: 65-250°C, 250-500°C and 500-1100°C. While discussion of the low temperature region will be deferred to a later section on NO adsorption, the 250-500°C region indicates an oxygen saturated surface with a coverage of between 1.2 and 1.3 monolayers and a surface structure resulting in a (1x3) LEED pattern. Above 500°C, the O coverage decreases without evidence of any specific oxygen desorption temperature and the LEED pattern undergoes a transition to a 1x1. Since the oxygen coverage did not decrease to zero and the diffraction pattern exhibited no increase in background intensity, this is indicative of oxygen dissolution in the bulk. The temperature dependence

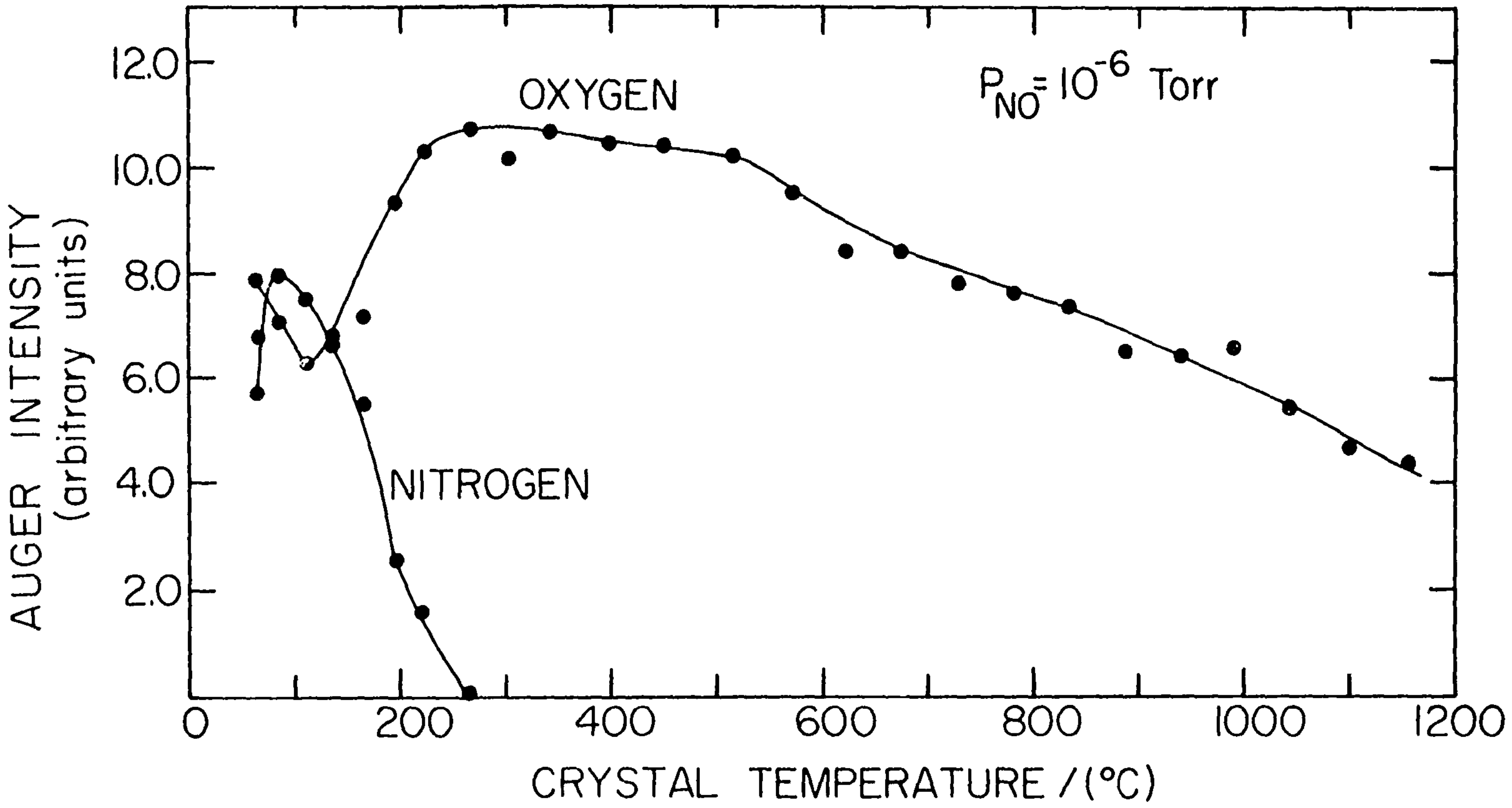

Figure 16. Auger intensity of N and O peaks as a function of crystal temperature with the pressure of NO constant at 10^{-6} Torr

of the decrease qualitatively confirms this as no sharp decrease is noted due to the desorption of volatile ruthenium oxides or oxygen.

If the (1x3)-O surface structure were simple then the oxygen coverage would be 1/3; a coverage of ∿1.3 indicates a coincidence type lattice superstructure. As the oxygen atoms are unreactive to removal by H_2 treatment and undergo penetration of the ruthenium lattice easily, it is reasonable to model the (1x3)-O surface with the adsorbate residing within surface or sub-surface layers. The (1x3)-O LEED pattern and a ball model of the surface are illustrated in Figure 17. This model requires only minor reconstruction with the elevated row of ruthenium atoms paralleling the $(\bar{2}\bar{1}1)$ direction being pushed upward by the penetrating oxygen atoms. The atomic arrangement is modeled in Figure 18. As the temperature was increased above 500°C, the bulk mobility of the oxygen could increase allowing O penetration and the surface would return to its initial lattice configuration. The facile oxygen transport makes it unlikely that the oxygen is ionic as two electron transfer to the oxygen atom would cause an increase in atomic radius from 0.67 to 1.32 Å.

The transport of oxygen into the bulk was confirmed by depth profiling the surface layers utilizing argon bombardment. An oxygen contaminated surface with a (1x3)-O structured overlayer was heated to 810°C for 36 hrs; this reduced

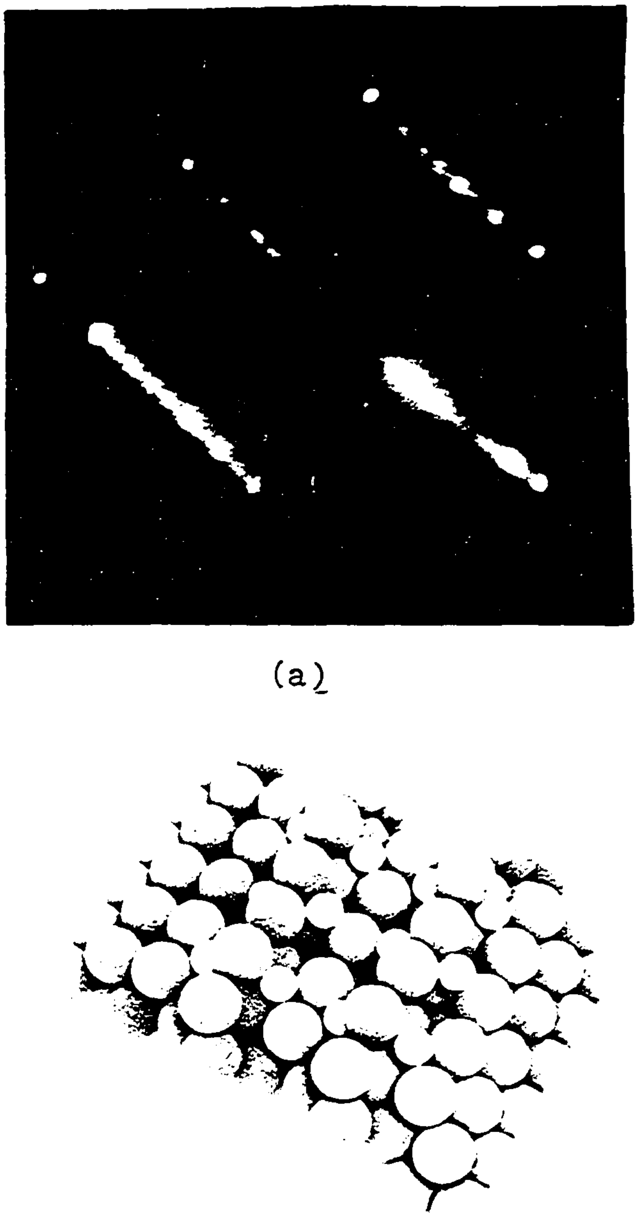

(a)

(b)

Figure 17. LEED pattern (a) observed following NO adsorption using a beam energy of 82 eV, (1x3)-O; (b) ball model of the proposed overlayer structure

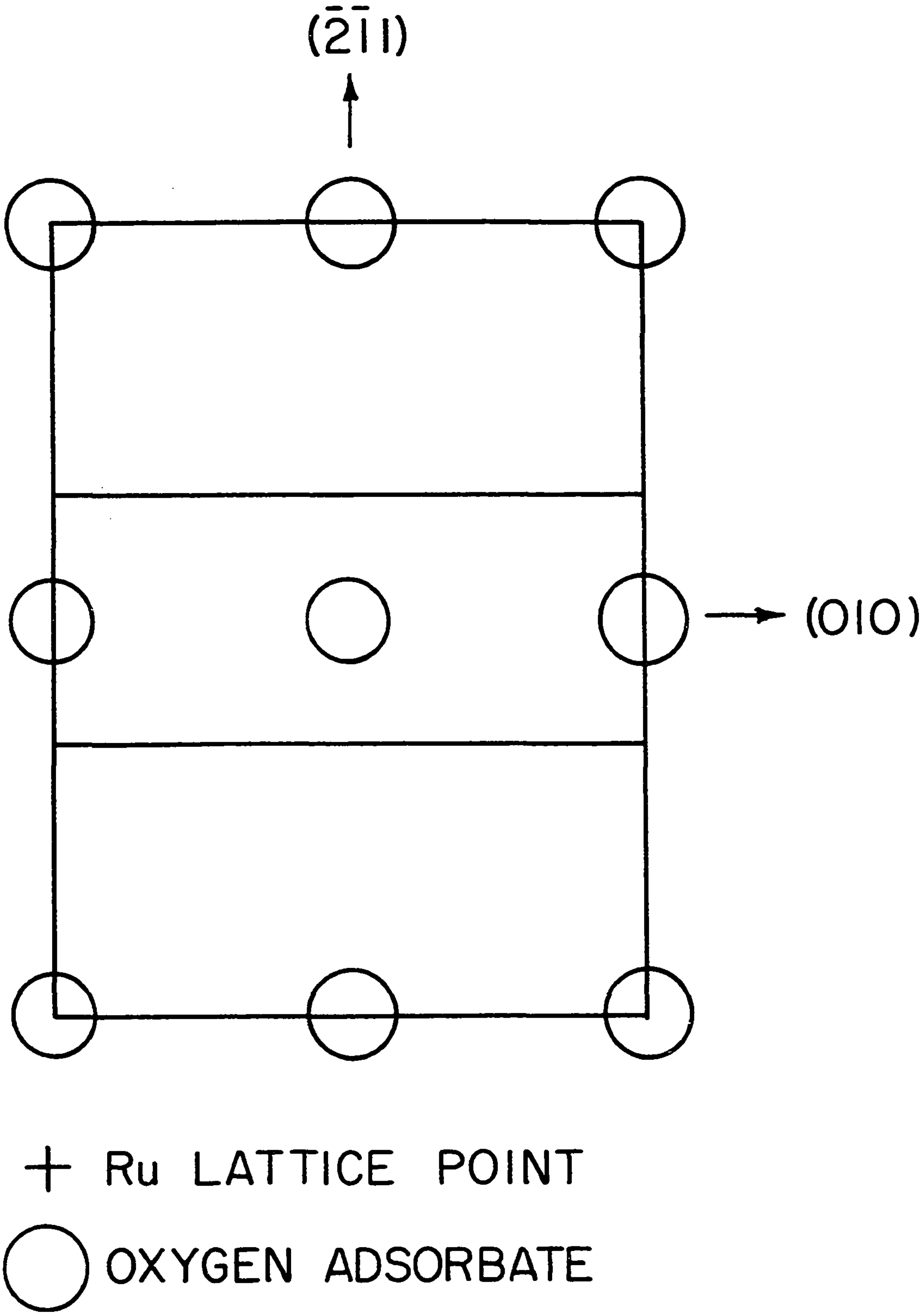

Figure 18. Oxygen overlayer due to NO interaction with Ru (102); nonprimitive unit cell of the (1x3)-O overlayer

the oxygen coverage from 1.31 to 0.95. Upon heating to 1000°C for several minutes, the coverage was reduced to 0.28 and the LEED pattern was a sharp (1x1). Ion bombardment of the surface increased the oxygen coverage to 1.25 which indicates that the oxygen had previously penetrated the ruthenium lattice during heating. Further bombardment using high ion energies and currents reduced the coverage to zero as the atomic layers containing the oxygen were removed.

Unreactive surface oxygen has been noted on other platinum group metals including iridium (68,69), platinum (70,71) and palladium (72,73). Most have been reported as oxides due to their low reactivity and little is known concerning their catalytic properties. A study investigating NO reduction by CO on iridium (69) found that the surface "oxide" acted as a poison.

This study shows that three types of oxygen can be associated with a ruthenium surface. The chemisorbed oxygen which results from the dissociation of molecular oxygen was found to be strongly bound as it could only be desorbed above 800°C, but was reactive to removal by H_2 at 500°C. The second type is oxygen which is not bonded to the ruthenium surface but within the ruthenium surface lattice; it forms a (1x3)-O LEED pattern and is unreactive. Upon heating, this oxygen diffuses into the bulk and subsurface layers to form the third type. The adsorption characteristics of nitric oxide were not greatly affected by the presence of the latter type of oxygen in the bulk.

The differences in the adsorption characteristics of nitric oxide and oxygen are interesting and could possibly be due to the large variance between the thermodynamic equilibria using NO or O_2 for the formation of a ruthenium oxide. Using the thermodynamic parameters for ruthenium dioxide, the respective equilibrium constants for the reactants oxygen and nitric oxide are $K_{O_2} = 1.84 \times 10^{12}$ atm^{-1} and $K_{NO} = 3.61 \times 10^{23}$ atm^{-1} at 475°C. By calculating the ratio K_{NO}/K_{O_2}, which yields the NO dissociation equilibrium constant, and using an average partial pressure of nitrogen under reaction conditions, a relation can be determined between the pressures of oxygen and NO. It was determined that in the presence of 13 μm of nitrogen an actual pressure of 7×10^{-6} Torr of NO was equivalent to a virtual oxygen pressure of one atmosphere at the ruthenium crystal.

Using this relation, a possible explanation for the adsorption differences is that if equivalent reactant partial pressures are dosed into a reaction chamber the corresponding partial pressures in terms of an oxygen partial pressure are different enough to lead to the formation of two different surface phases. Using 10^{-5} Torr of oxygen only adsorption to the ruthenium surface results. Upon using an equivalent pressure of NO for which the corresponding oxygen pressure is greater than one atmosphere, a surface phase change occurs resulting in the formation of the (1x3)-O structure. This state could be viewed as a precursor state to bulk ruthenium oxides which may form at higher NO pressures; this point will be addressed later.

One difficulty with this model is that upon comparing the oxygen dissociation pressures of the two phases one would expect the O_2 partial pressure at a given temperature to be greater for the (1x3)-O phase than for the chemisorbed phase as the coverages within the two states are 1.3 and 0.5, respectively. Upon flashing the crystal to 1000°C, the oxygen coverage was found to decrease only for the chemisorbed state.

This seeming discrepancy can be understood if it is considered that the oxygen atoms which reside in the subsurface layer are limited in their association rate by their binding to the ruthenium atoms. This would kinetically limit the decrease in oxygen coverage within the time span of the high temperature flash experiment. The dissociation pressure of the higher oxygen coverage state would then have a seemingly low value as the system is continuously pumped. An additional effect which would lead to a seemingly low pressure is that at higher temperatures the rate of oxygen dissolution into the ruthenium bulk is enhanced.

The adsorption pathway of carbon monoxide was found to be altered by the presence of the subsurface oxygen. CO was dosed at pressures ranging from 10^{-8} to 0.5 Torr in the temperature range 300-500°C. The doses in the 10^{-8} to 10^{-5} Torr range did not change the Auger spectrum and a 1x1 LEED pattern was maintained during the dose. This result was expected as carbon monoxide desorption from the Ru(102) face occurs below 250°C, as will be discussed later.

Upon dosing 150 μm of CO onto a clean oxygen-free ruthenium surface at 490°C for 100 sec, the F' value was found to decrease from 0.88 to 0.58 while the oxygen coverage remained virtually unchanged. This is evidence of the CO disproportionation reaction occurring on ruthenium:

$$2CO_{(g)} + Ru \longrightarrow RuC + CO_{2(g)}. \qquad (45)$$

While the mechanism of this reaction on ruthenium is unknown, it is believed to occur on nickel by interaction of an adsorbed CO molecule with a gas-phase molecule (74,75) and not via a CO dissociation mechanism. The occurrence of reaction (45) on ruthenium has been used, possibly erroneously, as evidence of CO dissociation (76-78).

The carbon overlayer could be removed easily by dosing nitric oxide onto the catalyst at 490°C. The F' value increased to 0.93 and the oxygen coverage increased to 1.22. Since the removal was rapid and complete, this implies mechanistically that if carbon monoxide were to dissociate on ruthenium under reaction conditions:

$$2Ru + CO_{(g)} \rightleftharpoons RuC + RuO \tag{46}$$

then the surface concentration of RuC would be approximately zero.

On ruthenium with a subsurface oxygen layer, the result of a similar experiment was no carbon overlayer formation. Starting with a surface with an oxygen coverage of $\theta_O = 0.45$, several hundred microns of CO were dosed at 490°C for 500 seconds. Following evacuation, the F' and θ_O values were unchanged and a sharp (1x1)-Ru LEED pattern was observed. The lack of carbon overlayer formation is evidence of a difference in the type of CO bonding. The specific relevance of this to the catalysis is that it eliminates or at least diminishes the possibility that the reaction mechanism involves a type of CO bonding (β-CO) that occurs on a metal surface if a high carbon monoxide surface coverage is found to exist under reaction conditions. This possibility will be discussed in the Thermal desorption section.

If the carbon monoxide were dosed for periods of up to 1500 seconds at 490°C, a sulfur contaminant segregated to the surface, as detected by an increase in intensity of the Auger 150 eV peak. While the mechanism of segregation is unknown, it is interesting that only under reducing conditions was it detected. Previous research from this group has shown that sulfur contamination was a continuous inconvenience (79) in

Auger investigations on ruthenium. As this crystal was cut from the same boule as the previous work, it was anticipated that this would be a problem. That it was not is due to the facile oxidation of the sulfur by treatment with nitric oxide. This has an indirect mechanistic implication as Unland (22) found that the isocyanate reaction intermediate was drastically reduced in coverage upon pretreatment of a ruthenium/Al_2O_3 sample with SO_2. If the sulfur were segregating to the surface between kinetic runs and the isocyanate were an active intermediate then the reaction rate would be expected to be low with low NO/CO ratio reactant mixtures. Since the rate did not seem abnormally low under these conditions, the isocyanate complex is unlikely to be a significant reaction intermediate in the present work.

The lack of interaction of CO with the NO treated surface also indicates the stability of the catalyst with regard to oxygen removal. Since the O coverage was not found to decrease, this is evidence that the catalyst for the NO-CO reaction is not a ruthenium surface but possibly the ruthenium/oxygen surface.

This was confirmed by dosing an NO-CO gas mixture of 340 μm each into the bell jar with the catalyst at 490°C. Following reaction for 500 seconds, the system was evacuated and a (1x3)-O diffraction pattern was observed. The oxygen coverage was 1.32. Removal of the oxygen was found to be as difficult as that resulting from nitric oxide dissociation. Using gas mixtures with different NO/CO ratios, the LEED pattern was determined to consistently be a (1x3)-O with an oxygen coverage range of between 1.25 and 1.41 as Table 2 indicates. The calculated nitrogen coverage was zero.

Table 2. Oxygen coverages and LEED patterns as functions of P_{NO}/P_{CO} gas mixture ratios

P_{NO}/P_{CO} ratio	θ_O (±0.1)	LEED Pattern
0.071	1.40	(1x3)-O
0.29	1.38	(1x3)-O
0.50	1.36	(1x3)-O
1.0	1.32	(1x3)-O
1.0	1.36	(1x3)-O
1.0	1.25	(1x3)-O
8.9	1.41	(1x3)-O

The pressure of nitric oxide used in this study never exceeded 500 μm indicating that in regions I and II (Figure 5), where the surface had a metallic finish, the catalyst is metallic ruthenium with oxygen atoms bonded in the first atomic layer. Taylor, Sinkevitch and Klimisch (5) had proposed that under reducing condition, the catalyst is ruthenium metal. Voorhoeve and Trimble considered the state of the ruthenium to be either ruthenium nitride or nitrogen covered. Clearly both interpretations are incorrect.

If a series of runs were performed under the same given set of reaction conditions over the ruthenium catalyst, the oxygen coverage underwent a slight increase of approximately 0.1 to 0.15 monolayers per 500 second reaction interval. The reaction conditions used were similar to those in region II of Figure 5. Since the (1x3)-O pattern remained virtually unchanged except for an increase in background intensity, it appears as though the additional oxygen is randomly adsorbing on the surface as there is no transformation into another overlayer structure. It is possible that the additional oxygen is diffusing into the bulk but this seems unreasonable as this effect is not significant in a 500 second time interval until ∿1000°C.

The LEED/Auger study mentioned thus far has characterized the catalyst used under reducing conditions. Catalysis under oxidizing conditions could not be studied directly in the LEED/Auger system because at the high pressures of nitric oxide (∿10 Torr) required it was found that to maintain the crystal at 500°C resulted in reduction of heater lifetimes to a matter of minutes. Hence, the ruthenium disc was used as a catalyst in the reactor system under oxidizing conditions; this established the formation of a tarnished overlayer. The crystal was then transferred in air, mounted on the manipulator and installed in the LEED/Auger system. Following evacuation without baking, the system analysis was undertaken. The tarnished disc had previously been shown to be stable to extensive evacuation in the reactor system.

The crystal was initially heated to approximately 250°C to remove any contaminants from the transfer. LEED revealed no diffraction pattern so the overlayer was not ordered, implying the formation of a noncrystalline surface. Auger analysis revealed that the elemental composition was ruthenium and oxygen and that the surface was somewhat heterogeneous as the oxygen coverage was found upon scanning the surface to vary by up to one-half of a monolayer. The mean oxygen coverage was 1.9 monolayers using the average of four Auger spectra.

The Auger line shape was considerably different from that observed in the previously discussed results. It was observed, Figure 19, that the most intense ruthenium Auger transition was shifted in energy from 273 to 270 eV and that transitions at 184, 156 and approximately 125 eV appeared. It also was noted that the oxygen peak was shifted to 508 eV and broadened as can be seen on comparing Figures 19b and c.

Since the Ru:O ratio was found to be approximately two, this is initial evidence that the chemical state of ruthenium is ruthenium oxide. It would then be expected that the Auger

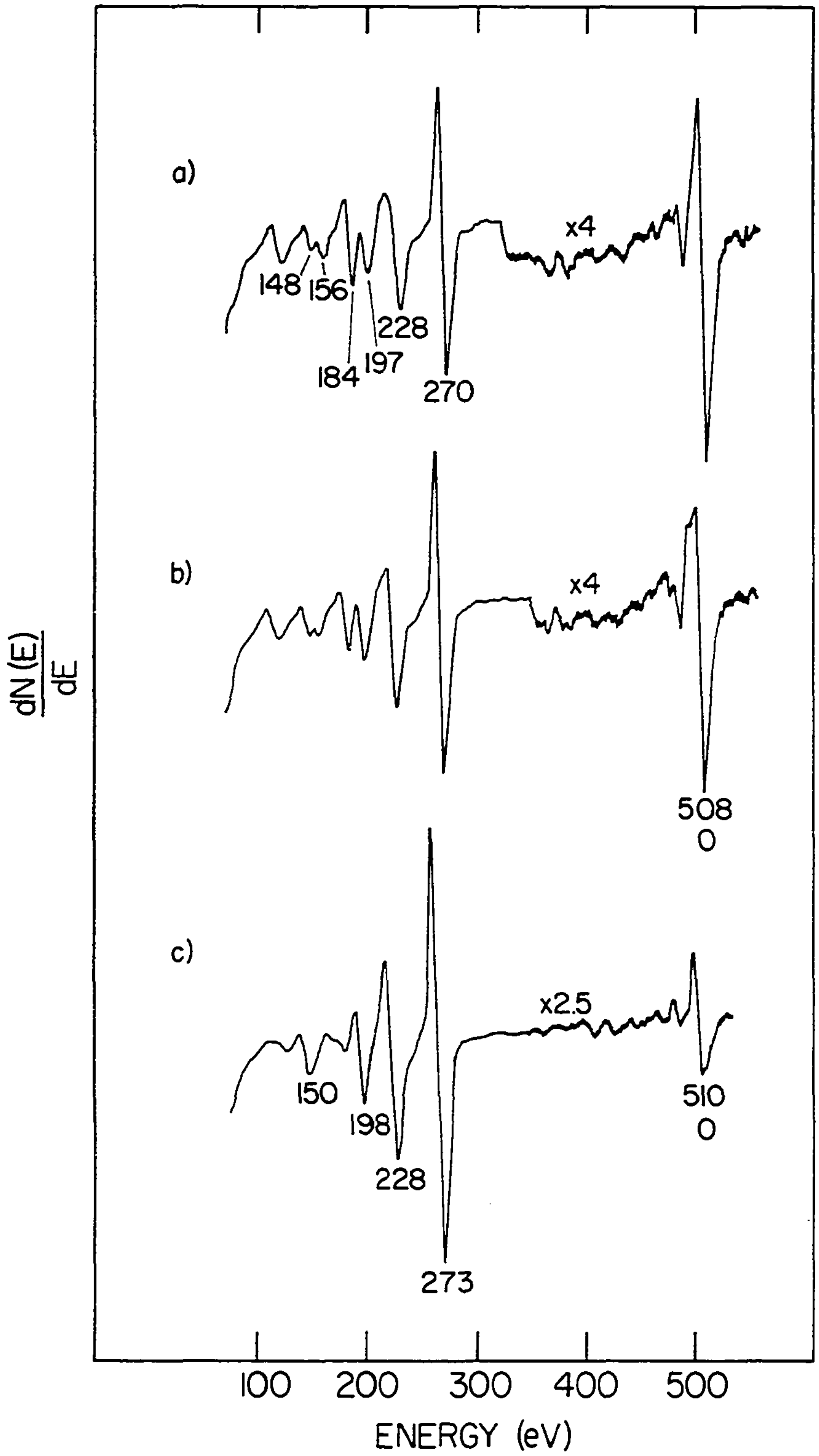

Figure 19. Auger spectra of ruthenium catalysts: a), b) spectra of catalysts used under oxidizing conditions (RuO_2), c) spectra of catalyst used under reducing conditions, (1x3)-O

line shape would change and chemical shifts could occur. Such Auger chemical shifts have been observed upon oxidation of several metals in research including Pt (80), Cu (81), Co (82), Rh (83) and Ni (84-86), as well as several other metals including Ti and Mo (87). The shifts were generally less than ∿6 eV and if any interpretation was given it was generally in terms of interatomic interactions (88). Some of the shifting observed could be due to sample charging as it appears that the surface is oxidic, meaning a positive space change could result. This, however, is expected to be minimal with RuO_2 as it has a "very high electrical conductivity" (89).

With regard to the oxygen shift of 2 eV, it is possible that the shift is due to a chemical state change as the peak at 510 eV is due to KVV or $KL_{2,3}L_{2,3}$ transitions. Since oxidation would change the electron distribution within the valence band, this would cause the Auger electron to be emitted with a different energy resulting in the shift. A similar argument could be used to interpret the two Ru peaks at 184 and 197 eV. If 197 eV is due to emission from ruthenium metal then the 184 eV transition could be due to emission from the oxide. For the metal the line at 197 eV is due to a M_4N_1V transition (90) and changes in the ruthenium valence band could lead to the chemical shift. The Ru peaks at 125 and 156 eV are more difficult to understand as they arise from electron transitions involving nonvalence orbitals. The Auger transitions for these peaks are either $M_5N_1N_{2,3}$ or $M_5N_{2,3}N_{2,3}$ indicating that $4P_z$ or $4P_{x,y}$ orbitals are involved whereas the valence electrons are either 4d or 5s electrons. No detailed explanation of these oxide lines will be given as analysis would probably not be pertinent to the catalysis. The overall conclusion that was drawn is that the ruthenium surface undergoes a chemical change going from reducing to oxidizing conditions. It progresses from a state in which oxygen resides within the first atomic layer to a state that resembles a bulk ruthenium oxide.

XPS characterization

Following the observation of tarnish formation under high nitric oxide pressure conditions, the ruthenium (102) disc was removed from the reactor system and transferred to the AEI XPS spectrometer. The purpose of the XPS work was to undertake an elemental analysis of the film and to determine the composition from chemical shift data. A scan of the binding energy from the Fermi edge to 850 eV is shown in Figure 20. A literature survey of ruthenium and oxygen binding energies is presented in Table 3.

Using the peak assignments given in Table 3, it can be seen that the principal surface contaminant was oxygen; in the 330 to 350 eV range two peaks were detected which

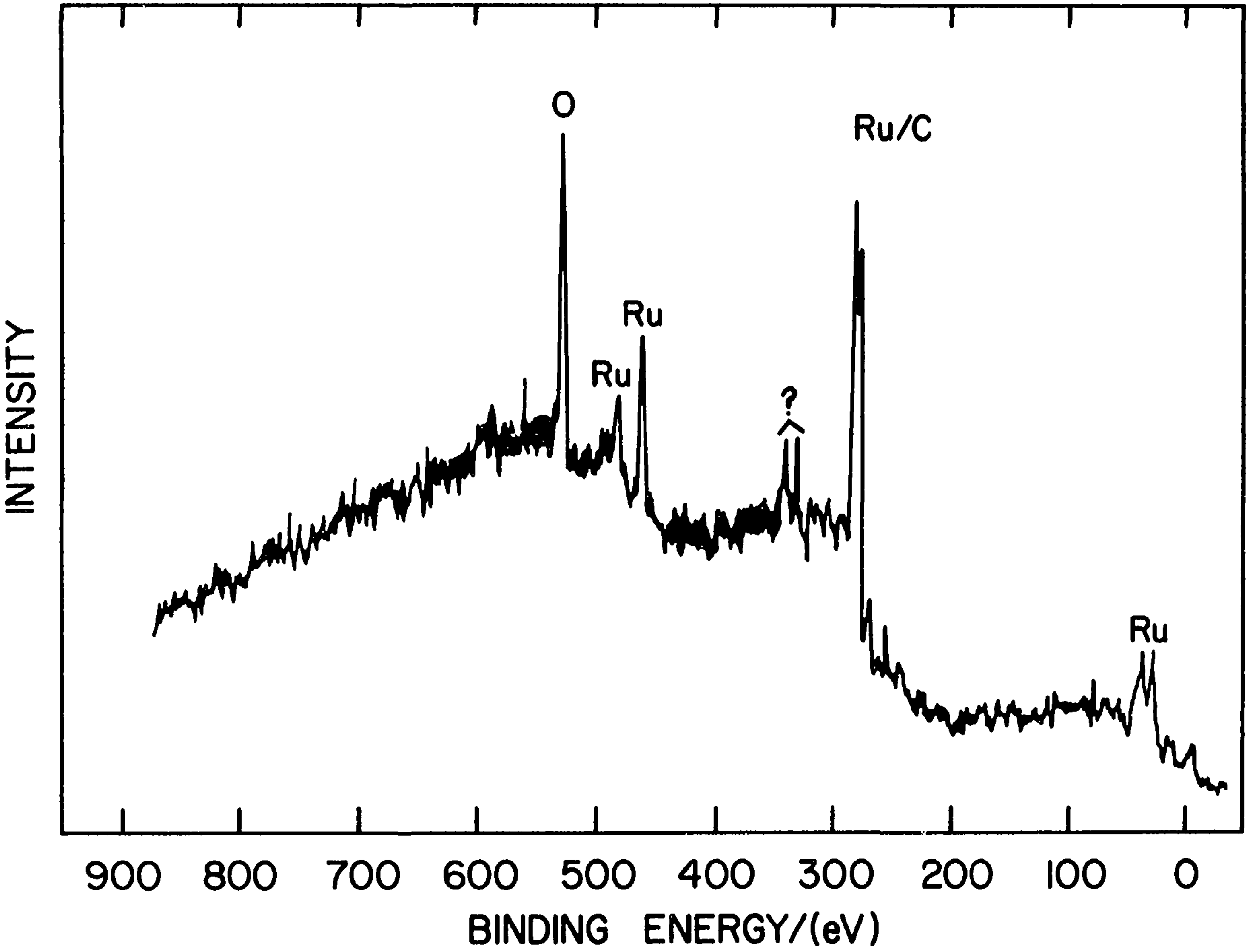

Figure 20. X-ray photoelectron spectrum of ruthenium sample used under oxidizing conditions, high P_{NO}/P_{CO} ratio gas mixture

Table 3. Binding energies of Ru, Ru oxides, adsorbates

Substance (Level)	Binding energy (eV)	Reference
Ru^o ($3d_{5/2}$)	280.0	91
Ru^o ($3d_{5/2}$)	279.9 ± 0.2	92
Ru^o ($3d_{5/2}$)	279.4 ± 0.3	90
Ru^o ($3d_{3/2}$)	284.1	92
Ru^o ($3d_{3/2}$)	283.6 ± 0.3	90
RuO_2 (Ru $3d_{5/2}$)	280.7	91
RuO_2 (O 1s)	529.4	91
RuO_3 (Ru $3d_{5/2}$)	282.5	91
RuO_3 (O 1s)	530.7	91
RuO_4 (Ru $3d_{5/2}$)	283.3	91
RuO_{ads} (Ru $3d_{5/2}$)	280.0	91
RuO_{ads} (O 1s)	531.5/529.9[a]	91
RuO_{ads} (O 1s)	529.8 ± 0.2	92
RuO_{ads} (O 1s)	529.8 ± 0.1	93
C (graphite) (C 1s)	284.3	94

[a] 531.5 eV was designated for surface adsorbed oxygen and 529.9 eV for oxygen within the first two ruthenium surface layers.

possibility could be due to thorium $4f_{5/2}$ and $4f_{7/2}$ (95) electron emissions. Using ruthenium and thorium sensitivities, the surface concentration of the thorium was calculated to be less than 10%. Due to the 0.3 eV difference in binding energy, the Ru $3d_{3/2}$ and C 1s transitions overlap within the resolution capabilities of the instrument and the Ru $3d_{5/2}$ had to be used to determine chemical shifts. An initial mild argon bombardment of the sample (30 s, 5 μA, 0.5 kv) was undertaken to remove surface contaminants due to the atmospheric transfer. The oxygen and ruthenium binding energy ranges were then scanned in the ranges 526 to 537 eV and 275 to 290 eV, respectively. The ruthenium spectrum, illustrated in Figure 21, shows that the Ru $3d_{5/2}$ peak, following work function correction, lies at 280.8 eV. By comparing this value with the ruthenium photoelectron values in Table 3, it can be seen that this identifies the catalytic state under oxidizing conditions as ruthenium dioxide. The oxygen spectrum, Figure 22, confirms this analysis with a maximum in intensity at 529.4 eV. All binding energies reported are accurate to ±0.2 eV.

Assuming the XPS peak shape to be symmetric around the maximum, it can be shown that the shoulder at higher binding energies in the oxygen spectrum has a maximum of about 531.3 eV. Kim and Winograd also detected this shoulder in a Ru/O_2 study and assigned it to the oxygen resulting from RuO_3.

Figure 21. XPS spectrum of ruthenium in the binding energy range 275-295 eV. The sample had served as a catalyst under oxidizing conditions; the solid line represents the experimental data and the dashed line was drawn assuming a symmetric peak at 280.8 eV

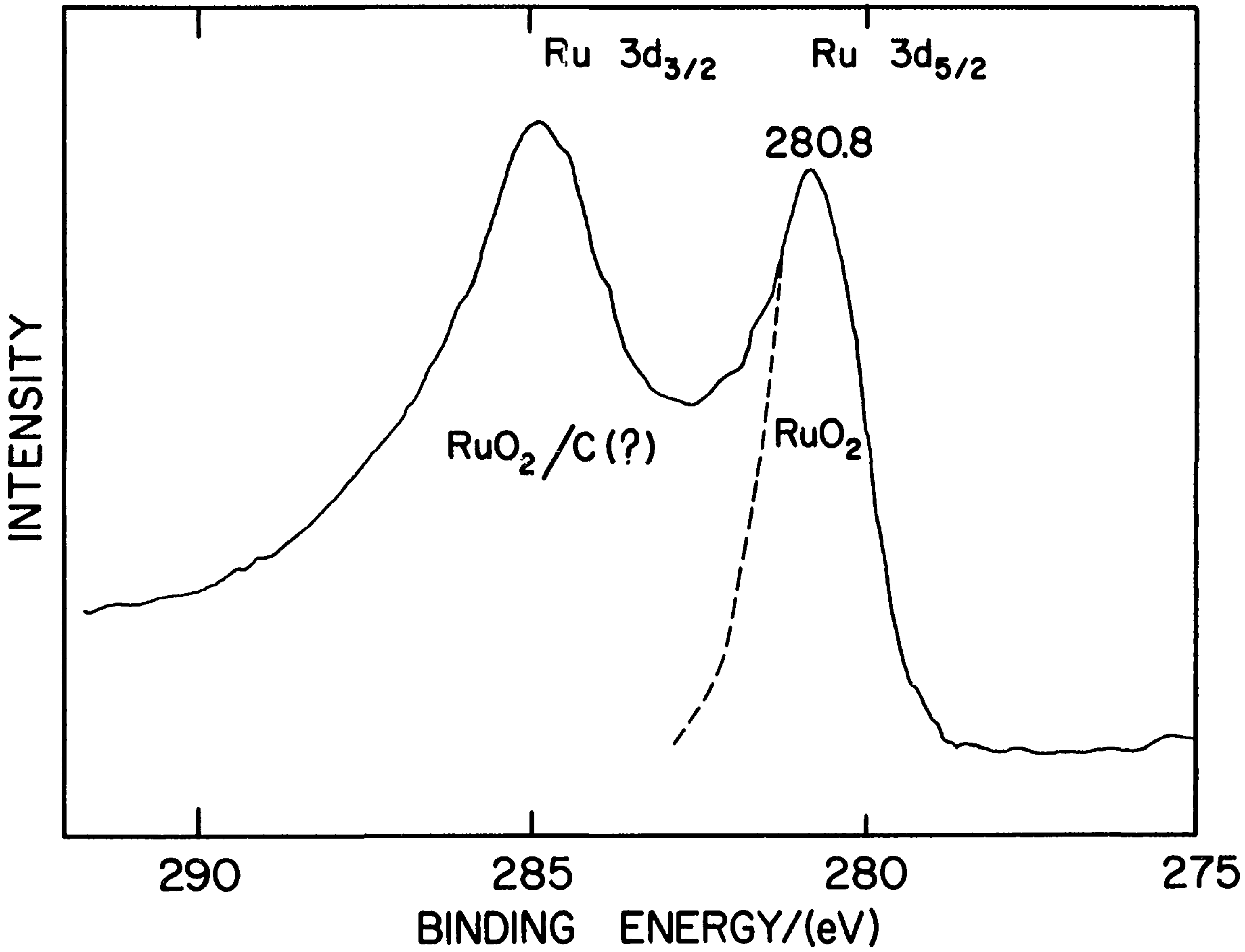
Ru 3d$_{3/2}$
Ru 3d$_{5/2}$
280.8
RuO$_2$/C (?)
RuO$_2$
INTENSITY
290
285
280
275
BINDING ENERGY/(eV)

Figure 22. Oxygen XPS spectrum of ruthenium crystal catalyst used under oxidizing conditions. The solid line represents the experimental data, the dashed line was drawn assuming a symmetric peak at 529.4 eV, and the peak at 531.0 eV represents the difference between the experimental and symmetric curves

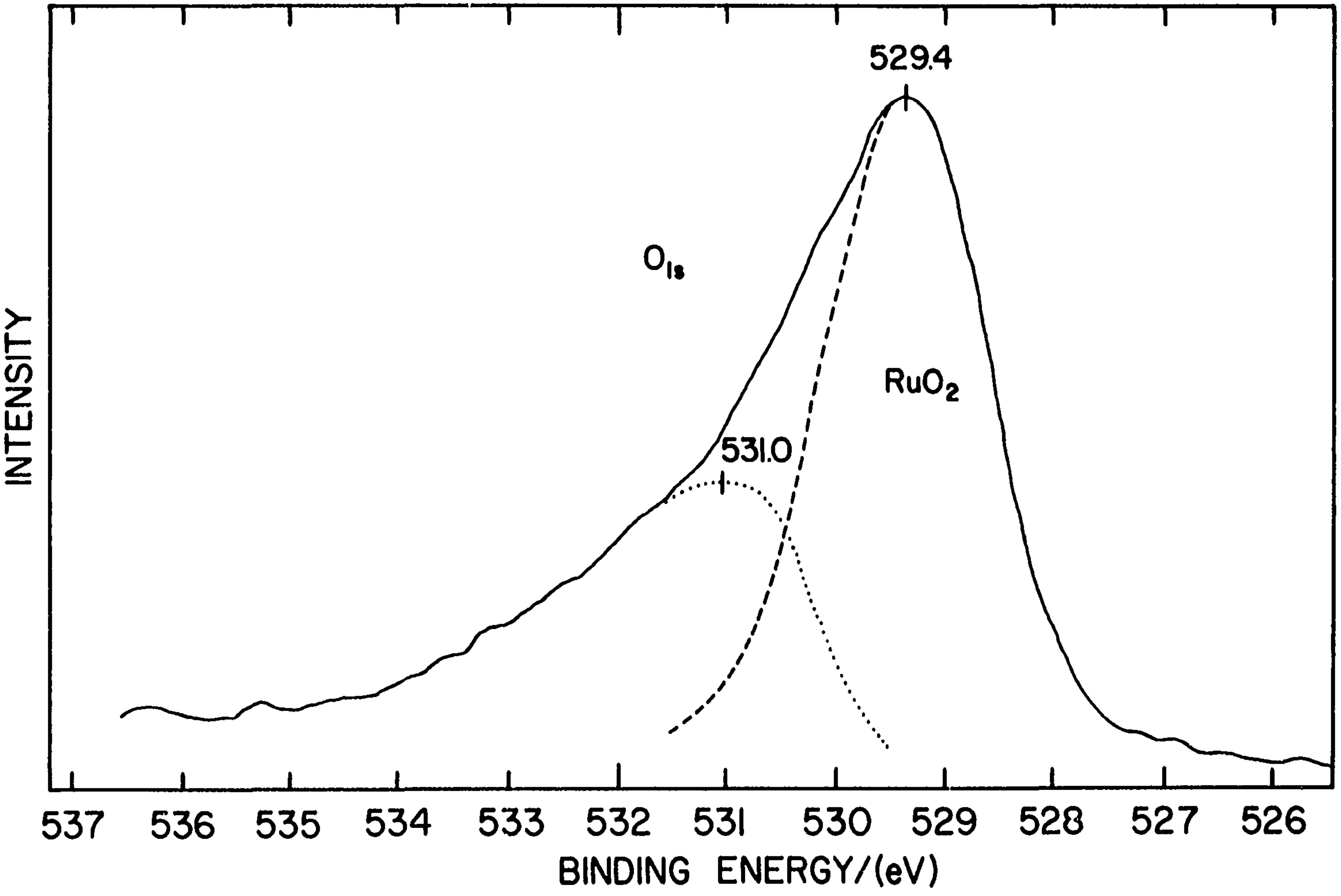
INTENSITY
O_{1s}
529.4
531.0
RuO_2
537
536
535
534
533
532
531
530
529
528
527
526
BINDING ENERGY/(eV)

This assignment, it is believed, is incorrect. Their assignment was based on the dependence of the Ru $3d_{5/2}$ peak position on the oxidation state of the ruthenium; the peak assignments for Ru, RuO_2 and RuO_4 were 280.0, 280.7 and 283.3 eV, respectively. Using a spectrum similar to the spectrum in Figure 21, they separated the Ru $3d_{5/2}$ peak into two peaks with maxima at 280.7 and 282.5 eV on the assumption that the peaks were symmetric. Since the maximum of the calculated peak was between 280.7 and 283.3 eV, it was assigned as RuO_3. As their assignment was debatable, a ruthenium dioxide sample was prepared (96) by passing dry oxygen over a ruthenium sample of 99.99% purity for 12 hours at 1000°C. Under these conditions, the only stable condensed oxide is RuO_2 (97,98). Bell and Tagami undertook an analysis of a similarly oxidized ruthenium sample and found that the product was ∿99% RuO_2. X-ray diffraction analysis was also undertaken and only lines for the Ru (s) and RuO_2 (s) were detected.

Following the procedure used in this laboratory, the sample was transferred to the AEI XPS spectrometer and spectra of ruthenium and oxygen were recorded. The peak shape and binding energies were the same as those recorded from the ruthenium sample oxidized by the NO-CO reaction. This conclusively establishes RuO_2 as the state of oxidation of the catalyst under oxidizing conditions; Kim and Winograd are in error in assigning the 531.3 eV shoulder to RuO_3 (91).

The sample used in the NO-CO reaction chamber was then extensively bombarded until the oxygen was removed. The ruthenium spectra, Figure 23, indicated that the $3d_{5/2}$ electron binding energy was 280.0 eV, suggesting that the surface is zero-valent ruthenium. The ratio of Ru $3d_{5/2}$ to Ru $3d_{3/2}$ peak areas was found to be $\sim$1.4 which is close to the theoretically expected value for metallic ruthenium.

A sample which had served as a catalyst only under reducing conditions was also analyzed; it was found to have a ruthenium spectrum not unlike that in Figure 23 and a binding energy of 280.0 eV. This implies that the oxygen which penetrates the ruthenium surface is nonionic and that the surface is nonoxidic.

An *in situ* study was attempted to examine the effect of gas dosing pressure and catalyst temperature on the chemical state of the adsorbates. This was accomplished by allowing a clean ruthenium sample to be exposed to pressures of up to 10^{-6} Torr in NO or CO. This provided little information as the spectrometer seemed to be insensitive to coverage changes of a monolayer or less. Changes could be observed but were not always reproducible. A UPS spectrum change was repeatedly observed at 50°C when nitric oxide was dosed at room temperature and the crystal then heated. This possibly could

Figure 23. Ruthenium XPS spectrum of catalyst used under oxidizing conditions following extensive argon bombardment

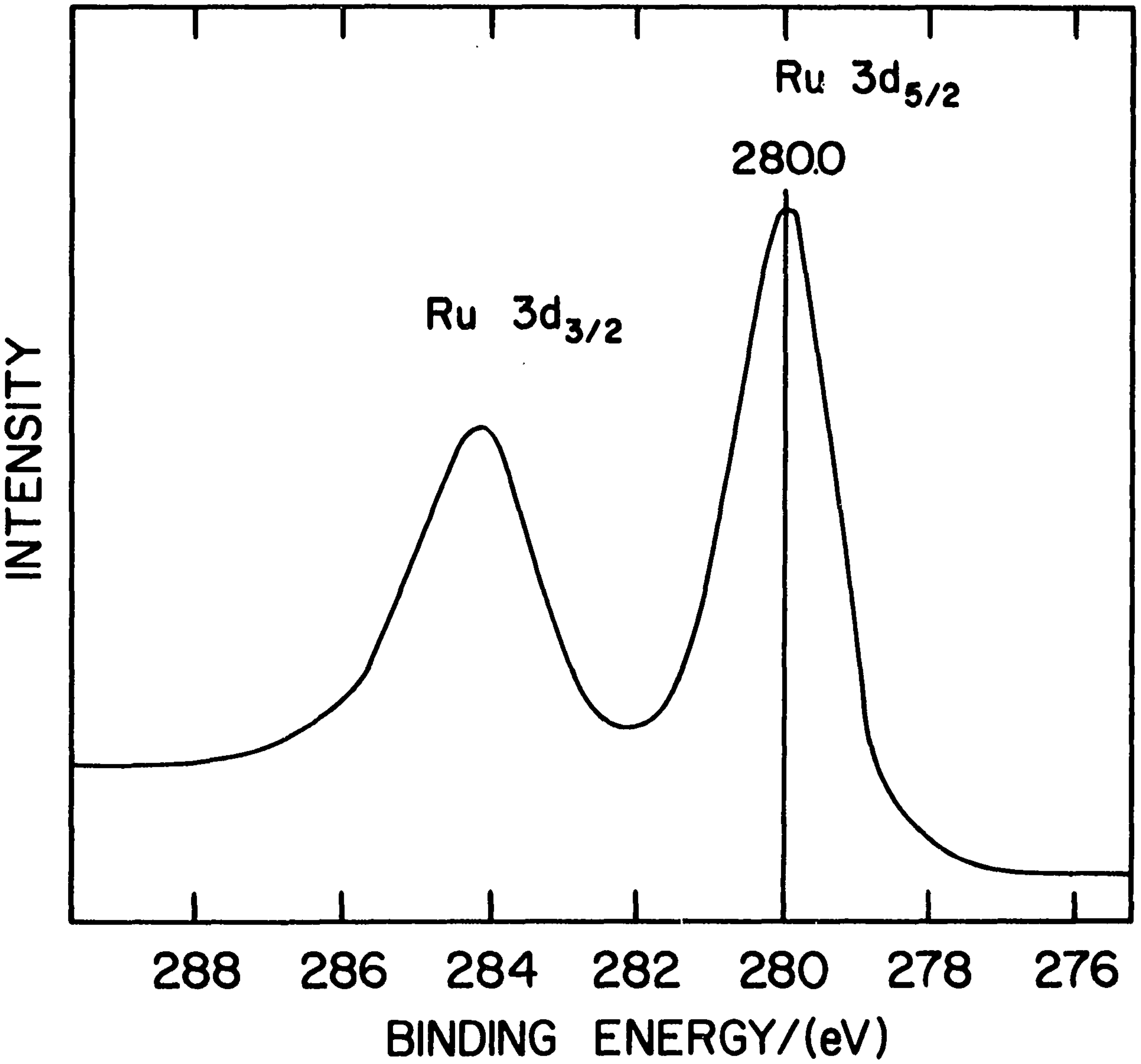
Ru 3d5/2
280.0
Ru 3d3/2
INTENSITY
288
286
284
282
280
278
276
BINDING ENERGY/(eV)

be due to the dissociation of the nitric oxide overlayer into nitrogen and oxygen atoms.

To summarize, the XPS results confirmed what was suspected from the LEED/Auger results, that mechanism B was occurring on a Ru catalyst that has a RuO_2 overlayer. The oxidized catalyst state of ruthenium is not, as Taylor, Sinkevitch and Klimisch (5) suspected, a reconstructed metal surface.

Thermal desorption spectroscopy

A series of experiments was performed using the technique of thermal desorption spectroscopy (TDS). For the low dosing pressure ($< 10^{-7}$ Torr) studies the (102) ruthenium crystal was cleaned by outgassing at ∿1000°C for several hours. This, from the LEED/Auger studies, should result in the surface having an oxygen coverage of approximately zero.

The first gas studied was carbon monoxide, which was dosed in the 0 to 10 L range. It was found that the desorption peak maximum was independent of coverage, an indication of first order desorption kinetics (99). Using a heating rate, β', of 4° per second, the maximum desorption temperature, T_p, was 212°C. Assuming first order desorption kinetics, Redhead's equation (99):

$$\frac{E}{RT_p} = \ln \frac{\nu T_p}{\beta'} - 3.64 \qquad (47)$$

was utilized to calculate an activation energy, E, of 30.1 kcal/mole assuming a vibrational frequency, ν, of 10^{13} s^{-1}. Previous studies on other single crystals of ruthenium have resulted in similar calculated desorption activation energies as shown in Table 4. A second state, α, has been shown to to exist, which has a lower activation energy than the β state just discussed. This state was not detected as the system had a low pumping speed which reduces peak resolution; however, no evidence could be found to dispute its occurrence on a (102) face.

Table 4. Carbon monoxide desorption activation energies ($\nu = 10^{13}$ s^{-1})

Crystal orientation	Activation energy (kcal/mole)	Reference
102	30.1	This work
101	28.2	59
100	31.2	47
001	28.0	100
001	29.0	93

The small (3 kcal) variation in activation energy over the series of crystal faces implies that the adsorption of carbon monoxide is structurally insensitive. The kinetics indicate that low pressure adsorption is molecular and that mechanistically the adsorption equilibrium of carbon monoxide must be considered.

The adsorption of nitric oxide was found to be more complex. Upon dosing in the 0-2 L range, the nitric oxide dissociated and the nitrogen desorbed in the 280-325°C temperature range under a heating rate of 10.5° per second. No nitric oxide or oxygen desorbed. The lack of oxygen desorption was due to its incorporation into the ruthenium surface. Figure 24 illustrates that the peak maxima shifts to lower temperatures, spectra a-d, with an increase in dose. As the surface coverage of nitrogen increases with the dose in nitric oxide, this is an indication of second order desorption.

As the number of langmuirs dosed was increased, the desorption spectra, Figure 24e-h, maxima became coverage independent with the maximum occurring at 228°C. In addition with the higher doses, nitric oxide desorption was observed though the peak was very broad. The reason it was broad was not due to multiple state desorption but probably can be attributed to its adsorption on the internal reactor surfaces of the system, resulting in an apparent low pumping speed.

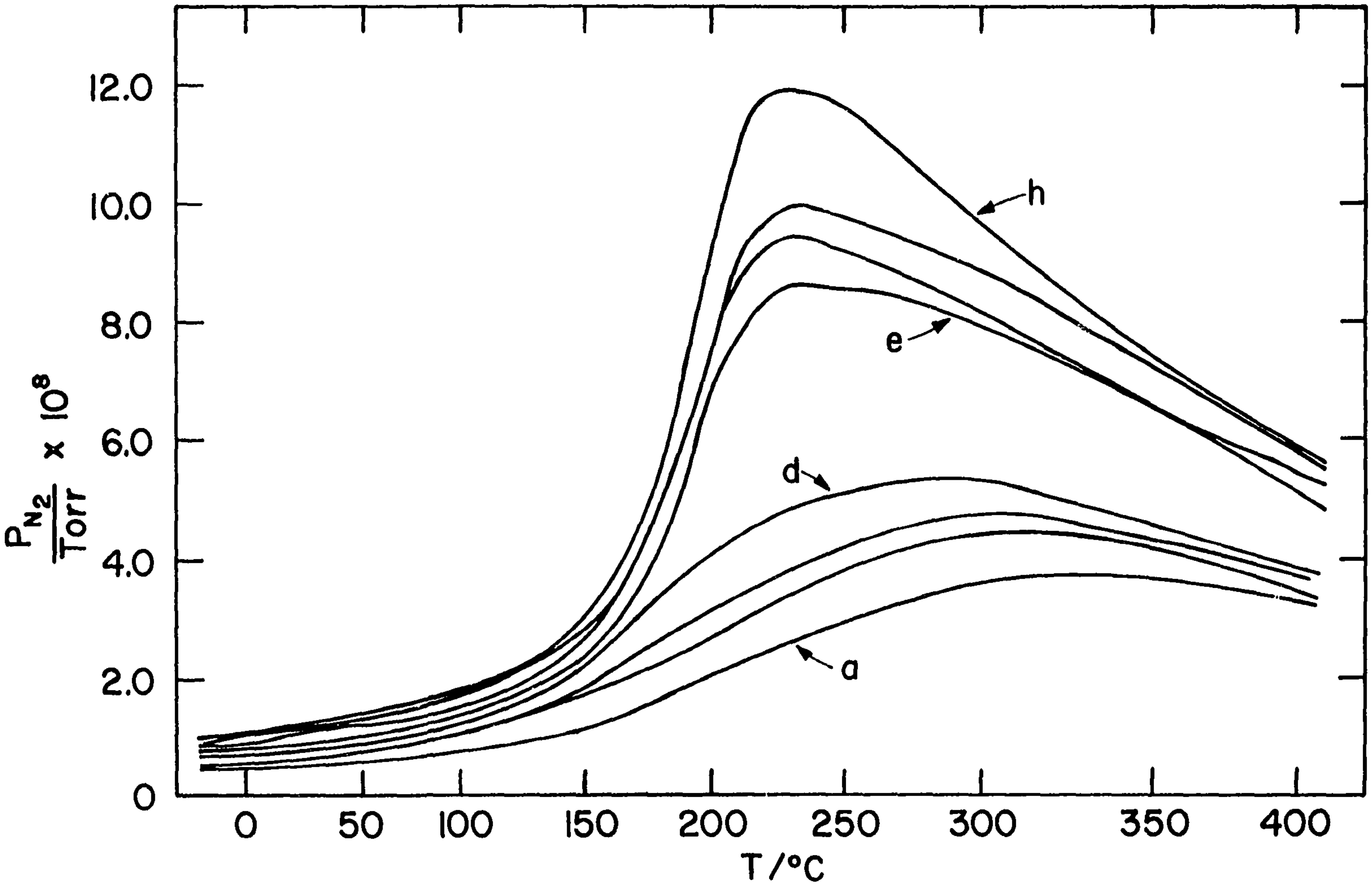

Figure 24. Thermal desorption spectra of N_2 following NO dose of the ruthenium a) 0.4 L dose, b) 0.5 L dose, c) 0.7 L dose, d) 1.0 L dose, e) 2.4 L dose, f) 4.8 L dose, g) 5.7 L dose, h) 7.4 L dose

Again, no oxygen was detected even at crystal temperatures above 1000°C.

The second order desorption kinetics can be accounted for quite easily by the bimolecular association of two nitrogen adatoms. The first order behavior could be accounted for either by assuming formation of a dinitrogen complex on the ruthenium surface or by assuming that there is a repulsive interaction between the nitrogen atoms. The latter possibility has been treated by Adams (101) and will not be discussed further.

The formation of a ruthenium dinitrogen complex, which possibly could account for the first order behavior, is unreasonable. While compounds with the molecular formula $[Ru(NH_3)_5-N_2]-X_2$ where X = Cl, Br, I, BF_4 and PF_6 have been prepared (102) in solution formation of dinitrogen complexes under low pressure conditions by gas phase NO is dubious. Actually, no N_2 compounds where the ruthenium oxidation state is Ru(O) are known (103,104). The only recorded case of the retention of an N_2 species by a ruthenium catalyst required the incorporation of an alkaline metal, K or Cs, into the ruthenium. Potassium reacted with the ruthenium in the presence of nitrogen (105) to form a ternary compound of the type $(K-N_2-Ru)_n$ at 350°C under 1 atmosphere of nitrogen. Since the zero-valent ruthenium catalyst used in this study was not doped, it is unreasonable to consider an N_2 complex as a stable species leading to first order desorption behavior.

The desorption of nitric oxide is indicative of molecular adsorption. The reason it was only observed at higher doses was simply that as the surface became saturated with N and O adatoms, which occurs following a 2 L dose, the number of adjacent empty sites diminishes and decomposition ceases. This allows for the possibility of molecular and dissociative adsorption of NO on ruthenium. Such a model was proposed by Bonzel and Fischer (41) on the basis of an UPS study.

It was observed that, in the same dosage region where nitrogen starts to desorb via first order kinetics, NO also desorbs. In addition only a small fraction, approximately 3%, of the nitric oxide which had been dosed did desorb. A possible model accounting for these observations assumes that the molecular nitric oxide is a precursor state which is weakly bound. The nitric oxide would then undergo rapid migration at lower temperatures. This was observed to commence at 250K by Klein and Shih (106). Upon heating the crystal, the mobility of the nitrogen atoms increased and the probability of the molecular NO finding an adjacent vacant site would increase. Dissociation occurs and the coverage of nitrogen atoms would increase. This would lead to repulsive N-N interactions so that as the temperature increased these would give rise to the low temperature nitrogen desorption peak. As the coverage decreased, the repulsive interactions would diminish thus allowing the peak which follows second order kinetics to occur at higher temperatures.

With the desorption of molecular nitrogen upon the association of the N adatoms, the oxygen atoms were incorporated into the first surface layer. The oxygen coverage was then observed to increase following N_2 desorption indicating a negligible NO precursor lifetime at higher temperatures. This is depicted in Figure 16 in the 65 to 250°C temperature range.

Using Figure 16, it is initially assumed that at 65°C the surface overlayer is composed of both molecular and dissociated NO. This is supported in the literature by the dissociation of one of two adsorption states of NO on Ru (001) at 43°C (107) as detected by (HREELS). An UPS study by Bonzel and Fischer (41) at approximately 100°C observed both molecular and dissociated NO on Ru (100); this was confirmed by this work which noted a change in the UPS spectrum at 50°C, possibly indicating the initiation of dissociation. More detailed studies (106) have also noted first order desorption of NO from a (100) crystal face at 237°C. No second order desorption of NO was ever observed. Upon heating the crystal above 65°C, the nitrogen AES peak to peak value increased and the oxygen correspondingly decreased. This is evidence of NO dissociation. The increase in the nitrogen signal could be interpreted on the basis that NO is adsorbed linearly through the N atom. As dissociation occurs, the oxygen atom, which had attenuated the nitrogen signal as it had acted as an overlayer adsorbed on the N atom, would adsorb on a ruthenium site. An increase in the nitrogen peak to peak value would result. This could be an oversimplification of the signal increase as it may be due to a change in the cross section of the N atom due to NO dissociation. The oxygen signal decrease is probably due to such a cross section change as it seems unreasonable to expect O incorporation at less than 100°C.

At approximately 100°C, the nitrogen starts to desorb which was confirmed by the flash results (Figure 24); as desorption occurs, oxygen incorporation is initiated. This leads to an oxygen coverage of $\sim$1.3 at 265°C where the N coverage has decreased to zero.

At 475°C, from the expected nitric oxide adsorption mechanism, the gas phase NO would be in equilibrium with adsorbed NO; the NO coverage at this temperature would be expected to be negligible. This is a consequence of the two pathways available to the molecularly adsorbed nitric oxide. It can either desorb or dissociate. Since only 3% of the adsorbed NO ever desorbs, dissociation is expected to be the predominant pathway followed. Following dissociation, the nitrogen adatoms would associate and desorb as N_2. The oxygen would then be incorporated into the surface which would result in a (1x3)-O pattern. If the surface were already saturated, the oxygen atom could react with carbon monoxide to form the second product, CO_2.

With regard to carbon monoxide adsorption, it has been shown that β-type CO adsorbs associatively on ruthenium metal surfaces. A HREELS study (65) has shown that β-type carbon monoxide is adsorbed linearly with the Ru-C bond having a bond order of one. Using the force constant derived from the C-O vibrational frequency, it was determined, using a bond energy bond order correlation, that the bond energy is 250 kcal/mole as opposed to 256 kcal/mole in the gas phase. This indicates that the CO molecule is only slightly perturbed upon chemisorption.

Using a ruthenium (101) crystal with oxygen in the subsurface region, Reed, Comrie and Lambert (60) found that upon CO adsorption and subsequent desorption, in addition to desorption of α and β-CO, a third type desorbed at ∿525°C (γ-CO). In attempting to saturate the states, they found that the β and γ states were in competition thus implying a common adsorption site. The γ state was not due to the association of C and O which resulted from CO dissociation.

When applied to this research, these results lead to the conclusion that the CO disproportionation reaction occurs through the reaction of β-CO. It will be recalled that in dosing 400 μm of CO onto a nitric oxide pretreated surface the disproportionation reaction was not favored, while on a metal ruthenium surface the reaction occurs resulting in the formation of a carbon overlayer. Since the α and β states occur only on the metallic surface and on the "oxidic" surface the β and γ are in competition, it can be stated that the α state is unreactive to disproportionation, the γ state possibly has a high coverage concentration on the "oxide" surface and the β state is the only state active in disproportionation. The coverage of linearly bonded CO would therefore be expected to be quite low under the NO-CO reaction conditions used in this study. If in curve fitting the NO and CO plots, Figures 4 and 5, to a rate law the coverage of reactive CO is found to be high, then it would have to be attributed to either α or γ-type CO. Since the γ-CO desorbs at a higher temperature than the α or β-CO and it is not due to the association of C and O atoms, it seems conceivable that the bonding configuration involves the interaction of both the oxygen and carbon atoms with the surface. This would be consistent with the blocking of β sites and is compatible with the large unit cell of the (102) surface.

The desorption spectra of the reactive surfaces were also recorded following reaction under both reducing and oxidizing conditions. These spectra could lead to a conception of the reaction intermediates. The spectra were recorded after reaction at 475°C and a decrease in crystal temperature to ∿100°C. This allows for the possibility of reactant adsorption which would complicate the interpretation.

Following reaction under reducing conditions, nitrogen desorption transpired at 275°C and a broad nitric oxide peak was perceived. No oxygen desorbed and only a small partial pressure increase in CO was seen. Considering that the NO probably displaced most of the adsorbed CO, the desorption spectrum was very similar to that obtained using the individual reactants.

Under oxidizing conditions, the results were analogous except that a large quantity of nitric oxide desorbed and oxygen evolved with a maximum desorption rate at 800°C. The oxygen desorption is believed to be due to the dissociation of ruthenium dioxide. Since the oxygen dissociation pressure of RuO_2 at 800°C is $\sim 10^{-3}$ Torr and the O_2 pressure during the crystal heating was greater than 10^{-7} Torr (97,108), the conclusion seems reasonable. This was confirmed by placing a ruthenium dioxide sample in the reaction system which was prepared in the manner already discussed. Upon heating, the RuO_2 using a focused light beam oxygen "desorption" occurred at 800°C. The RuO_2 disc then returned to its metallic luster which parallels the removal of the tarnished overlayer from the (102) crystal following the desorption experiment.

Exchange Studies

During the course of this investigation, the NO-CO reaction was performed using reactants $N^{16}O$ and $^{12}C^{18}O$. This was done in order to observe whether or not carbon monoxide dissociation was to be considered a viable step in the reaction mechanism. The result observed under both oxidizing and reducing conditions was that exchange occurred resulting in the formation of the three possible carbon dioxide isotopes. This could transpire by one of three possible mechanisms. The first could be that exchange occurred between carbon dioxide molecules.

This mechanism could not be confirmed by mixing both $^{12}C^{18}O^{18}O$ and $^{12}C^{16}O^{16}O$ for no exchange was observed in the reaction chamber with the crystal at 475°C. The $^{12}C^{18}O^{18}O$ was produced by allowing $^{12}C^{18}O$ and $^{18}O_2$ to react over the catalyst until completion.

The two other mechanisms involve C-O bond dissociation either by unimolecular dissociation or by interaction with another adsorbate. The first mechanism which would involve an elementary step not unlike reaction (46) was shown to be feasible by dosing both $^{13}C^{16}O$ and $^{12}C^{18}O$ into the reaction cell, with each having a pressure of 445 μm. Isotopic mixing between the two reactants was observed as shown in Figure 25. A similar result was observed by McCarthy and Wise (42) with a flow reactor. The rate of exchange past 50 seconds decreased and became approximately zero after 100 seconds. This may have been due to formation of a carbon overlayer via the disproportionation reaction. This would imply that the surface used in this exchange study was more metallic than oxidic. Since an unreactive surface oxygen layer or a ruthenium dioxide layer is associated with the catalyst under reaction conditions, this does leave open the question of unimolecular CO dissociation under stated conditions.

Considering the strong oxidizing tendencies of nitric oxide, it seems unreasonable to consider the second mechanism as the carbon, once formed, would be quickly oxidized back to carbon monoxide. This was also substantiated by the LEED/Auger experiments.

The third mechanism would involve C-O bond rupture which is enhanced by the carbon monoxide interacting with another adsorbate. Since γ-type CO adsorption does occur on ruthenium surfaces with an associated oxygen layer, a possible exchange mechanism could be:

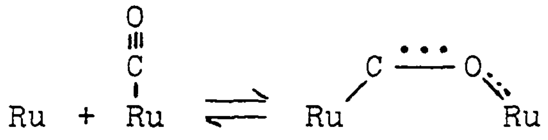

(γ-CO) (48)

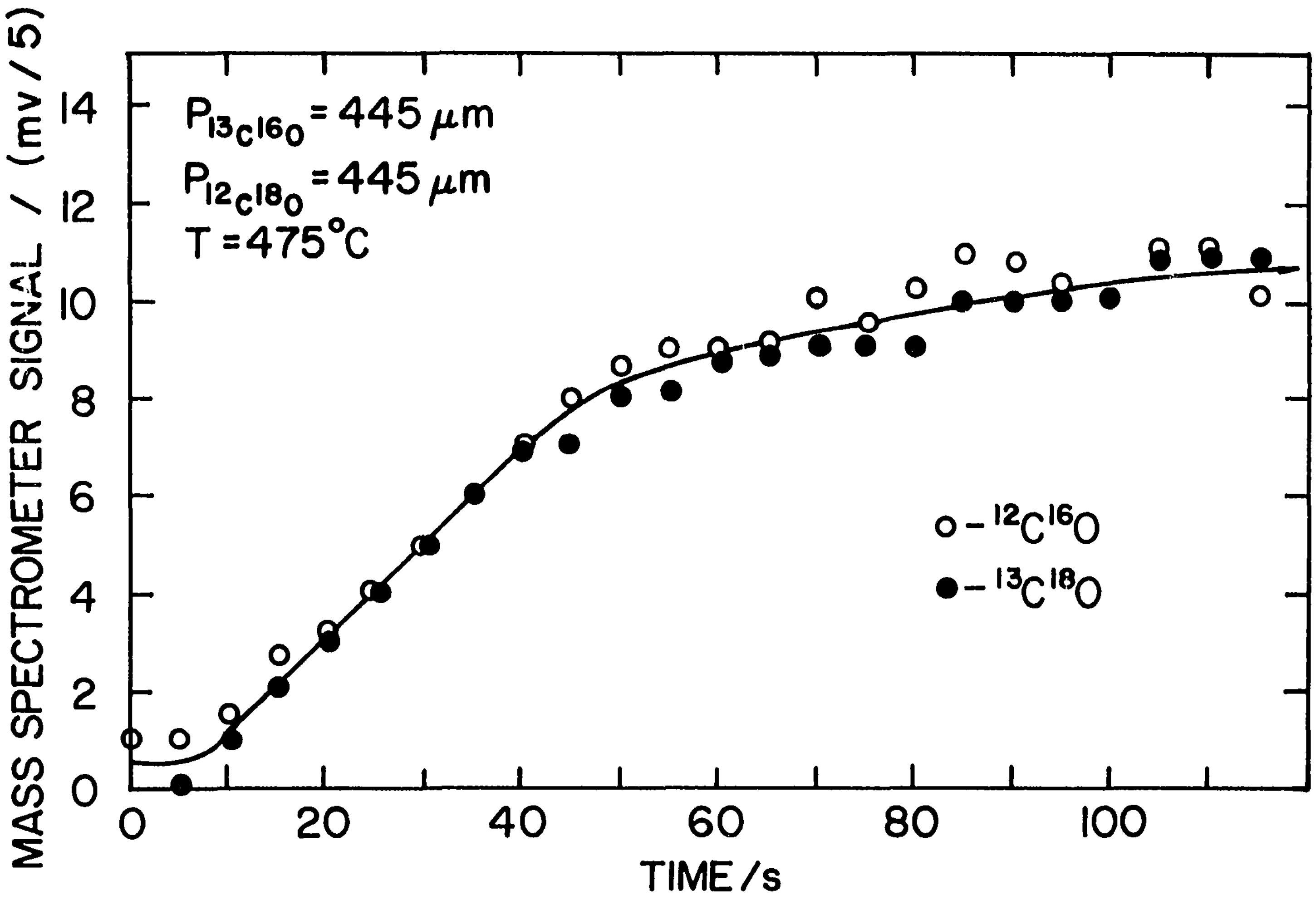

Figure 25. Exchange reaction of $^{12}C^{18}O + {}^{13}C^{16}O \rightleftharpoons {}^{13}C^{18}O + {}^{12}C^{16}O$: mass spectrometer signal intensity of products as a function of time

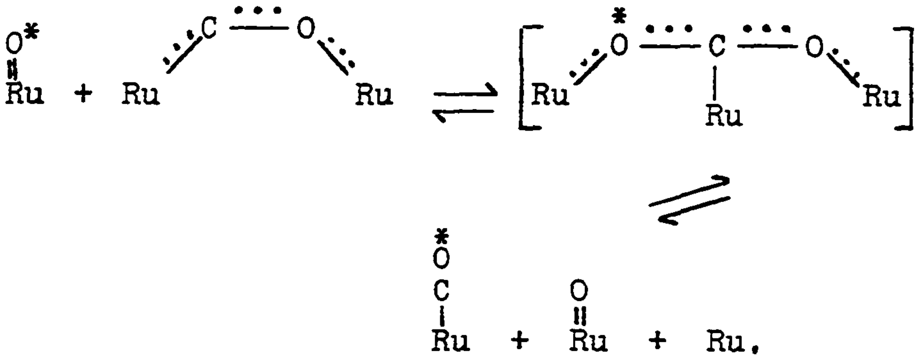

(49)

Another mechanism which has been considered is that involving bimolecular exchange. Webb and Eischens (109) have considered an exchange complex on iron:

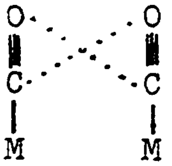

where an oxygen atom becomes bonded to two carbon atoms and it never exists as a separate adatom. A similar complex has been postulated to occur on tungsten (110).

On ruthenium such a complex seems unreasonable as recent publications (111) have shown using HREELS and LEED that as the CO coverage increases, the ν_1 stretching frequency, C-O, increases. This could not be attributed entirely to dipole-dipole interaction nor to modification of the chemisorptive bond, Ru-C, as ν_2 remained constant with coverage. The decrease was considered to be due to repulsive interadsorbate interactions. The interaction was significant enough that the CO molecules would adsorb on sites with low binding energies as the coverage increased to maximize the CO-CO distance and avoid CO occupancy of the nearest neighbor site. Thus, a biomecular complex could not be considered favorable.

A final point must be made concerning CO dissociation on ruthenium. As mentioned, the C-O bond energy of chemisorbed CO is only approximately 6 kcal/mole less than the gas phase value of 256 kcal/mole. By approximating the bond energies of the Ru-C, Ru-O and Ru-CO bonds it can be shown that the enthalpy change for dissociation is positive. The Ru-CO bond energy is 30 kcal/mole as ascertained from the CO desorption activation energy. A confirmation of this value is available from the isosteric heat of adsorption of CO on Ru (001) which is 29 kcal/mole (100). The dissociation energy of a high temperature $RuO_{(g)}$ species has been determined to range from 88 ± 5 to 116 kcal/mole (112) though the most commonly reported value is 115 ± 15 kcal/mole (113). Using an O_2 desorption activation energy of 75 ± 3 kcal/mole which is in the range of energies for ruthenium (001) and (101) surfaces (53,60) and an O-O bond energy of 118.9 kcal/mole, the chemisorption bond energy was calculated to be 97 kcal/mole in agreement with the Ru-O dissociation energy.

An estimate of the Ru-C bond enthalpy was available from the dissociation energy of $RuC_{(g)}$, 154.0 ± 3.0 kcal/mole (114). An alternate estimate of the Ru-C chemisorptive bond energy was calculated using the heat of formation of ruthenium carbide, $RuC_{(s)}$, ≈ +20 kcal/mole (115). Using the heats of sublimation of carbon and ruthenium, 171.3 and 155.5 kcal/mole, respectively, the total bond enthalpy within the solid was calculated to be 306.8 kcal/mole. Ruthenium carbide is known to have the WC structure (116) thus indicating that the carbon is bonded within a trigonal prismatic ruthenium unit cell giving it a coordination number of six. Since the Ru-Ru distances in the hexagonal solid are only slightly greater than the Ru-Ru single bond distance of 2.492 Å (117) an estimate of the metal-metal bond energy must be subtracted from the calculated total bond energy value. Employing the empirically derived formula (117), $D(n) = D(1) - 0.60 \log n$, the bond order, n, of the ruthenium-ruthenium bond was determined using the metal-metal bond distances, D(n) and the single bond distance, D(1) = 2.492 Å. Each ruthenium atom in the trigonal prismatic unit cell is bonded to two ruthenium atoms 2.821 Å apart and six atoms separated by 2.908 Å. The bond orders were calculated to be 0.28 and 0.20, respectively. The total metal-metal bond order was then determined by multiplying the respective values by two and six and dividing by two to avoid overcounting, then adding the results; the total order was 0.88. An estimate of the bond energy was determined by reducing the ruthenium heat of vaporization by a factor of six which is the ruthenium valency and multiplying the result by the total metal-metal bond order. The interaction was determined to be 23 kcal/mole. Reducing the total bond enthalpy in RuC by 23 kcal/mole determined the Ru-C bond strengths in the carbide. This value could then be utilized to estimate the carbon binding energy to different adsorption sites on the ruthenium surface. The binding energy of carbon to a 3-fold site, Ru_3C, is therefore determined to be 142 kcal/mole assuming the carbon single bonds to each site atom. It will be recalled that this value is within 12 kcal/mole of the $RuC_{(g)}$ dissociation energy; this could imply that the bond order of carbon to a top site is three with a bond energy of between 142 and 154 kcal/mole. If the single Ru-C bond energy were used as a measure of binding energy to a top site, the value would be 47 kcal/mole.

The enthalpy change for the dissociation of chemisorbed carbon monoxide can therefore be estimated by adopting the estimates of the binding energies of the adsorbates. Assuming that the carbon would bond to a 3-fold site or triply bond to a single ruthenium atom, the enthalpy change for the reaction is between +29 and 41 kcal/mole. The entropy change for the elementary step would be small. The configurational change could possibly be the major contribution to the entropy shift which would be on the order of 0 to +1 cal/mol•deg. The free energy change for the reaction would therefore be positive at 475°C.

It is therefore unexpected that dissociation would occur; exchange would thereby have to occur through a γ-type CO intermediate under the reaction conditions used in this dissertation.

Rate Reproducibility and Mechanistic Considerations

During the course of this investigation, the stability of the reaction rate and the reproducibility of the nitric oxide order plot were found to vary by an amount greater than can be attributed to instrumental noise. At low nitric oxide pressures, region I in Figure 5 and over the entire range of the CO order plot, the rates would vary by less than 10%. In regions II-IV of the NO order plot, the rates appeared to be essentially time dependent.

In region II this is exemplified by Figure 26. Using pressures of nitric oxide and carbon monoxide of 75 μm and 285 μm, respectively, it was found that a rate decrease occurred with time. The experimental procedure used to determine the plot was to allow the reaction to proceed for up to 200 seconds, evacuate the reaction cell and then redose the reactants. The rate of the second reaction would be less than the previous one. Only initial rates were again measured to insure that the decrease was not due to depletion of nitric oxide. It will be recalled from the LEED/Auger

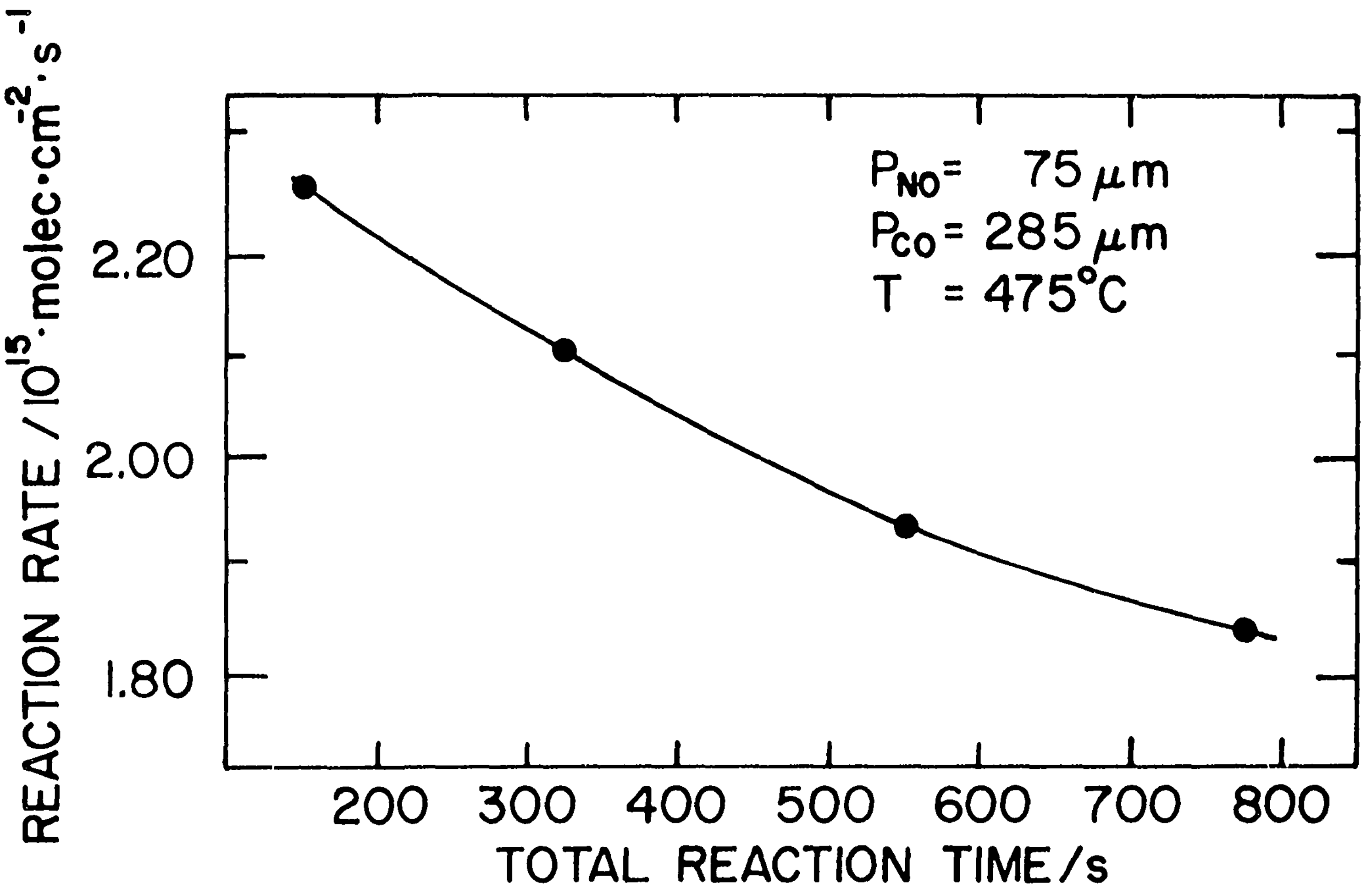

Figure 26. Reaction rate decrease using region II reactant partial pressures as a function of total reaction time

results that sequential reactions using the same reaction conditions and concentrations led to an increase in the coverage of oxygen with each run. This indicates that the reduction in reaction rate is probably due to oxygen poisoning of a reaction site. This was confirmed by pretreating the reduced surface with 320 μm of oxygen for 1650 seconds with the catalyst at 565°C. Upon reacting NO and CO over the pretreated surface, the rate was found to have decreased by 48% as compared to that obtained using an untreated surface. All reaction conditions utilized were similar to those in region II.

Under conditions more favorable to oxidation, the rate was found to increase with respect to total reaction time as illustrated in Figure 27. Initially, the rate of increase was rapid but decreased to approximately zero above 5000 seconds. This indicates that under reaction conditions, the active catalytic surface is being generated. Above 1000 seconds, the rate was established to be proportional to $(\text{time})^{\frac{1}{2}}$. Since ruthenium dioxide formation has previously been shown to transpire under oxidizing conditions, high nitric oxide pressures, then it appears that oxide growth occurs under catalytic conditions and follows a parabolic rate law. This result establishes RuO_2 as the catalyst under oxidizing conditions. The rapid reduction in the rate in region IV can then be attributed only to a kinetic effect

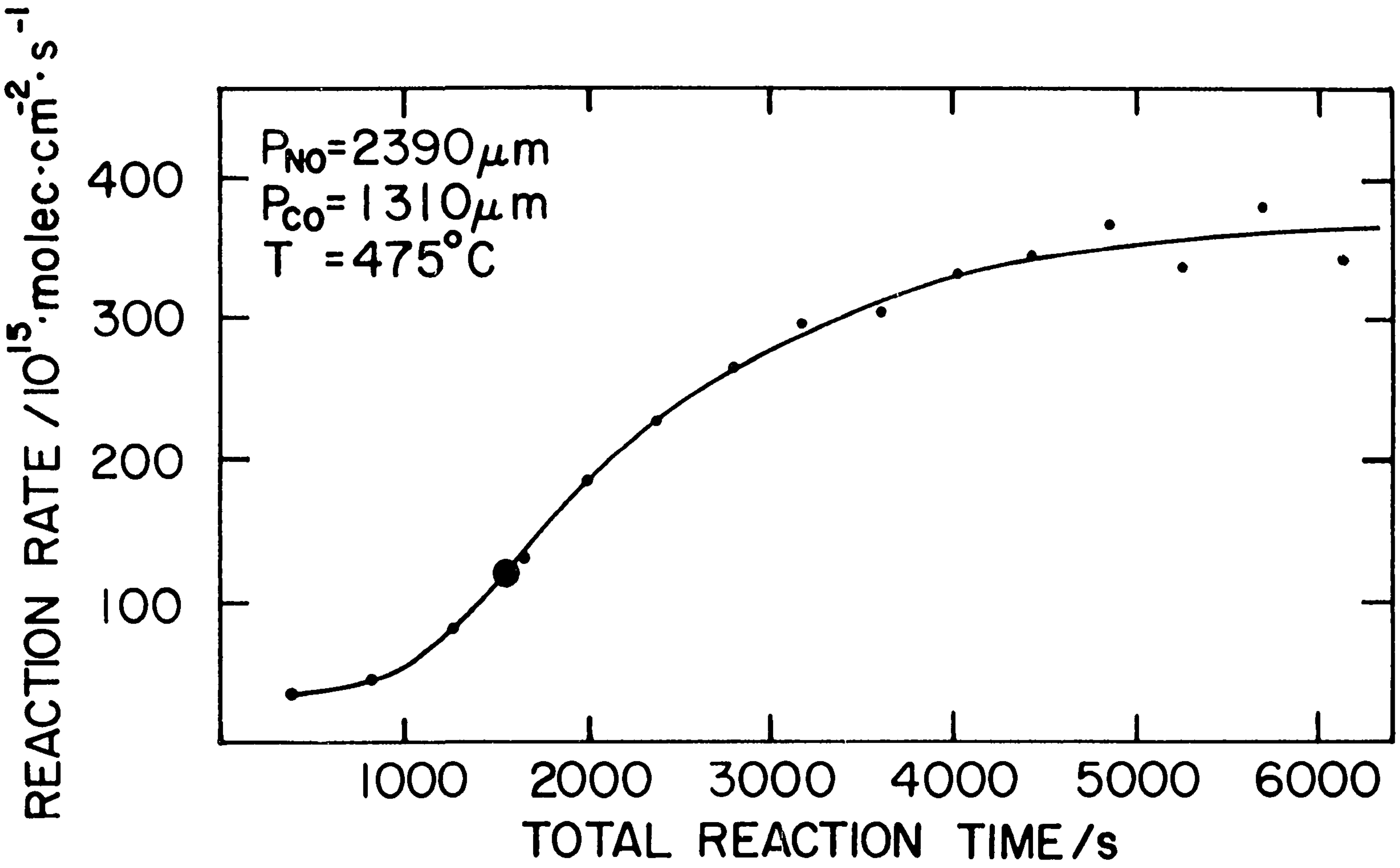

Figure 27. Reaction rate increase using region IV reactant partial pressures as a function of total reaction time. The enlarged point indicates the calculated reaction rate using the given reaction conditions in the determination of an NO order plot similar to Figure 5

and not to mass diffusional limitations. The large point at about 1600 seconds in Figure 27 is the calculated rate during an order plot determination similar to Figure 5 using the given reaction conditions. Since the total reaction time under oxidizing conditions is of the order of 4000 seconds and since the large point in Figure 27 is in a region where the rate is time dependent, the rate of oxide growth and its mechanism will have to be considered.

A metal oxide of the type under consideration has two interfaces, labelled A and B in Figure 28, which are the Ru/RuO_2 and $RuO_2/NO_{(g)}$, $CO_{(g)}$ interfaces, respectively. There are two limiting cases with regard to transport phenomena across these interfaces and through the oxide layer, both of which lead to oxide growth. The transport, which is considered to be rate determining, can occur according to case I by motion of ruthenium cations from interface A to B and to maintain neutrality, hole transport from B to A. The motion of the ruthenium cations could also be visualized as an anion vacancy undergoing diffusion to the Ru/RuO_2 interface. Case II would involve motion of interstitial oxygen anions to interface A; this could also be viewed as transport of cation vacancies from interfaces A to B. Electron flow would then be in the direction of the RuO_2/gas phase interface.

Figure 28. Model of Ru/RuO_2/gas phase interfaces and the transport direction of the defects and ions. Case I and Case II are explained in the text

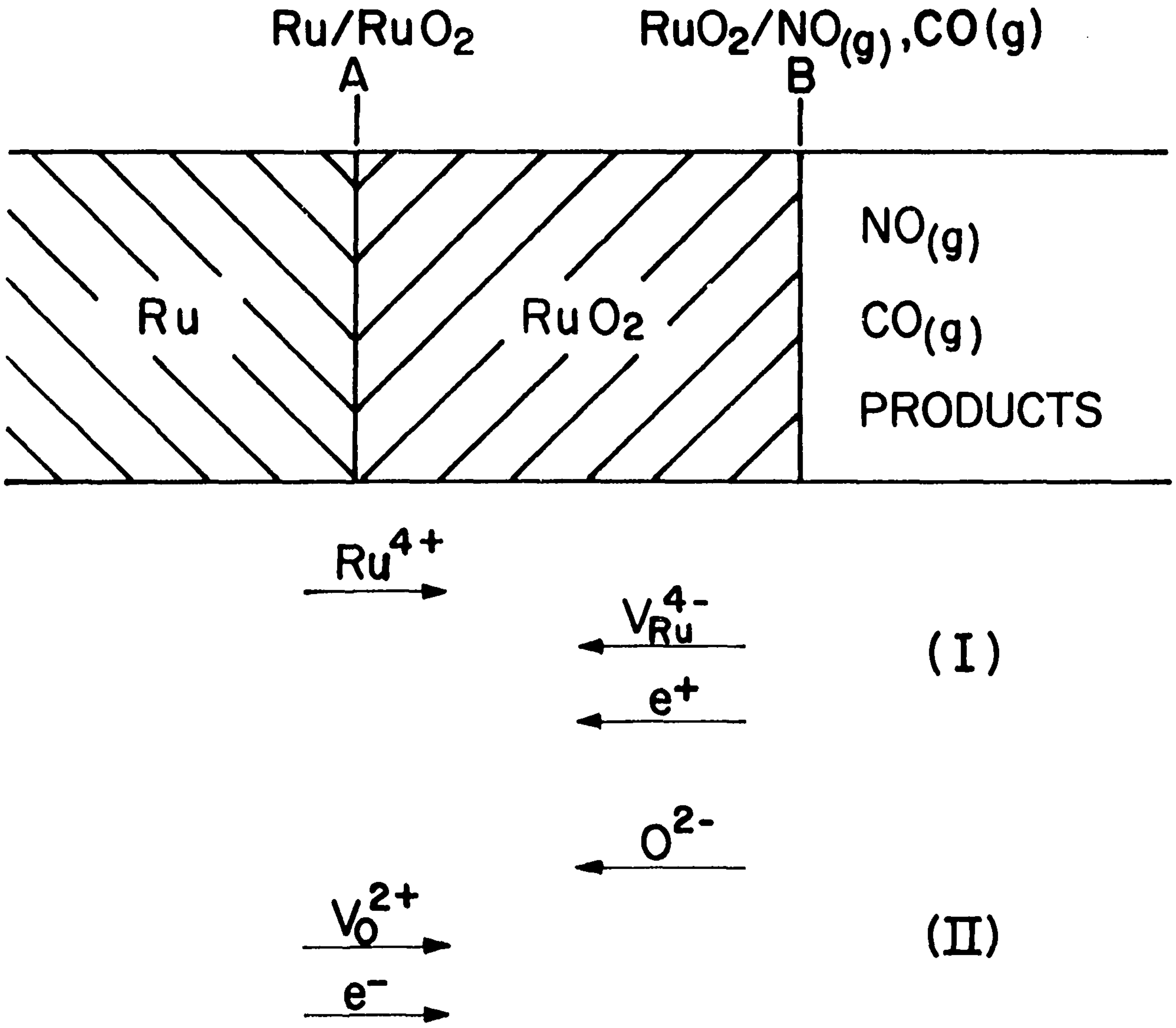
Ru/RuO2
A
RuO2/NO(g),CO(g)
B
Ru
RuO2
NO(g)
CO(g)
PRODUCTS
Ru4+
VRu4-
e+
(I)
O2-
VO2+
e-
(II)

Since the reactions (the ruthenium oxidation and not the NO-CO reduction) at the interfaces are usually rapid with respect to the transport phenomena, the rate of growth should decrease as the RuO_2 layer increases in thickness. This will lead to a parabolic type rate law. This rate law follows directly from Fick's law of diffusion:

$$\frac{dx}{dt} = \frac{k}{x} \tag{50}$$

where x is the film thickness. Upon integration of equation (50):

$$x = (2kt)^{\frac{1}{2}} \tag{51}$$

the thickness is found to be proportional to $t^{\frac{1}{2}}$. In this study, no direct measure of the thickness was available but beyond approximately 1000 seconds it appears that the reactive catalytic surface area is proportional to it. The rate constant, k, is dependent on the diffusing species, temperature, and may depend on reactant pressure according to the growth mechanism.

In order to develop a mechanism, it must be determined whether the ruthenium or oxygen ion is involved in the transfer. Most researchers agree that the predominant species that undergoes migration is the cation (118-120). Two recent publications (121,122) on the application of the field ion microscope and the atom probe to oxidized ruthenium films presented a compositional profile of the oxide layer.

The analysis throughout the oxide film indicated an O/Ru ratio of two, but in a narrow region just before the Ru/RuO_2 interface, the layer was found to be oxygen deficient. There was no significant evidence in the sample of an oxygen solution in a ruthenium metal substrate.

If the anions had been mobile, an oxygen rich layer would have been found in a narrow region just beyond the oxide/oxygen interface. As a ruthenium rich layer was found near the Ru/RuO_2 interface, this supports the idea of cation movement during the formation of RuO_2.

On the basis of the Wagner-Schottky theory, the rate of growth of RuO_2 is dependent on the nature and the number of defects within the lattice. It is, of course, the defects which will control the cation transport rate. For the present discussion, these defects will be viewed as ion vacancies; a specific discussion of the effect of the various types of vacancies, Frenkel, Schottky or surface defects, has been undertaken by Harrison (123). At the present time the exact nature of the solid state defects in RuO_2 is not known.

The rate of oxidation is therefore proportional to the vacancy concentration:

$$\text{rate}_{RuO_2} = k\left[V_{Ru}{}^{4-}\right]. \tag{52}$$

Assuming the oxidation mechanism involves the reaction of surface oxygen with a ruthenium cation:

$$2[O_{ads}] \underset{\longleftarrow}{\xrightarrow{K}} RuO_{2(s)} + V_{Ru}^{4-} + 4e^{+} \tag{53}$$

then

$$[V_{Ru}^{4-}][e^{+}]^{4} = K[O_{ads}]^{2} \tag{54}$$

where K is the equilibrium constant for the oxidation process. It is considered that:

$$4[V_{Ru}^{4-}] = [e^{+}] \tag{55}$$

as it is necessary to maintain charge neutrality of the crystal. Substituting equation (55) in (54) then:

$$[V_{Ru}^{4-}]^{5} = K'[O_{ads}]^{2} \tag{56}$$

where K' equals 256(K). Utilizing the adsorption and dissociation equilibria of nitric oxide on ruthenium at 475°C, it can be shown that the surface coverage of oxygen is linearly related to the NO pressure. Therefore, the rate of oxidation of RuO_2 will be proportional to $P_{NO}^{0.4}$:

$$\text{rate of growth } (P_{NO}) = k[V_{Ru}^{4-}] = k'P_{NO}^{0.4} \tag{57}$$

where k' includes the constants for the oxidation equilibrium, adsorption equilibria and the diffusion constant of the metal cations. Incorporating equation (51) the rate of growth, which according to Figure 27 is actually the rate of increase of surface area, is:

$$\mathrm{rate}(t,P_{NO}) = UP_{NO}{}^{0.4}\ t^{\frac{1}{2}} \tag{58}$$

Since an oxide layer is formed as the nitric oxide pressure is increased, in the evaluation of the NO order plot two experiments were undertaken to observe the effect of increased carbon monoxide pressure on the stability and reactivity of the oxide layer.

The ruthenium dioxide layer following evacuation was found to be reducible by reaction with carbon monoxide at 475°C. This was evidenced by the removal of the tarnished overlayer and the production of carbon dioxide. The partial pressure increase in CO_2 was generally in the range of 2 to 20 μm depending on the total reaction time under oxidizing conditions. Using the ruthenium (102) site density, 5.85×10^{14} atoms·cm^{-2}, the thickness of the oxide layer was calculated to be equivalent to approximately 180 to 1800 monolayers of RuO_2. Assuming an arbitrary RuO_2 layer thickness of 4 Å, this is equivalent to an oxide thickness of 700 to 7000 Å. The oxide that forms can then truly be considered a bulk oxide and not a surface oxide of one to two monolayer thickness such as is known to form on nickel.

Another experiment that characterized the overlayer entailed using the oxidized catalyst under reducing conditions. Upon dosing a low NO/CO ratio gas mixture into the reaction cell, the RuO_2 was immediately reduced via the reaction discussed above:

$$RuO_{2(s)} + 2CO_{(g)} \rightleftharpoons Ru_{(s)} + 2CO_{2(g)} \qquad (59)$$

The reaction then proceeded with a rate which was about three times faster than that measured using an initially reduced catalyst. Upon subsequent reactions using the same reducing gas mixture, the rate decreased to within 10% of the expected value. Since the initial reduction of the film was rapid this implies, as does Figure 27, that the oxide layer is quite permeable by the reactants NO and CO. Following the removal of the oxide by the carbon monoxide, a ruthenium structure with a high surface area and a high porosity remains. Upon the interaction of a NO-CO mixture on this catalyst, the rate would therefore be expected to be high. Since the ruthenium temperature is about 475°C and transition metal films sinter as low as 0°C (124), the porous structure would be expected to degrade resulting in a reduction in the surface area. This explains the diminution of the reaction rate to its expected value.

After extensive oxidation, the reflectivity was found to be diminished following reduction of the oxide film. The most reasonable explanation is that though sintering does occur, upon annealing, the surface does not return to its original (102) orientation. LEED analysis confirmed this as the pattern was very complex. It was only following extensive annealing (several days, 1000°C) that the (102) LEED pattern could be restored.

An effort has been made to develop a reaction mechanism which is quantitatively consistent with the kinetic studies. Such a mechanism would also have to at least be qualitatively related to the results obtained from the thermal desorption, XPS, LEED/Auger, isotopic exchange and rate reproducibility studies. The NO-CO reaction kinetics will be modelled by considering that the catalytic surface exists in two states; one is a ruthenium surface with an associated oxygen layer and the other is ruthenium dioxide. Due to the differences in the surface structures this leads to two different reaction mechanisms, each of which is favorable only while the catalyst is in a particular state.

Since the rate reproducibility experiments demonstrated that the rates measured in the carbon monoxide order plot were time independent as well as that part of the nitric oxide plot in region I then these regions will be curve fit simultaneously to the mechanism which corresponds to the reduced state. The rate measurements within region II of the NO plot will be incorporated in the fit of the reduced mechanism though the rate law will have to be adapted to include catalyst poisoning. Within these regions, the ruthenium was not in the form of the dioxide as no oxygen desorption occurred at 800°C upon heating. ESCA spectrum of the ruthenium indicated it was in a metallic form and the ratio of the lattice parameters from the LEED pattern was 2.34 as expected for the (102) crystal face.

A $N^{16}O$, $^{12}C^{18}O$ reaction mixture over the catalyst resulted in a mixture of the carbon dioxide isotopes; this indicates that the reaction does not proceed via a Rideal-Eley type mechanism. As the CO reactant order in Figure 4 decreases to a negative value, the class of mechanisms initially chosen was Langmuir-Hinshelwood. A rate law of the type utilized was:

$$\text{rate} = \frac{AP_{CO}P_{NO}}{[1 + BP_{NO}^{\frac{1}{2}} + CP_{CO} + DP_{NO} + EP_{CO}^{2}]^{2}} \qquad (60)$$

in which any of the terms in the denominator could be zero. Included in the analysis were terms of the type $P_{CO}^{n}P_{NO}^{m}$ where m and n are in the range -2 to 2 and have either integral or half order values. In an attempt to fit the CO order plot and region I by arbitrarily varying the constants, A-E, it was found that if the low NO pressure region were fit to within 10% then the maximum in the CO order plot occurred at ∿200 μm instead of the desired ∿5 Torr maximum.

To correct this, the rate law was modified by including a high order CO term in the numerator:

$$\text{rate} = \frac{A\,P_{NO}P_{CO} + FP_{CO}^{X}}{[1 + BP_{NO}^{1/2} + CP_{CO} + DP_{NO} + EP_{CO}^{2}]} \qquad (61)$$

The values of X considered were 3/2 and 2. This shifted the maximum to higher pressures but resulted in a plot with greater than 100% error in the 0.1 to 1.0 Torr pressure range.

An additional problem with this rate law was that it required that the term $BP_{NO}^{1/2}$ be significant to simulate the curvature of the NO plot in region I. This half order term in nitric oxide is related directly to the surface coverage of nitrogen. For a LH mechanism this would require that at 475°C the nitrogen coverage be appreciable, contradicting results from both Auger spectroscopy and flash desorption showing it to be negligible by 250°C. Consequently, this required modification of the type of mechanism chosen.

The modification consisted of allowing the reduced reaction surface to be composed of two different types of sites. Adsorption would then occur independently on each type of site and displacement of one species by another could not occur. From the infrared studies by Davydov and Bell (35) and Brown and Gonzalez (36), it was observed that adsorption of nitric oxide onto a carbon monoxide predosed ruthenium metal surface occurred with displacement of the CO without reaction. The reactants would therefore be required to adsorb on the same site, at least in the pressure range investigated by the infrared investigation.

Since the catalyst under reduced conditions consists of a ruthenium surface with oxygen atoms bonded within the first atomic layer as shown in Figure 17, it is not inconceivable that two types of sites could exist. Bonding could occur on an oxygen site or a ruthenium site. If the oxygen atoms were to be considered inactive, then the two sites could consist of ruthenium sites, Ru and Ru'. The Ru sites, for example, could be those ruthenium atoms residing in the trough and the Ru' sites, those which make up the row atoms elevated by the partially penetrated oxygen atoms. The exact nature of the sites is unknown though it is reasonable to assume that one site is more highly influenced by the oxygen than the other. The "oxidic" site will therefore have less d electrons available for bonding due to the change in coordination and the oxygen bonding.

A marked feature of ruthenium metal chemistry is the formation of nitric oxide complexes which are of the general type $Ru(NO)L_5$. It is postulated (32) that an electron transfer occurs from NO to the metal, Ru, which in the complex results in $Ru{=}N^{+}{=}\ddot{O}{:}$. Such a transfer would be enhanced on the oxide site due to the reduction in the electron density in the ruthenium atom. This would strengthen the N-O bond due to transfer out of the π^*

anti-bonding orbital. For carbon monoxide adsorption on an oxide site, there would be less d electrons available for back donation into the π^* orbital which results in a weak metal to carbon bond. On a ruthenium metal site back donation could occur into the anti-bonding orbitals of carbon monoxide resulting in a weak C-O bond and a strong Ru-C bond. A similar result would be expected for NO; not only would transfer from the π^* orbital be hindered but, in addition, the N-O bond could be further weakened by d electron donation into those bonds.

Considering that molecular nitric oxide appears to exist in a metastable state on ruthenium at 475°C, it seems unreasonable that it would initially adsorb on a site which would strengthen the N-O bond. It is for this reason that the binding site of the reactants is chosen to be on the ruthenium metal sites, Ru, though the assignment is almost arbitrary.

Two possible reaction mechanisms which were considered to occur over the reduced state of the catalyst will now be discussed. For clarity, the sites which are associated with the oxygen layer will be designated Ru' and the metal sites Ru. The first mechanism to be discussed will consider multiple carbon monoxide adsorption on a single ruthenium site:

$$Ru + NO_{(g)} \underset{k_{-1}}{\overset{k_1}{\rightleftharpoons}} RuNO \tag{62}$$

$$Ru' + RuNO \xrightarrow{k_2} Ru'O + RuN \tag{63}$$

$$Ru + CO_{(g)} \underset{k_{-3}}{\overset{k_3}{\rightleftharpoons}} RuCO \tag{64}$$

$$RuCO + CO_{(g)} \underset{k_{-4}}{\overset{k_4}{\rightleftharpoons}} Ru(CO)_2 \tag{65}$$

$$RuCO + Ru'O \xrightarrow{k_5} Ru + Ru' + CO_{2(g)} \tag{66}$$

$$2RuN \xrightarrow{fast} 2Ru + N_{2(g)} \tag{67}$$

The derivation of a rate expression from the mechanism can be accomplished by one of two means. It can be assumed that the reactions in equations (62), (64) and (65) are not in true equilibrium; this would then require a steady state development for each of the five adsorbates: RuNO, RuCO, Ru'O, $Ru(CO)_2$ and RuN. The resultant simultaneous equations are solvable, but not straightforwardly. A more direct approach which also lends greater physical significance to the rate law is one discussed by Kemball (125). The method presented involves the establishment of equilibria between the gas and surface phases and between the species on the surface. Each equilibrium will exert a thermodynamic influence on the coverages of the adsorbed species which take part in a kinetically controlled process. This non-steady state method will be used in the derivation of the rate law.

In the development of the rate expression, the surface coverage of nitrogen will be considered to be virtually zero; as the nitric oxide dissociates via reaction (63), the association of the nitrogen adatoms by equation (67) is considered to be sufficiently rapid to maintain a negligible coverage. The elementary step designated by reaction (66) was chosen as the rate determining step but it will be seen from the rate law evaluation that equations (63) and (66) are related and in a sense both are rate limiting. The mathematical derivation of the rate expression proceeds in the following manner.

The equilibria can be expressed as:

$$\frac{k_1}{k_{-1}} = K_1 = \frac{[\mathrm{RuNO}]}{[\mathrm{Ru}][\mathrm{NO}]} \qquad (68)$$

$$\frac{k_3}{k_{-3}} = K_3 = \frac{[\mathrm{RuCO}]}{[\mathrm{Ru}][\mathrm{CO}]} \qquad (69)$$

$$\frac{k_4}{k_{-4}} = K_4 = \frac{\mathrm{Ru(CO)_2}}{[\mathrm{RuCO}][\mathrm{CO}]} \qquad (70)$$

Equation (69) can be substituted into (70) and an expression for the surface coverage of $\mathrm{Ru(CO)_2}$ can be obtained. The

RuCO and RuNO expressions are obtained from equations (68) and (69) directly:

$$[RuNO] = K_1 P_{NO} [Ru] \tag{71}$$

$$[RuCO] = K_3 P_{CO} [Ru] \tag{72}$$

$$[Ru(CO)_2] = K_4 K_3 P_{CO}{}^2 [Ru] \tag{73}$$

Concerning equation (65), the formation of $Ru(CO)_2$ could have been considered as the product of a bimolecular surface reaction:

$$2RuCO \underset{k'_{-4}}{\overset{k'_4}{\rightleftharpoons}} Ru(CO)_2 + Ru \tag{74}$$

whereby equation (73) would become

$$[Ru(CO)_2] = K'_4 K_3{}^2 P_{CO}{}^2 [Ru]. \tag{75}$$

It can be shown <u>via</u> curve fitting that it is not possible to distinguish between (73) and (75) from a kinetic viewpoint.

The surface oxygen coverage, Ru'O, was derived using the steady state approximation:

$$\frac{d[Ru'O]}{dt} = 0 = k_2 [RuNO][Ru'] - k_5 [RuCO][Ru'O] \tag{76}$$

which upon incorporation of equations (71) and (72) yields:

$$[Ru'O] = \frac{k_2 K_1}{k_5 K_3} \frac{P_{NO}}{P_{CO}} [Ru']. \tag{77}$$

This same expression could have been derived on the basis that reaction stoichiometry dictates that the production rate of nitrogen will be half that of carbon dioxide. Since the rate of equation (67) is fast, then reactions (63) and (65) must proceed at equal rates.

It is convenient to express the surface concentrations as fractional coverages. The sum of the coverages of the intermediates and vacant ruthenium sites must therefore be unity. Since two different independent sites are postulated, two relationships concerning the concentration of surface sites are necessary:

$$[\mathrm{Ru}] + [\mathrm{RuNO}] + [\mathrm{Ru(CO)_2}] + [\mathrm{RuCO}] = 1 \tag{78}$$

and

$$[\mathrm{Ru'}] + [\mathrm{Ru'O}] = 1. \tag{79}$$

Substitution of the above expressions for the surface complex concentrations into (78) and (79) yields two equations for the fractional coverage of empty surface sites:

$$[\mathrm{Ru}] = 1/\{1 + K_1P_{NO} + K_3P_{CO} + K_4K_3P_{CO}^{\,2}\} \tag{80}$$

and

$$[\mathrm{Ru'}] = 1/\left\{1 + \frac{k_2K_1}{k_5K_3}\,\frac{P_{NO}}{P_{CO}}\right\}. \tag{81}$$

The rate can now be expressed using the rate determining equation as:

$$\frac{d[CO_2]}{dt} = k_5[RuCO][Ru'O] = k_2K_1P_{NO}[Ru][Ru'] \qquad (82)$$

which upon using the fractional coverage expression for vacant sites yields:

$$\frac{d[CO_2]}{dt} = \frac{k_2K_1P_{NO}}{\{1 + K_1P_{NO} + K_3P_{CO} + K_4K_3P_{CO}{}^2\}\{1 + \frac{k_2K_1P_{NO}}{k_5K_3P_{CO}}\}} \qquad (83)$$

From the flash desorption results the surface coverage of nitric oxide is expected to be low at 475°C; consequently, the K_1P_{NO} term is zero. The K_3P_{CO} expression which is proportional to the RuCO coverage would be considered to be approximately zero if β-type carbon monoxide were the active carbon monoxide component. Assuming that only β-CO is involved and using these approximations equation (84) becomes

$$\frac{d[CO_2]}{dt} = \frac{k_2K_1P_{NO}}{\{1 + K_4K_3P_{CO}{}^2 + \frac{k_2K_1}{k_5K_3}\frac{P_{NO}}{P_{CO}} + \frac{k_2}{k_5}K_1K_4P_{CO}P_{NO}\}} \qquad (84)$$

This expression can be rewritten as:

$$\frac{d[CO_2]}{dt} = \frac{A\ P_{NO}}{\{1 + BP_{CO}{}^2 + \frac{CP_{NO}}{P_{CO}} + DP_{CO}P_{NO}\}} \qquad (85)$$

The other reaction mechanism which was considered to occur in the reducing regime involves carbon monoxide adsorption on both the Ru and Ru' sites. The reaction sequence is very similar to that given in equations (62)-(67).

$$\mathrm{Ru} + \mathrm{NO}_{(g)} \underset{k_{-1}}{\overset{k_1}{\rightleftharpoons}} \mathrm{RuNO} \tag{86}$$

$$\mathrm{Ru'} + \mathrm{RuNO} \xrightarrow{k_2} \mathrm{Ru'O} + \mathrm{RuN} \tag{87}$$

$$\mathrm{Ru} + \mathrm{CO}_{(g)} \underset{k_{-3}}{\overset{k_3}{\rightleftharpoons}} \mathrm{RuCO} \tag{88}$$

$$\mathrm{Ru'} + \mathrm{CO}_{(g)} \underset{k_{-4}}{\overset{k_4}{\rightleftharpoons}} \mathrm{Ru'CO} \tag{89}$$

$$\mathrm{RuCO} + \mathrm{Ru'O} \xrightarrow{k_5} \mathrm{Ru} + \mathrm{Ru'} + \mathrm{CO}_{2(g)} \tag{90}$$

Nitrogen association is again expected to be rapid as indicated by equation (67). The surface coverage of the Ru'CO adsorbate is derived from the equilibrium in reaction (89):

$$\frac{k_4}{k_{-4}} = K_4 = \frac{[\mathrm{Ru'CO}]}{[\mathrm{Ru'}]P_{CO}} \longrightarrow [\mathrm{Ru'CO}] = K_4 P_{CO}[\mathrm{Ru'}]. \tag{91}$$

The conservation of surface site relationships are therefore:

$$[\mathrm{Ru}] + [\mathrm{RuNO}] + [\mathrm{RuCO}] = 1 \tag{92}$$

and

$$[\mathrm{Ru'}] + [\mathrm{Ru'O}] + [\mathrm{Ru'CO}] = 1, \tag{93}$$

Using equations (71), (72), (77) and (91) in equations (92) and (93), the fractional surface coverages of the vacant active sites are:

$$[\mathrm{Ru}] = 1/\{1 + K_1 P_{NO} + K_3 P_{CO}\} \tag{94}$$

and

$$[\mathrm{Ru'}] = 1/\{1 + \frac{k_2 K_1}{k_5 K_3} \frac{P_{NO}}{P_{CO}} + K_4 P_{CO}\}. \tag{95}$$

The rate of production of carbon dioxide is therefore:

$$\frac{d[CO_2]}{dt} = \frac{k_2 K_1 P_{NO}}{\{1 + K_1 P_{NO} + K_3 P_{CO}\}\{1 + \frac{k_2 K_1}{k_5 K_3} \frac{P_{NO}}{P_{CO}} + K_4 P_{CO}\}} . \tag{96}$$

Using the same assumption that RuNO ≈ 0 at 475°C, the rate law reduces to:

$$\frac{d[CO_2]}{dt} = \frac{k_2 K_1 P_{NO}}{\{1 + K_3 P_{CO} + \frac{k_2 K_1}{k_5 K_3} \frac{P_{NO}}{P_{CO}} + K_4 P_{CO} + \frac{k_2}{k_5} K_1 P_{NO} + K_3 K_4 P_{CO}{}^2\}} \tag{97}$$

which can be rewritten as:

$$\frac{d[CO_2]}{dt} = \frac{F\ P_{NO}}{\{1 + GP_{CO} + \frac{HP_{NO}}{P_{CO}} + JP_{CO} + LP_{NO} + MP_{CO}{}^2\}} , \tag{98}$$

where the constants G and J could be combined. These mechanisms will predict the reactant order of carbon monoxide to vary from +1 to -2 and the nitric oxide order to vary from

+1 to 0. They both gave an adequate fit to the CO and NO rate plots. The fits are illustrated in Figures 29 and 30. It can be seen that the theoretical curves lie within 10% of the experimental points in region I and over most of the carbon monoxide plot. A disagreement arises at the maximum in the CO order plot as the theoretical curve is not as sharp as desired.

The maximum divergence was 25% or less; that is greater than can be explained due to instrumental deviations. This could possibly be due to nonideal behavior of the adspecies. The fractional coverage which can be calculated from the reaction mechanism inherently incorporates an assumption that the gases adsorb ideally and that the coverage of the adsorbates can be related to a Langmuir adsorption isotherm. Implicit in the derivation of such an isotherm is the concept that the adsorbates are bonded to the surface at a definite, localized site. Each site can accommodate only one adsorbate; the adsorption energy is the same at all sites and is independent of the presence or absence of other adsorbed species at neighboring sites. This, of course, would eliminate the possibility of any interactions between the surface complexes. Rarely does any adsorption system fit the criteria necessary to truly meet the Langmuir assumptions. While a deviation is observed, especially with the mechanism involving Ru'CO complexes, it is not believed

Figure 29. Theoretical fits using the Ru'CO, RuCO mechanism, equation 98: a) nitric oxide order fit to region I, b) carbon monoxide order fit. The constants used in equation 98 are listed in Table 5

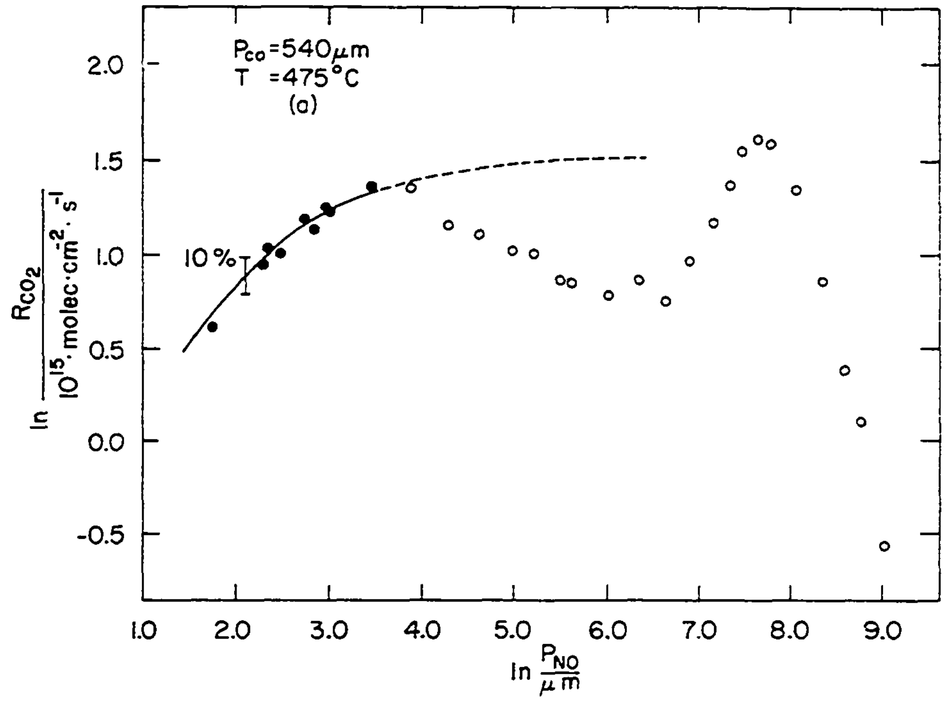
P_{co}=540μm
T =475°C
(a)
10%
$\ln \frac{R_{CO_2}}{10^{15}\cdot\text{molec}\cdot\text{cm}^{-2}\cdot\text{s}^{-1}}$
2.0
1.5
1.0
0.5
0.0
-0.5
1.0
2.0
3.0
4.0
5.0
6.0
7.0
8.0
9.0
$\ln \frac{P_{NO}}{\mu m}$

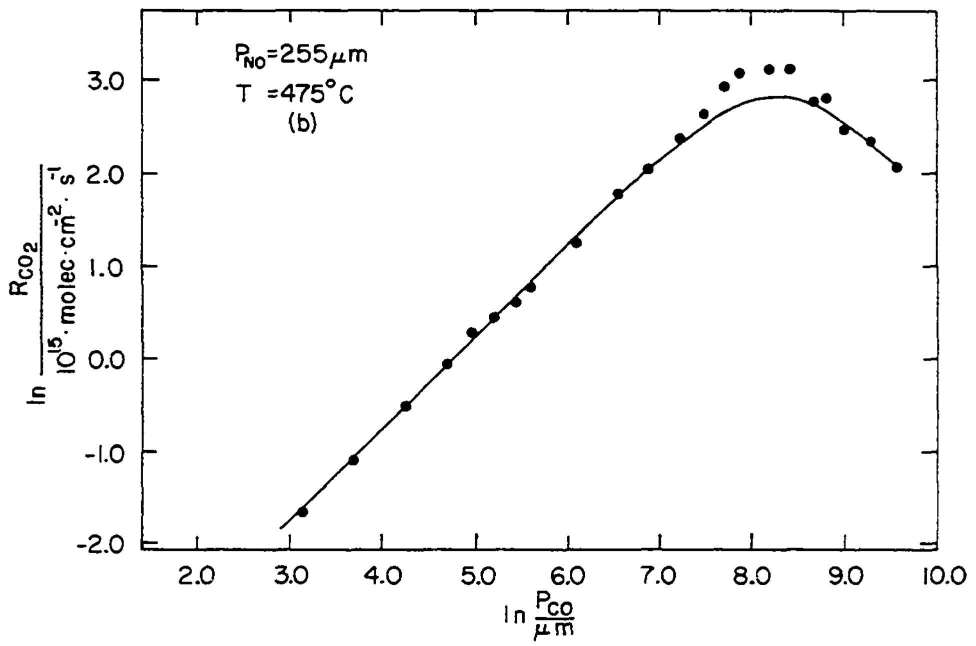
P_{NO}=255μm
T =475°C
(b)
$\ln \frac{R_{CO_2}}{10^{15}\cdot\text{molec}\cdot\text{cm}^{-2}\cdot\text{s}^{-1}}$
3.0
2.0
1.0
0.0
-1.0
-2.0
2.0
3.0
4.0
5.0
6.0
7.0
8.0
9.0
10.0
$\ln \frac{P_{CO}}{\mu m}$

Figure 30. Theoretical fits using the $Ru(CO)_2$ mechanism, equation 85: a) nitric oxide order fit to region I, b) carbon monoxide order fit

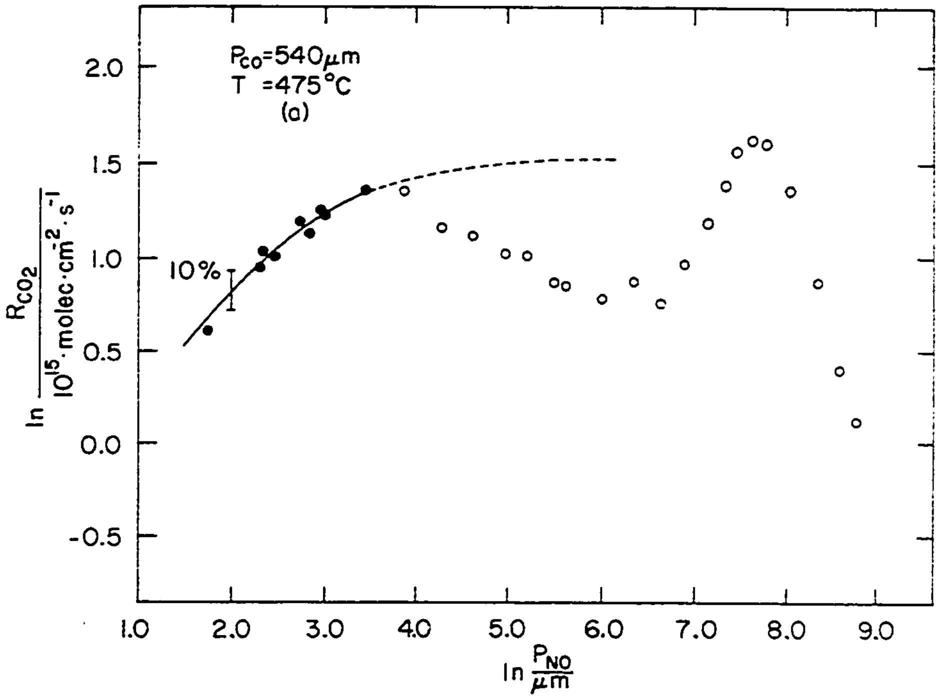
P_{CO}=540μm
T =475°C
(a)
10%
$\ln \frac{R_{CO_2}}{10^{15}\cdot \text{molec}\cdot\text{cm}^{-2}\cdot\text{s}^{-1}}$
2.0
1.5
1.0
0.5
0.0
-0.5
1.0
2.0
3.0
4.0
5.0
6.0
7.0
8.0
9.0
$\ln \frac{P_{NO}}{\mu m}$

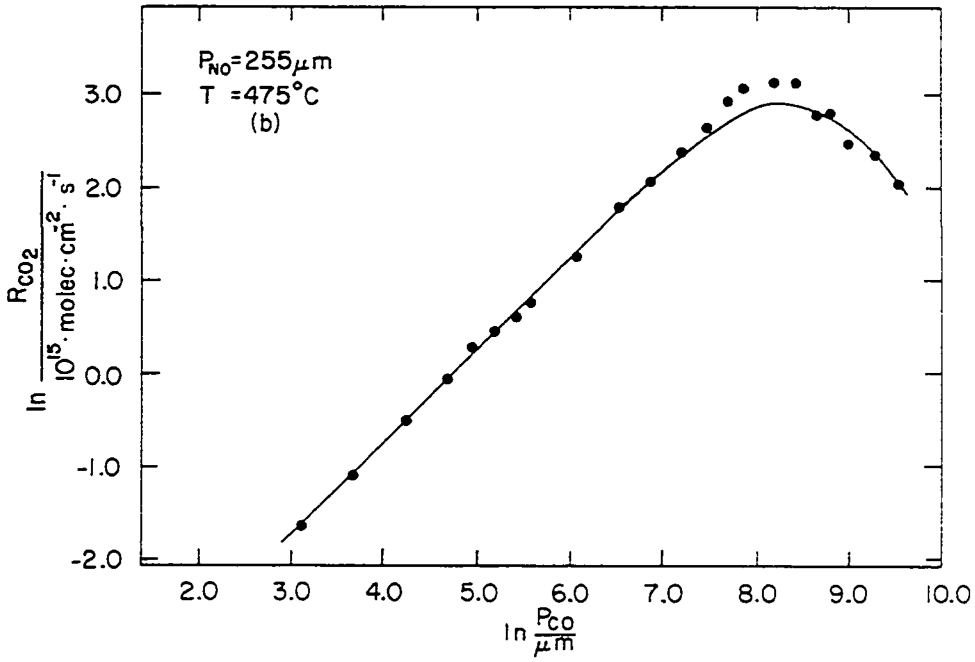
P_{NO}=255μm
T =475°C
(b)
$\ln \frac{R_{CO_2}}{10^{15}\cdot \text{molec}\cdot\text{cm}^{-2}\cdot\text{s}^{-1}}$
3.0
2.0
1.0
0.0
-1.0
-2.0
2.0
3.0
4.0
5.0
6.0
7.0
8.0
9.0
10.0
$\ln \frac{P_{CO}}{\mu m}$

that the accuracy of the data warrant the utilization of a more sophisticated adsorption isotherm.

The two mechanisms differ most significantly in the mode of carbon monoxide bonding. In both cases it singularly bonds with a metal site in the manner illustrated below:

$$\begin{array}{c} O \\ \| \\ C \\ | \\ Ru \end{array}$$

Since the lack of site competition between the adsorbates in the rate determining step will usually lead to an order plot which varies from +1 to 0 and since it was found that the CO order is negative at higher pressures, it was necessary to consider either multiple adsorption on a single site or carbon monoxide adsorption on the Ru$'$ sites. Incorporating these intermediates led to an order of -2 in CO.

The multiple adsorption complex, $Ru(CO)_2$, is not without precedence in the literature. It will be recalled that such species were postulated from infrared studies (24,26,28,29) at temperatures of less than 200°C and were confirmed by an EPR study (27) by Kobayashi and Shirasaki using supported catalysts. Such surface structures have generally been modelled from inorganic ruthenium carbonyls where up to 4 CO groups would be bonded to a single ruthenium atom. The polynuclear compound (126) $Ru_3(CO)_{12}$ has frequently served as a model of CO adsorption on ruthenium. However, more detailed investigations on metal surfaces, specifically the ruthenium (001) crystal face, have shown considerable evidence (65,111,127) to suggest that such surface species cannot exist. As previously mentioned, there is a considerable repulsive CO-CO interaction which is pronounced enough even at low coverages to cause the admolecules to occupy surface sites with lower binding energies in order to maximize the CO-CO distances. While the magnitude of the interaction must be less than the adsorption energy, it also must be greater than the variation in binding energies of the available sites. Williams and Weinberg (111) noted that the minimum CO-CO distance on ruthenium (001) was 3.35 Å. It would therefore be expected that the possibility of two carbon monoxide molecules occupying the same site would be remote.

A recent study by Madey (127) using the Electron Stimulated Desorption Ion Angular Distributions (ESDIAD) method determined that the desorbed CO$^+$ and O$^+$ ions had an angular distribution centered at the surface normal. The width of the desorbing ion beam was ∼16° at 300K which was attributed to CO bending vibrations.

Under no conditions were ion beams detected in the range of approximately 45-60° from the plane of the surface, indicative of a $Ru(CO)_2$ type structure. On this basis the first mechanism discussed is not favored, though no direct kinetic evidence is available to render its complete elimination.

The other mechanism which includes CO bonding on Ru and Ru' sites allows only for linear adsorption. This mechanism does allow for the possibility of CO adsorption on either of the two sites, each of which have different adsorption energies. Due to the presence of the oxygen, the Ru'-C bond would be expected to be weaker thus making it a less favored adsorption site relative to the ruthenium metal site.

In region II of Figure 5, the nitric oxide order is not zero, but negative. This is a direct result of the surface poisoning discussed earlier. From Auger, surface pretreatment and rate reproducibility data, it was surmised that oxygen was the catalyst deactivating agent. Since the oxygen, at least in region II, appeared to be irreversibly adsorbed it is necessary to consider how its concentration varies with time. Oxygen adsorbed on Ru' sites, while active, could possibly be inactive on the Ru sites due to the increased availability of d electrons. Transfer of electrons to the oxygen would thereby be enhanced, creating a stronger Ru-O bond with the possibility of some ionic character. The mechanistic equation considered as the pathway to poison formation is the transfer of an oxygen adatom on a Ru' site to a Ru site.

$$\mathrm{Ru'O} \;+\; \mathrm{Ru} \;\xrightarrow{k_p}\; \mathrm{RuO} \;+\; \mathrm{Ru'} \qquad (99)$$

The number of available Ru sites would thereby be diminished and the rate would decrease with time. It is assumed, on the basis of the constancy of the reaction rates, that at low NO pressure conditions, region I, the ruthenium poison, RuO, is reactive due to the conditions more highly favorable to reduction.

Under these conditions, the total number of ruthenium sites would be Ru_{tot} while under conditions more favorable to oxidation a smaller number, R_{av}, would be available due to the site poisoning by the oxygen. The number of Ru sites blocked, Ru_p, is related under all conditions, to the total number and the number of available sites by the following expression:

$$\mathrm{Ru}_{av} \;=\; \mathrm{Ru}_{tot} \;-\; \mathrm{Ru}_p . \qquad (100)$$

In region I, $\mathrm{Ru}_p = 0$.

Using the reaction mechanism involving adsorption of carbon monoxide on both Ru and Ru' sites, equation (92) can be rewritten as:

$$[Ru_V] + [RuNO] + [RuCO] = Ru_{tot} - Ru_p \tag{101}$$

where Ru_V is the fractional number of Ru_{av} sites that are vacant. Using equations (71) and (72), this can be rewritten as:

$$Ru_V = \frac{Ru_{tot} - Ru_p}{[1 + K_1P_{NO} + K_3P_{CO}]} \tag{102}$$

From equation (99) the rate of formation of the poison, RuO, is:

$$\frac{d[RuO]}{dt} = k_p[Ru'O][Ru_V]. \tag{103}$$

Since $[RuO] = Ru_p$, then equation (103), using expressions (77) and (95), can be manipulated to read:

$$\frac{d[RuO]}{dt} = \frac{\frac{k_pk_2K_1}{k_5K_3}\frac{P_{NO}}{P_{CO}}(Ru_{tot} - [RuO])}{\{1 + \frac{k_2K_1}{k_5K_3}\frac{P_{NO}}{P_{CO}} + K_4P_{CO}\}\{1 + K_1P_{NO} + K_3P_{CO}\}} \tag{104}$$

which, upon integration, results in:

$$Ru_{tot} - [RuO] = e^{-Bt} \tag{105}$$

where

$$B = \frac{\frac{k_pk_2K_1}{k_5K_3}\frac{P_{NO}}{P_{CO}}}{\{1 + \frac{k_2K_1}{k_5K_3}\frac{P_{NO}}{P_{CO}} + K_4P_{CO}\}\{1 + K_1P_{NO} + K_3P_{CO}\}} \tag{106}$$

Substituting equation (105) into (102), the resulting expression can be used to determine the rate law which is appropriate in region II:

$$\frac{d[CO_2]}{dt} = \frac{k_2K_1P_{NO}\ e^{-Bt}}{\{1+K_1P_{NO}+K_3P_{CO}\}\{1+\frac{k_2K_1}{k_5K_3}\frac{P_{NO}}{P_{CO}}+K_4P_{CO}\}} . \qquad (107)$$

Using the parameters from the iterative trial and error fit of region I and the carbon monoxide order plot, equation (107) was fit to the medium nitric oxide pressure regime. The deviation between the theoretical curve and the experimental points was less than 5%. The final theoretical nitric oxide order plot and the fitting parameters will be reported following examination of the mechanism proposed under more oxidizing conditions.

In regions III and IV, it is necessary that two effects be taken into consideration: the nitric oxide reactant order behavior, which seems to vary from approximately 2 to ≤ -3, and the growth of the ruthenium dioxide as a function of time. The form of the rate law which will be fit to the high nitric oxide pressure region in Figure 5 is:

$$\text{rate} = \{\text{mechanistic rate law}\} \times \{UP_{NO}{}^{0.4}\ t^{\frac{1}{2}}\} \qquad (108)$$

where the second term arises from equation (58). A mechanism which yields the appropriate reactant orders is:

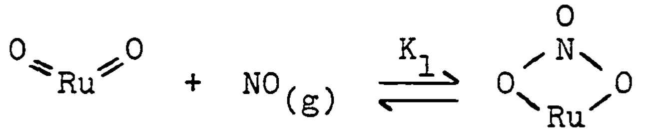
(109)

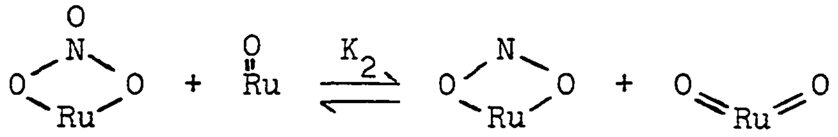
(110)

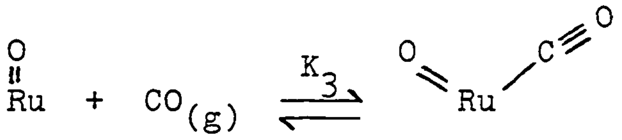
(111)

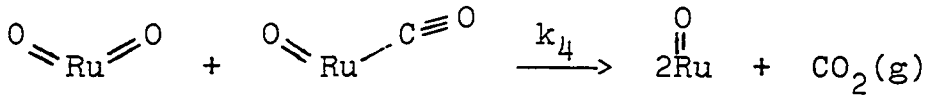
(112)

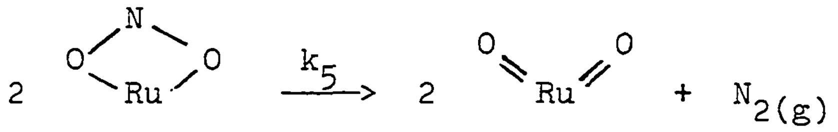
(113)

This is a two site mechanism as the reactants adsorb on different types of sites, RuO_2 and RuO. The difference between this and the reduced mechanism is that their numbers are not independent but are related by the equilibrium, K_2. On the basis of the stoichiometry, the rate of production of nitrogen must be half the rate of formation of carbon dioxide, therefore:

$$k_4[RuO_2][RuOCO] = 2k_5[RuO_2N]^2. \qquad (114)$$

Using (114) and the reaction equilibria in a method similar to that described in derivation of the reduced mechanism rate law, the fractional coverage equations of the surface complexes can be derived:

$$[RuO_2N] = K_1K_2P_{NO}[RuO] \tag{115}$$

$$[RuOCO] = K_3P_{CO}[RuO] \tag{116}$$

$$[RuO_2] = \frac{2k_5}{K_3k_4}(K_1K_2)^2\frac{P_{NO}{}^2}{P_{CO}}[RuO] \tag{117}$$

$$[RuO_2NO] = \frac{2K_1k_5}{K_3k_4}(K_1K_2)^2\frac{P_{NO}{}^3}{P_{CO}}[RuO] \tag{118}$$

Assuming that the rate limiting step is the production of carbon dioxide:

$$\frac{d[CO_2]}{dt} = k_4[RuO_2][RuOCO] = 2k_5[RuO_2N]^2 \tag{119}$$

then the rate law for the oxidizing mechanism is:

$$\frac{d[CO_2]}{dt} = 2k_5K_1K_2P_{NO}{}^2/\{1+\frac{2k_5}{K_3k_4}(K_1K_2)^2\frac{P_{NO}}{P_{CO}} + \frac{2K_1k_5}{K_3k_4}(K_1K_2)^2\frac{P_{NO}{}^3}{P_{CO}} + K_3P_{CO} + K_1K_2P_{NO}\}^2. \tag{120}$$

This rate expression can be rewritten using a constant P_{CO} as:

$$\frac{d[CO_2]}{dt} = \frac{N\ P_{NO}{}^2}{\{1 + QP_{NO}{}^2 + RP_{NO}{}^3 + SP_{NO}\}^2} \tag{121}$$

As mentioned earlier, the procedure used to heat the crystal restricted the maximum total pressure feasible in a kinetic study. With nitric oxide this maximum pressure was in the range of 7-8 Torr. If a carbon monoxide reactant order plot were to be made while the catalyst was in the oxidized state, a nitric oxide partial pressure of at least 7 to 8 Torr would be necessary. If the CO pressure were greater than 540 μm, a temperature of 475°C could not be maintained. This, along with an additional point to be made later, was the reason why such a plot was not feasible and cannot be reported with any accuracy.

From the thermal desorption spectrum obtained upon flashing the oxidized surface after reaction, it was observed that only a small, almost insignificant, partial pressure increase of carbon monoxide occurred. This is evidence that on the oxidized surface the coverage of CO is small, in agreement with the CO bonding model on oxidized surfaces already discussed. For this reason, the K_3P_{CO} term in the denominator of equation (120) is expected to be approximately zero.

In order to obtain a reaction mechanism that will give reactant orders of 2 to -4, it was found that the nitric oxide adsorption site had to be more highly oxidized than the CO adsorption site. In addition, the nitric oxide upon decomposition had to oxidize a more reduced active center to the type of site on which the molecular adsorption initially occurred. This mechanism fits both criteria.

Concerning the nitrogen and nitric oxide adsorbates, a bidentate chelate structure is proposed for the nitric oxide adsorption complex and a di-adsorbed nitrogen atom to a RuO_2 site for the surface nitrogen. The structures of the species in equations (109) and (110) are not meant to imply any specific bond order in the Ru-O or the O-N bonds. Bidentate nitrato complexes of heavy metals have been proposed from infrared results though no specific complex has been reported on ruthenium.

Using a SnO_2 catalyst, Niwa et al. (128) postulated, using infrared and EPR results, that a possible structure for the state of adsorbed nitrogen was similar to a chelated NO_2 group. Since ruthenium dioxide has the same rutile structure as SnO_2, this gives precedent to the RuO_2N group postulated as the structure of adsorbed nitrogen.

A general comment should be made with regard to NO adsorption. On metal surfaces there seems to be no question that the adsorption occurs with the nitrogen bonded to the metal; on oxides the configuration is less clear. Using the infrared results on ruthenium, one is led to the conclusion that for the oxidized form of the catalyst the bonding is through the nitrogen. Winter (129), in investigating the catalytic activity of 40 metallic oxides, postulated that NO adsorption occurred through the oxygen at an anion vacancy in the oxide lattice. Since mechanistically, nitric oxide must adsorb on a site that is already highly oxidized, it seems less reasonable to have it bond <u>via</u> the oxygen than the nitrogen.

The geometry of the carbon monoxide adsorption structure is consistent with the infrared results of Brown and Gonzalez (30) which state that the 2135 cm^{-1} band was due to CO adsorbed on a ruthenium oxide and the 2080 cm^{-1} band was due to adsorption on an oxygen perturbed ruthenium site. Since CO is adsorbing on a site that is bonded to oxygen, it seems reasonable to assign the 2135 cm^{-1} band to the CO adsorption structure as the M-C bond would be expected to be weak. This would promote high vibrational freqencies.

Using equations (109), (110) and (113), the mechanism can also be used to demonstrate the pathway of the initial oxidation of the ruthenium surface. Assuming nitric oxide will oxidize a metal surface to a RuO state, as has been observed under reducing conditions, at higher NO pressures the oxidation mechanism will be initiated by the formation of a RuO_2 site. A sequence would then start following an overall reaction of:

$$2NO_{(g)} + 2RuO \longrightarrow 2RuO_2 + N_2. \qquad (122)$$

Since four RuO_2 centers are generated for every two used in the sequence then in a sense the formation of RuO_2 could be considered to be autocatalytic and the rate of formation of a monolayer of RuO_2 would increase with time. Oxide growth would then proceed by the reaction (53) which involves cation transfer through the oxide layer. The accelerating rate of formation of the first monolayer of RuO_2 is similar to that observed in the nucleation and growth of the reaction interface during the oxidation of metals (123). The rate is generally found to be proportional to t^n where $n > 1$; a value of $n \cong 3$ is commonly reported as the nuclei, once formed, often experience linear growth in three dimensions.

The mechanism also demonstrates the pathway to partial RuO_2 reduction *via* reaction (112). If carbon monoxide were dosed onto a RuO_2 surface CO_2 would be produced. In the experiment whereby just CO was passed over the surface, the oxide returned to the metallic state indicating that the RuO sites were also reduced.

The mechanistic rate law, equation (121), was substituted into equation (108) and curve fit to within $\sim$10% of the experimental points in the NO order plot. The final NO order plot incorporating both the reduced and oxidized mechanisms, the effect of catalyst poisoning in region II and the growth of the RuO_2 layer in regions III and IV, is shown in Figure 31. In the region where the rate was time dependent, the theoretical rates were necessarily calculated at the same nitric oxide pressure at which the experimental points were obtained and in the order in which they were

Figure 31. Final theoretical fit of the nitric oxide order plot incorporating the kinetic mechanisms which apply under oxidizing and reducing conditions and the surface site poisoning and RuO_2 growth mechanisms. The rate laws utilized are given in equations 58, 98, 107 and 121; their constants are enumerated in Table 5. The dashed line illustrates the rapid reduction of the reaction rate of the reduced mechanism with increase in nitric oxide pressure due to oxide nucleation and growth

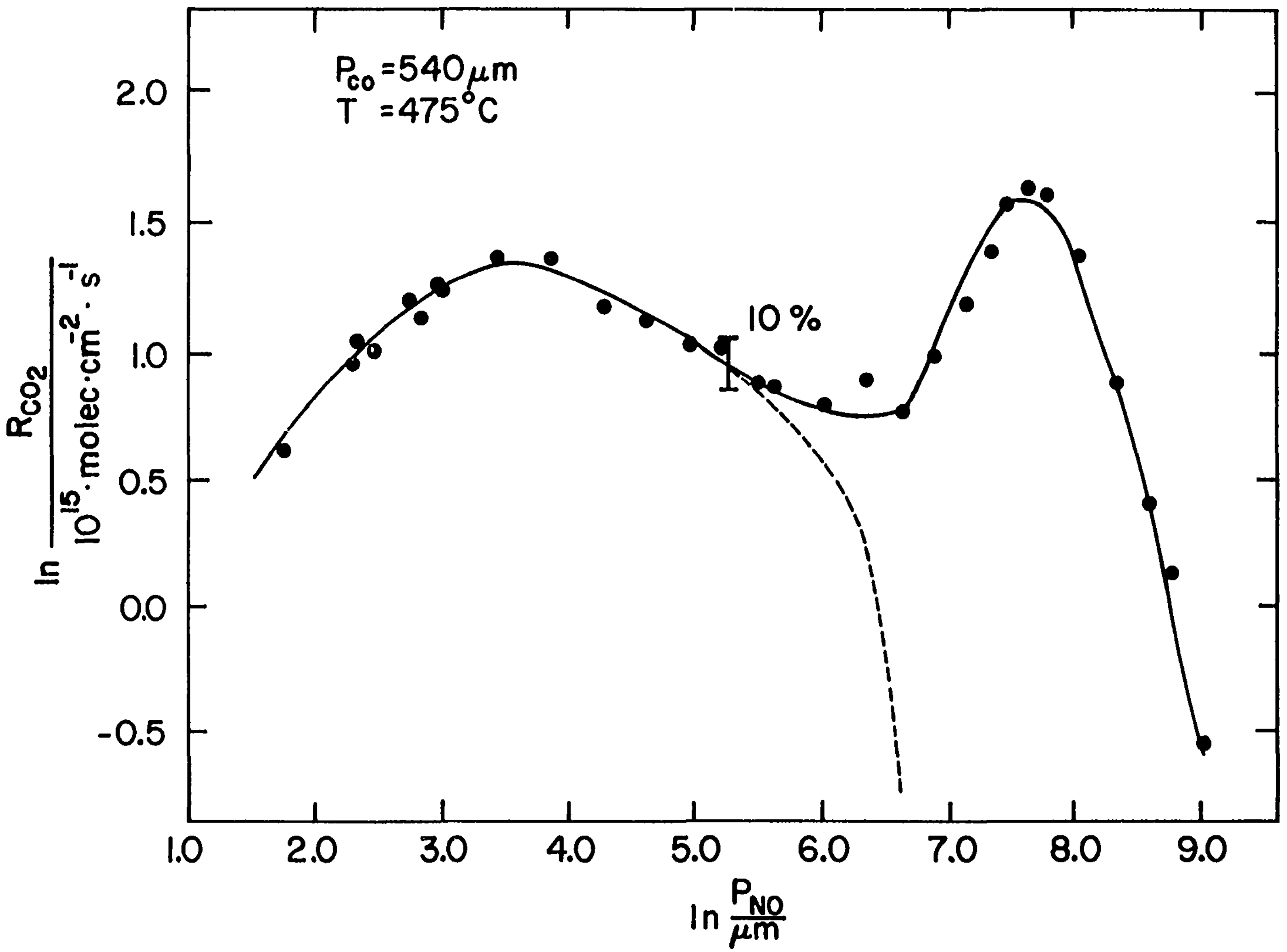
P_{CO} =540 μm
T =475°C
10 %
$\ln \frac{R_{CO_2}}{10^{15} \cdot \text{molec} \cdot \text{cm}^{-2} \cdot \text{s}^{-1}}$
2.0
1.5
1.0
0.5
0.0
-0.5
1.0
2.0
3.0
4.0
5.0
6.0
7.0
8.0
9.0
$\ln \frac{P_{NO}}{\mu m}$

recorded. The curve illustrated is therefore actually a line drawn through the theoretical rate points.

Since no independent analysis was available to ascertain at which pressure the formation of ruthenium dioxide was initiated, it was imperative to set t=0 in equation (108) at an experimental point that gave the best fit of the experimental points. Upon the nucleation of the oxide, the ruthenium metal sites would be blocked and effectively poisoned; therefore the number of sites available for the reduced mechanism will decrease rapidly. The dashed line in Figure 31 indicates this decrease in the rate as the RuO_2 overlayer forms. The parameters used to obtain the fit to the data are given in Table 5. Using these parameters, it

Table 5. Values of the constants used in the rate expressions

Constant	Value	Units
F	1.50×10^{15}	$\text{molec}\cdot\text{cm}^{-2}\cdot\text{s}^{-1}\cdot\mu\text{m}^{-1}$
G	9.23×10^{-6}	μm^{-1}
H	1.70×10^{2}	---
J	2.60×10^{-3}	μm^{-1}
L	1.57×10^{-3}	μm^{-1}
M	2.40×10^{-8}	μm^{-2}
k_p	3.60×10^{-4}	s^{-1}

Table 5. (Continued)

Constant	Value	Units
N	8.89×10^{9}	$\text{molec} \cdot \text{cm}^{-2} \cdot \text{s}^{-1} \cdot \mu\text{m}^{-2}$
Q	3.37×10^{-7}	μm^{-2}
R	4.50×10^{-11}	μm^{-3}
S	0	μm^{-1}
U	1.25×10^{3}	$\mu\text{m}^{-0.4} \cdot \text{t}^{-0.5}$

can be shown that for the oxide at high NO pressures the major surface complex is adsorbed nitric oxide. This was substantiated by the thermal desorption results as following a reaction the major desorbing species was nitric oxide. For nitrogen, the coverage was found to be zero under all reaction conditions as the best fit was obtained letting $S=0$. Plots of the complex coverages for the two reaction mechanisms as functions of nitric oxide pressure are illustrated in Figures 32 and 33. For the reduced mechanism, the coverage of adsorbed nitric oxide and nitrogen was found, as assumed, to be negligible over the entire pressure range which is in agreement with the flash desorption and LEED/Auger results. Those results indicated that the

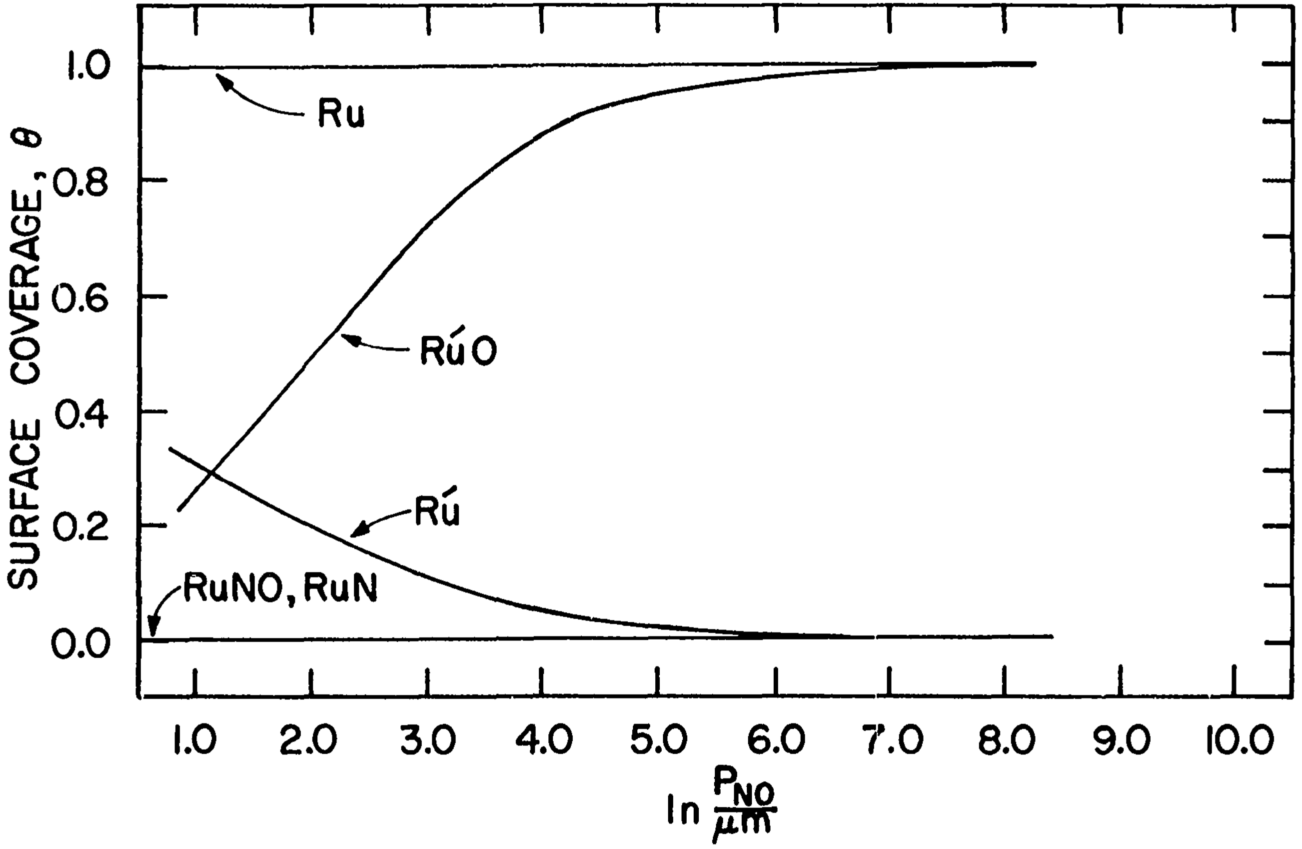

Figure 32. Surface intermediate coverages as a function of nitric oxide pressure using the Ru'CO, RuCO mechanism. The coverages were calculated from equation 98 using a carbon monoxide pressure of 540 μm

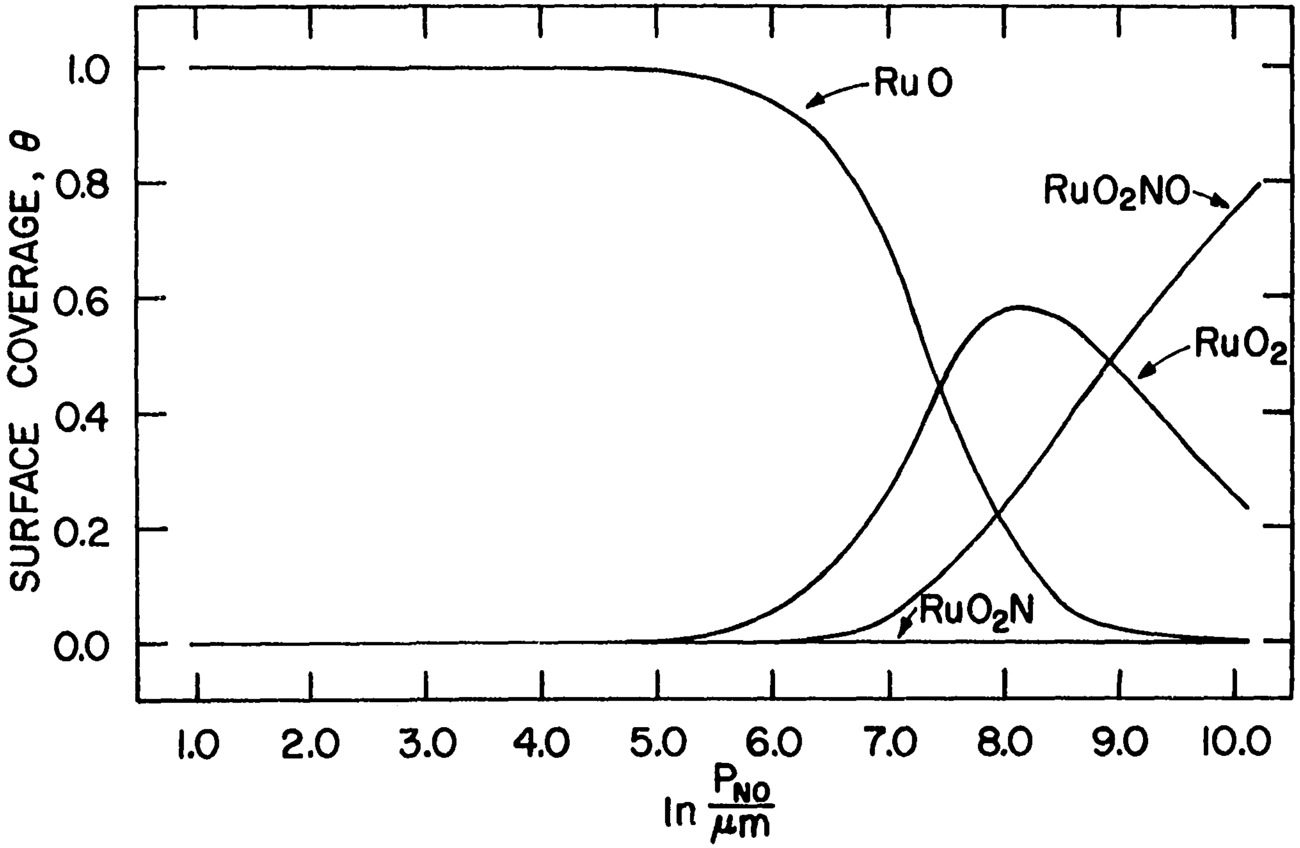

Figure 33. Surface intermediate coverages as a function of nitric oxide pressure as calculated from the mechanism operative on a RuO_2 catalyst

decomposition is rapid and the association of the N adatoms is fast mechanistically.

For the carbon monoxide order plot, it can be shown that the coverage of RuCO in the range studied was never greater than 0.003. This could possibly be a confirmation that the actual type of reactive carbon monoxide bound to the surface is the β-type. Since its coverage is low, it would not be expected that bimolecular exchange could occur; as already indicated, it is not believed that CO dissociates on a ruthenium surface. The only other possible mechanism for exchange which would lead to a mixture of carbon dioxide isotopes would involve a γ-bonded carbon monoxide species. The proposed mechanism for this exchange is given in equations (48,49).

As written, the exchange mechanism would not explicitly be included in the reaction mechanism as the reactants and products are molecularly the same. The rate of exchange was rapid as the product distribution of the carbon dioxide isotopes was time independent using reactants $N^{16}O$ and $^{12}C^{18}O$. An attempt was made to incorporate a γ-type CO intermediate into a mechanism similar to that proposed in equations (86-90); it could not be fit to the order plots unless the γ-CO coverage was zero. The interpretation of this could be that either the other steps in the attempted mechanism were incorrect or that the γ-CO is not to be considered as an intermediate in the reaction mechanism, but must be treated as an activated complex. A more reasonable explanation is that the exchange and reaction mechanisms are to be treated independently. The formation of the γ-CO species would occur via reaction (48) and the exchange by reaction (49).

Using the parameters presented in Table 5, three equilibrium constants and one rate constant can be determined. For the reduced mechanism using the assignments given in equation (98) by (97) the quantity F/(H)(G) yields the value of k_5 which is the rate limiting rate constant. The value of k_5 was 9.56×10^{17} molec$\cdot$cm$^{-2}\cdot$s^{-1}. For bimolecular surface reactions, the value of the rate constant tends to fall in the range 10^{12} to 10^{17} molec$\cdot$cm$^{-2}\cdot$s^{-1}. While the calculated value is high, it is not unexpected as a typical turnover number using a site density of 5.84×10^{14} sites$\cdot$cm^{-2} is 8. For most reactions the range in turnover numbers (TON) is 10^{-3} to 1; the calculated rate constant would then be expected to be high as the TON is unexpectedly high.

The equilibrium constants K_3 and K_4 are directly obtainable from constants G and J, respectively. The equilibrium constants for the adsorption of CO on a Ru' site is $K_4 = 2.60 \times 10^{-3}$ μm^{-1} and for the Ru site is $K_3 = 9.23 \times 10^{-6}$ μm^{-1}. While the values of the constants differ by approximately three orders of magnitude, their relative values seem correct as CO generally desorbs from ruthenium in the 200-250°C range. The difference between the values is a manifestation of the nonreactivity of the Ru'CO species; the K_4 value would consequently be expected to be higher than the K_3 value as the Ru'CO coverage would be greater. No reported value for either constant is available for comparison. The third equilibrium constant obtainable is the adsorption equilibrium of nitric oxide on the RuO_2 surface. The quotient R/Q equals $K_1 = 1.34 \times 10^{-4}$ μm^{-1}.

It is interesting to observe that on the basis of activity per unit surface area, the oxide catalyst is approximately 10^3 less active than the reduced surface. This is due to one of two effects. Assuming that each ruthenium site is available for reaction, it could simply be due to activity differences per site. Since the oxide catalyst seems to promote the NO dissociation reaction to a lesser extent than the reduced catalyst, it seems reasonable. Another inference could be that only one in 10^3 possible sites are active. A means of rationalizing this would be to view the site, RuO, upon which the carbon monoxide adsorbs, as a defect in an RuO_2 lattice. This would give a defect concentration of approximately 7×10^{19} defects/cm^3. Considering that the proportion of defects (Schottky) in an ionic crystal falls in the range of

10^{-3} - 10^{-4} only near the melting point, such a model will not be suggested, at least not on the basis of the normal distribution of point defects in a solid.

It is proposed from the suggested models that the (1x3)-O structure becomes poisoned by the random adsorption of oxygen atoms on Ru sites and that under more oxidizing conditions this surface undergoes a transition to RuO_2. Ruthenium dioxide, which has a rutile structure (89) with lattice parameters of a = 4.491 and c = 3.106 Å (130,131), has been shown to have similar surface and bulk structures (132). Using a field ion microscope, Cranstoun and Pyke (121) found that upon oxidation of ruthenium a coincident oxide layer formed. In order to create such an epitaxial layer it is necessary that the lattice distortion be minimal as a RuO_2 layer is formed on a Ru substrate. The ruthenium (102) lattice parameters are 2.71 x 6.35 Å. For RuO_2 the orientation which would give the minimum distortion is the (110) face which has dimensions of 3.11 x 6.35 Å; the lattice distortion required to place a (110) RuO_2 plane parallel to a (102) Ru face is 14.8%. Assuming that the (110) RuO_2 plane forms epitaxially on the Ru catalyst face, it can be seen why a LEED pattern could not be acquired for the RuO_2 sample. The distortion, while minimal, could only be maintained over short distances on the ruthenium surface lattice; a faceted surface with a nonplanar morphology would result. This is most clearly recognized by calculating the ratio of the molar volumes of RuO_2 and Ru. The ratio is $\bar{V}_{RuO_2}/\bar{V}_{Ru} = 2.3$, thus indicating that a porous, nonprotecting overlayer will form.

Formation of the first surface layer of RuO_2 could follow the model proposed in Figure 34. The (1x3)-O structure exhibited in 34a would start to become poisoned and the Ru sites deactivated by oxygen blockage of the active centers as illustrated in Figure 34b. The oxygen atoms within the (1x3)-O structure which are bonded to two row atoms would shift to a possibly more stable 3-fold site with the oxygen bonding to one row atom. By doing this the oxygen would then be indirectly increasing its coordination and availability to d electrons. As the oxygens shift, a ruthenium dioxide nucleus will form, Figure 34c, and nucleation and growth will be initiated. The relative size of the ruthenium and oxygen atoms in Figure 34c is not intended to imply the degree of electron transfer from the ruthenium to the oxygen. It is expected that the Ru-O bond would have a large percentage of ionic character and that the oxygen may have a greater radius than the ruthenium atoms.

From Figure 31, decrease in the reduced rate due to RuO_2 formation follows a power law of the form:

$$\alpha = kt^n \tag{123}$$

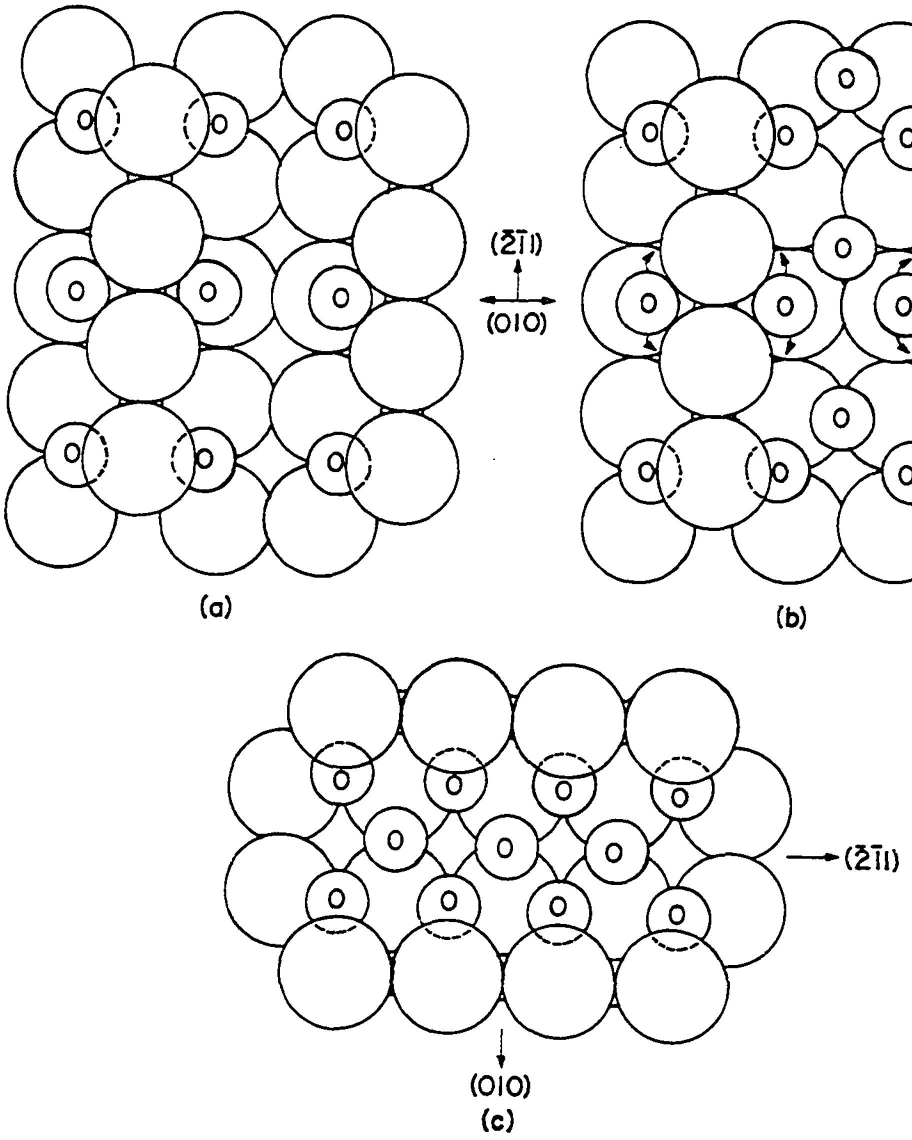

Figure 34. Model of surface structures formed during oxide nucleation: a) (1x3)-O surface structure, b) (1x3)-O surface structure with random oxygen adsorption in trough; arrows indicate transfer of "metastable" oxygen to 3-fold site, c) model of RuO_2 (110)-first surface layer

where α is the extent of the reaction and k is a rate constant. Using the rate reduction as a measure of the extent, n was found to be approximately 1.6. This value falls within the broad range 0.125 to 22.8 expected (123) for solid phase reactions though most n values are in the range from 1 to 3. As the curve did have the form of equation (123) and the n value was reasonable, it lends credence to the RuO_2 nucleation model proposed on ruthenium.

The model illustrated in Figure 34 is probably valid only during the initial stages of catalyst utilization. It will be recalled that if the ruthenium was extensively oxidized, following reduction the crystal would have reduced reflectivity. LEED analysis indicated a complex diffraction pattern after a mild annealing (24 hours, ∿700°C). This type of annealing was undertaken before data collection. The reflectivity of the crystal therefore decreased as a function of the total time that the catalyst was actually in the oxidized state, as the surface rearrangements were not annealed enough to restore the crystal to a (102) geometry. Therefore, the reaction did not always occur on a (102) crystal face under reducing conditions. Since the order plots were found not to change with catalyst usage, though the crystal surface structure was changing, this indicates that the reaction is not highly structure sensitive. This does not imply that the same initial order plot will be observed on any given ruthenium crystal face. Some differences might be expected due to the varying rates of oxide formation on different faces. The mechanism proposed supports the structure insensitivity as all surface complexes utilized only a single adsorption site.

Finally, an additional point needs to be made concerning the pressure dependence of the rate of oxide growth. From the discussion thus far it would be supposed that the growth rate would be independent of CO pressure under oxidizing conditions. This was found not to be the case as a NO/CO mixture would convert the Ru to RuO_2 at a more rapid rate than solely NO, using the same nitric oxide pressure. This rate enhancement was not due to the CO oxidizing the Ru as the oxygen composing the RuO_2 came only from the nitric oxide. This was checked by using a $N^{16}O$-$^{12}C^{18}O$ gas mixture to oxidize the ruthenium and $^{13}C^{16}O$ to reduce the RuO_2. Only $^{13}C^{16}O^{16}O$ was found as a reaction product. A possible rationale is that the carbon monoxide reacts with the oxygen within the surface RuO_2 lattice resulting in the formation of an anion vacancy. As the number of anion vacancies is increased, rate of growth will increase according to equation (52). An alternate explanation could be that the carbon monoxide reacts with the oxide layer in such a manner as to produce capillary-type pores in the overlayer. The ruthenium cations could then undergo rapid transfer from the metal surface to the oxide/gas phase interface in the pores thus increasing the oxide growth rate. While either hypothesis cannot be experimentally supported, this dependence on the growth rate creates an additional difficulty in the measurement of a CO order plot for the RuO_2 mechanism. Since the effect of the CO on the growth rate cannot be easily characterized either experimentally or theoretically, the fitting of a CO order plot to a mechanism would not be possible.

SUMMARY AND SUGGESTIONS FOR FUTURE INVESTIGATIONS

The ruthenium catalyzed nitric oxide reduction reaction by carbon monoxide has been studied using kinetic and isotopic techniques and a variety of surface analysis methods including LEED/Auger and x-ray photoelectron spectroscopy. In the pressure and temperature range of one micron to 10 Torr and 25 to 900°C, the results have led to an understanding of the reaction pathway to the formation of nitrogen and carbon dioxide and the role of the ruthenium. The state of the catalyst was found to be determined by the oxidation-reduction characteristics of the reactant NO-CO gas mixture. Under reducing (low NO/CO ratio) condition, the ruthenium existed in a metallic form with the first surface layer incorporating a coverage of unreactive oxygen atoms equalling $\sim$1.3 monolayers. Using a ruthenium single crystal (102), this surface phase was characterized by a (1x3)-O pattern. A more oxidizing reaction gas mixture (high NO/CO ratio) at temperatures greater than 400°C resulted in the formation of bulk RuO_2 which served as the catalyst. Mechanistically, the state of the catalyst, either reduced or oxidized, was found to dictate the types of surface intermediates formed. This led to the postulation of two reaction mechanisms which were consistent with the observations of dissociation of nitric oxide, oxygen overlayer removal by carbon monoxide, lack of formation of a carbon overlayer and the type available sites in each state of the catalyst. The reduced mechanism required the incorporation of two different adsorption sites resulting in a theoretical NO order variation of from +1 to 0. Since the surface was observed to poison following oxygen treatment and the NO order was negative (-0.3) at moderate nitric oxide pressures, a site poisoning mechanism was also incorporated into the kinetic data treatment. The reaction mechanism under oxidizing conditions required the inclusion of a RuO_2 growth mechanism involving diffusion controlled transport of ruthenium cations to the oxide/gas phase interface.

Though the two mechanisms proposed for the NO-CO reaction are consistent with the observed results, they are only to be regarded as speculative and not necessarily unique. The nature of the surface intermediates could be clarified by reflectance infrared spectroscopy or nuclear magnetic resonance studies. These techniques would allow for the identification of the adspecies under reaction conditions.

An additional area of investigation pertinent to these results concerns the kinetics of ruthenium dioxide growth. The reactor system employed was not easily amenable to the measurement of the pressure dependence of the growth rate. The postulated rate law (rate α $P_{NO}^{0.4}$ $t^{\frac{1}{2}}$) is therefore in need of experimental determination of the nitric oxide and carbon monoxide orders.

An extension of this dissertation using a ruthenium catalyst could be a study of the NO-H_2 reaction or the NO-CO-H_2 ternary system, as both are relevant to exhaust emission catalysis. An interesting endeavor would also be an investigation of any poisoning effects by SO_2.

LITERATURE CITED

1. Wei, J. Adv. Catal. 1975, 24, 57.

2. Shelef, M.; Gandhi, H. S. Ind. Eng. Chem. Prod. Res. Dev. 1972, 11, 393.

3. Klimisch, R. L.; Taylor, K. C. Environ. Sci. Tech. 1973, 7, 127.

4. Taylor, K. C.; Klimisch, R. L. J. Catal. 1973, 30, 478.

5. Taylor, K. C.; Sinkevitch, R. M.; Klimisch, R. L. J. Catal. 1974, 35, 34.

6. Kobylinski, T. P.; Taylor, K. C. J. Catal. 1974, 33, 376.

7. Klimisch, R. L.; Taylor, K. C. Ind. Eng. Chem. Prod. Res. Dev. 1975, 14, 26.

8. Otto, K.; Shelef, M. Z. Phys. Chem. NF 1973, 85, 308.

9. Schleppy, R.; Shah, Y. T. Ind. Eng. Chem. Prod. Res. Dev. 1975, 14, 26.

10. Shelef, M.; Otto, K. J. Catal. 1968, 10, 408.

11. Butler, J. D.; Davis, D. R. J. Chem. Soc., Dalton Trans. 1976, 21, 2249.

12. Klimisch, R. L.; Barnes, G. L. Environ. Sci. Tech. 1972, 6, 543.

13. Shelef, M.; Gandhi, H. S. Ind. Eng. Chem. Prod. Res. Dev. 1972, 11, 2.

14. Matson, S. L.; Harriott, P. Ind. Eng. Chem. Prod. Res. Dev. 1978, 17, 322.

15. Voorhoeve, R. J. H.; Trimble, L. E. J. Catal. 1975, 38, 80.

16. Schleppy, R.; Shah, Y. T. Ind. Eng. Chem. Prod. Res. Dev. 1977, 16, 47.

17. Ohara, H.; Yokota, K.; Fujitani, Y. Nippon Kagaku Kaishi 1978, 1978, 1612.

18. Guyer, A.; Guyer, P.; Schneider, F.; Marfurt, H. R. *Helv. Chem. Acta* 1955, 38, 798.

19. Thomas, J. M.: Thomas, W. J. "Introduction to the Principles of Heterogeneous Catalysis", Academic Press: New York, 1967; Chapter 8.

20. Franzen, H. F. *Prog. Solid St. Chem.* 1978, 12, 1.

21. Unland, M. L. *Science* 1973, 179, 567.

22. Unland, M. L. *J. Catal.* 1973, 31, 459.

23. Lynds, L. *Spectrochem. Acta* 1964, 20, 1369.

24. Guerra, C. R.; Schulman, J. H. *Surf. Sci.* 1967, 7, 229.

25. Eischens, R. P.; Pliskin, W. A. *Adv. Catal.* 1958, 10, 1.

26. Kobayaski, M.; Shirasaki, T. *J. Catal.* 1973, 28, 289.

27. Kobayaski, M.; Shirasaki, T. *J. Catal.* 1974, 32, 254.

28. Davydov, A. A.; Bell, A. T. *J. Catal.* 1977, 49, 332.

29. Dalla Betta, R. A. *J. Phys. Chem.* 1975, 79, 2519.

30. Brown, M. F.; Gonzalez, R. D. *J. Phys. Chem.* 1976, 80, 1731.

31. Brown, M. F.; Gonzalez, R. D. *J. Catal.* 1977, 47, 333.

32. Cotton, F. A.; Wilkinson, G. "Advanced Inorganic Chemistry", 3rd ed.; Interscience Publishers: New York, 1972; Chapter 26.

33. Blyholder, G. *J. Phys. Chem.* 1964, 68, 2772.

34. Blyholder, G.; Allen, M. C. *J. Amer. Chem. Soc.* 1969, 91, 3158.

35. Davydov, A. A.; Bell, A. T. *J. Catal.* 1977, 49, 345.

36. Brown, M. F.; Gonzalez, R. D. *J. Catal.* 1976, 44, 477.

37. Solymosi, F.; Raskó, J. *J. Catal.* 1977, 49, 240.

38. Maki, A.; Decius, J. C. *J. Chem. Phys.* 1959, 31, 722.

39. Dalla Betta, R. A.; Shelef, M. J. Molec. Catal. 1976, 1, 431.

40. Solymosi, F.; Kiss, J.; Sárkány, J. "Proceedings of the 7th International Vacuum Congress and the 3rd International Conference on Solid Surfaces", Vienna, 1977.

41. Bonzel, H. P.; Fischer, T. I. Surf. Sci. 1975, 51, 213.

42. McCarthy, J. G.; Wise, H. Chem. Phys. Lett. 1979, 61, 323.

43. Dushman, S. "Scientific Foundations in Vacuum Techniques Technique", 2nd ed.; Lafferty, J. M., Ed.; John Wiley & Sons: New York, 1962.

44. Hansen, R. S.; Mimeault, V. J. In "Experimental Methods in Catalytic Research", Anderson, R. B., Ed.; Academic Press: New York, 1968; Chapter 5.

45. Grayson, M. A. Int. J. Mass Spect. Ion Phys., in press.

46. Tomcsik, T. L. Ph.D. Dissertation, Iowa State University, Ames, Iowa, 1978.

47. Ku, R.; Gjostein, N. A.; Bonzel, H. P. Surf. Sci. 1977, 64, 465.

48. Hillard, J. C.; Wheeler, R. W. Combust. Flame 1977, 29, 15.

49. May, J. W. Adv. Catal. 1972, 21, 151.

50. Bauer, E. In "Topics in Applied Physics", Gomer, R., Ed.; Springer-Verlag: New York, 1975; Vol. 4, Chapter 6.

51. Bhasin, M. M. In "Catalysis in Organic Syntheses 1976", Rylander, P.; Greenfield, H., Eds.; Academic Press: New York, 1976; Chapter 2.

52. Hill, C. G. In "An Introduction to Chemical Engineering Kinetics and Reactor Design", John Wiley & Sons: New York, 1977; Chapter 6.

53. Madey, T. E.; Englehardt, H. A.; Menzel, D. Surf. Sci. 1975, 48, 304.

54. McDonnell, L.; Powell, B. D.; Woodruff, D. P. Surf. Sci. 1973, 40, 669.

55. Becker, G. E.; Hagstrum, H. D. J. Vac. Sci. Tech. 1974, 11, 284.

56. Orent, T. W.; Hansen, R. S. Surf. Sci. 1976, 67, 325.

57. Haas, T. W.; Grant, J. T.; Dooley, G. J. J. Appl. Phys. 1972, 43, 1853.

58. Grant, J. T.; Haas, T. W. Surf. Sci. 1970, 21, 76.

59. Reed, P. D.; Comrie, C. M.; Lambert, R. M. Surf. Sci. 1976, 59, 33.

60. Reed, P. D.; Comrie, C. M.; Lambert, R. M. Surf. Sci. 1977, 64, 603.

61. Korsch, D. Z. angew. Phys. 1969, 28, 43.

62. Kraemer, K.; Menzel, D. Ber. Bunsenges. Phys. Chem. 1974, 78, 649.

63. Roberts, M. W.; McKee, C. S. "Chemistry of the Metal-Gas Interface", Clarendon Press: Oxford, 1978; Chapter 3.

64. Thomas, G. E.; Weinberg, W. H. J. Chem. Phys. 1978, 69, 3611.

65. Thomas, G. E.; Weinberg, W. H. J. Chem. Phys. 1979, 70, 954.

66. Ibach, H. Festkörperprobleme 1971, 11, 135.

67. Dalmai-Imelik, G.; Bertolini, J. C.; Rousseau, J. Surf. Sci. 1977, 63, 67.

68. Ivanov, V. P.; Boreskov, G. K.; Savchenkov, V. I.; Egelhoff, W. F.; Weinberg, W. H. Surf. Sci. 1976, 61, 207.

69. Zhdan, P. A.; Boreskov, G. K.; Boronin, I.; Schepelin, A. P.; Egelhoff, W. F.; Weinberg, W. H. J. Catal. 1979, in press.

70. Ertl, G.; Koch, J. In "Adsorption - Desorption Phenomena", Ricca, F., Ed.; Academic Press: London, 1972; Sec. III, Chapter 10.

71. Close, J. S.; White J. M. J. Catal. 1975, 31, 185.

72. Weinberg, W. H.; Lambert, R. M.; Comrie, C. M.; Linnet, J. W. "Proceedings of the 5th International Congress on Catalysis", North Holland, Amsterdam, 1973.

73. Ducros, R.; Merrill, R. P. *Surf. Sci.* 1976, 55, 227.

74. Anderson, S.; Lundquist, B. I.; Norskov, J. K. "Pro- "Proceedings of the 7th International Vacuum Congress and the 3rd International Conference on Solid Surfaces", Vienna, 1977.

75. Madden, H. H.; Küppers, J.; Ertl, G. *J. Chem. Phys.* 1973, 58, 3401.

76. Singh, K. I.; Grenga, H. E. *J. Catal.* 1977, 47, 328.

77. Rabo, J. A.; Risch, A. P.; Poutsma, M. L. *J. Catal.* 1978, 53, 295.

78. Ekerdt, J. G.; Bell, A. J. *J. Catal.*, in press.

79. Slaughter, M. D. Ph.D. Dissertation, Iowa State University, Ames, Iowa 1979.

80. Matsushima, T.; Almy, D. B.; White, J. M. *Surf. Sci.* 1977, 67, 89.

81. Benndorf, C.; Egert, B.; Keller, G.; Thieme, F. *Surf. Sci.* 1978, 74, 216.

82. Bridge, M. E.; Lambert, R. M. *Surf. Sci.* 1979, 82, 413.

83. Theil, P. A.; Yates, J. T.; Weinberg, W. H. *Surf. Sci.* 1979, 82, 22.

84. Rieder, K. H. *Appl. Surf. Sci.* 1978, 2, 74.

85. Horgan, A. M.; Dalins, I. *Surf. Sci.* 1973, 36, 526.

86. Allen, G. C.; Tucker, P. M.; Wild, R. K. "Proceedings of the 7th International Vacuum Congress and the 3rd International Conference on Solid Surfaces", Vienna, 1977.

87. Benninghoven, A.; Bispinck, H.; Ganschow, O.; Wiedmann, L. "Proceedings of the 7th International Vacuum Congress and the 3rd International Conference on Solid Surfaces", Vienna, 1977.

88. Carrière, B.; Deville, J. P.; Maire, G.; Légaré, P. Surf. Sci. 1976, 58, 618.

89. Cotton, F. A.; Mague, J. T. Inorg. Chem. 1966, 5, 317.

90. Bearden, J. A.; Barr, A. F. Rev. Mod. Phys. 1967, 39, 125.

91. Kim, K. S.; Winograd, N. J. Catal. 1974, 35, 66.

92. Fuggle, J. C.; Madey, T. E.; Steinkilberg, M.; Menzel, D. Surf. Sci. 1975, 52, 521.

93. Fuggle, J. C.; Umbach, E.; Feulner, P.; Menzel, D. Surf. Sci. 1977, 64, 69.

94. Hamrin, K.; Johansson, G.; Gelius, U.; Nordling, C.; Siegbahn, K. Phys. Sci. 1970, 1, 277.

95. Wagner, C. D.; Riggs, W. M.; Davis, L. E.; Moulder, J. F.; Muilenberg, G. E. "Handbook of X-Ray Photoelectron Spectroscopy", Perkin-Elmer: Eden Prairie, Minnesota, 1979.

96. Cotton, F. A. In "Inorganic Syntheses", McGraw-Hill: New York, 1972; Vol. XIII, Chapter 5.

97. Bell, W. E.; Tagami, M. J. Phys. Chem. 1963, 67, 2432.

98. Norman, J. H.; Staley, H. G.; Bell, W. E. In "Advances in Chemistry", Gould, R. F., Ed.; American Chemical Society: Washington, D. C., 1968; Vol. 27, Chapter 8.

99. Redhead, P. A. Vacuum 1962, 12, 213.

100. Madey, T. E.; Menzel, D. Japan J. Appl. Phys. 1974, Supp. 2, Pt. 2, 229.

101. Adams, D. L. Surf. Sci. 1974, 42, 12.

102. Allen, A. D.; Bottomley, F.; Harris, R. O.; Reinsalu, V. P.; Stenoff, C. J. J. Amer. Chem. Soc. 1967, 89, 5595.

103. Sellmann, D. Angew. Chem. Int. Ed. Engl. 1974, 13, 639.

104. Kahn, M. M.; Martell, A. E. "Homogeneous Catalysis by Metal Complexes", Academic Press: New York, 1969; Vol. 1.

105. Ohya, A.; Uraba, K.; Aika, K.; Ozaki, A. J. Catal. 1979, 58, 313.

106. Klein, R.; Shih, A. Surf. Sci. 1977, 69, 403.

107. Thomas, G. E.; Weinberg, W. H. Phys. Rev. Lett. 1978, 41, 1181.

108. Pizzini, S.; Rossi, L. Z. Naturforschung 1971, 26A, 177.

109. Webb, A. N.; Eischens, R. P. J. Amer. Chem. Soc. 1955, 77, 4710.

110. Madey, T. E.; Yates, J. T.; Stan, R. C. J. Chem. Phys. 1965, 42, 1372.

111. Williams, E. D.; Weinberg, W. H. Surf. Sci. 1979, 82, 93.

112. Norman, J. H.; Staley, H. G.; Bell, W. E. Adv. Chem. Ser. 1968, 72, 101.

113. Brewer, L.; Rosenblatt, G. M. In "Advances in High Temperature Chemistry", Eying, L., Ed.; Academic Press: New York, 1969; Vol. 2, Chapter 1.

114. Gingerich, K. A. Chem. Phys. Lett. 1974, 25, 523.

115. Mollakov, B. M.; Glazunov, M. P.; Spitsyn, V. I. Izv. Akad. Nauk SSSR, Ser. Khim. 1973, 3, 660.

116. Kempter, C. P. J. Chem. Phys. 1964, 41, 1515.

117. Pauling, L. In "The Chemical Bond", Cornell University Press: Ithaca, New York, 1967, Chapter 11.

118. Fehlner, F. P.; Mott, N. F. Oxid. Metals 1970, 2, 59.

119. Cabrera, N.; Mott, N. F. Rept. Progr. Phys. 1948, 12,

120. Gomes, W. P.; Dekeyser, W. In "Treatise on Solid State Chemistry", Hannay, N. B., Ed.; Plenum Press: New York, 1976; Vol. 4, Chapter 2.

121. Cranstoun, G. K. L.; Pyke, D. R. Appl. Surf. Sci. 1979, 2, 359.

122. Cranstoun, G. K. L.; Pyke, D. R.; Smith, G. D. W. Appl. Surf. Sci. 1979, 2, 375.

123. Harrison, L. G. In "Comprehensive Chemical Kinetics", Tipper, C. F. H.; Bamford, C. H., Eds., Elsevier Publishing Company: New York, 1969; Vol. 2, Chapter 5.

124. Anderson, J. R.; Baker, B. G. In "Chemisorption and Reaction on Metallic Films", Anderson, J. R., Ed.; Academic Press: New York, 1971, Vol. 2, Chapter 1.

125. Kemball, C. *Faraday Discuss*., *Chem*. *Soc*. 1966, 41, 190.

126. Quicksall, C. O.; Spiro, T. G. *Inorg*. *Chem*. 1968, 7, 2365.

127. Madey, T. E. *Surf*. *Sci*. 1979, 575.

128. Niwa, M.; Minami, T.; Kodama, H.; Hattori, T.; Murakami, Y. *J*. *Catal*. 1978, 53, 198.

129. Winter, E. R. S. *J*. *Catal*. 1971, 22, 158.

130. Wyckoff, R. W. G. "Crystal Structures", 2nd ed.; Interscience Publishers: New York, 1963; Chapter IV.

131. Boman, C-E. *Acta Chem*. *Scand*. 1970, 24, 116.

132. Lythe, F. W.; Via, G. H.; Sinfelt, J. H. *J*. *Chem*. *Phys*. 1977, 67, 3831.

ACKNOWLEDGMENT

The completion of this project would not have been possible without the intervention of the Sovereign Lord. The Word of God states:

> If any of you lacks wisdom, he should ask God, who gives generously to all without finding fault, and it will be given to him. James 1: 5 (NIV)

and

> ...if you call out for insight and cry aloud for understanding, then you will understand the fear of the Lord and find the knowledge of God. For the Lord gives wisdom, and from his mouth come knowledge and understanding. Proverbs 2:3,5,6 (NIV)

By faith, through the shed blood and resurrection of God's only son, Jesus Christ, these promises were believed. They were fulfilled by God, for which He is given acknowledgment and praise.

Sincere gratitude is also extended to Dr. Robert S. Hansen for his guidance and encouragement during the course of my graduate career.

Thanks are given to Mr. Jim Andregg and Mr. Harlan Baker for their assistance in the collection of the XPS data and refinement of a ruthenium electropolishing technique, respectively. Additionally, appreciation is given to the members of the catalytic research group for the many hours of interesting and challenging discussion.

Finally, tender thanks are offered to my wife, Betty Anne, for her emotional support and encouragement. The love and patience she has given surpasses what I can even begin to provide (Proverbs 31:29).

APPENDIX

The two classical models for heterogeneous catalytic reactions are the Langmuir-Hinshelwood and the Rideal-Eley reaction mechanisms. The Rideal-Eley mechanism incorporates an elementary reaction between a chemisorbed species and a gas phase reactant as its rate limiting step. Considering the overall reaction:

$$A_{(g)} + B_{(g)} \rightleftharpoons AB_{(g)} \tag{A1}$$

a generalized Rideal-Eley mechanism using surface sites, S, is:

$$A_{(g)} + S \overset{K}{\rightleftharpoons} A\text{-}S \tag{A2}$$

$$A\text{-}S + B_{(g)} \xrightarrow{k} AB_{(g)} + S \tag{A3}$$

Treating reaction (A3) as the rate limiting reaction, the fractional surface concentration of species [A-S] and [S] are

$$[A\text{-}S] = K[P_A][S] \tag{A4}$$

$$[S] = 1/\{1 + K[P_A]\} \tag{A5}$$

and the rate law for the mechanism is:

$$\text{Rate}_{AB} = \frac{k\ K[P_A][P_B]}{\{1 + K[P_A]\}} \tag{A6}$$

The limiting order in a log-log plot of reactant A would be +1 at low pressures of gas A and would decrease to zero with an increase in P_A. The order with respect to reactant B would be +1 at all B pressures. Reactant B could also be thought of as weakly chemisorbed (physisorbed) to a chemisorbed overlayer of A and the result would be identical.

The Langmuir-Hinshelwood rate limiting step involves a bimolecular reaction between two adspecies competing for the same surface sites:

$$A_{(g)} + S \overset{K_A}{\rightleftharpoons} A\text{-}S \tag{A7}$$

$$B_{(g)} + S \overset{K_B}{\rightleftharpoons} B\text{-}S \tag{A8}$$

$$A\text{-}S + B\text{-}S \xrightarrow{k} AB_{(g)} + 2S. \tag{A9}$$

The fractional coverages of intermediates [A-S], [B-S] and [S], assuming that equilibria K_A and K_B are rapidly established and invoking a conservation of surface sites relationship, are:

$$[A\text{-}S] = K_A[P_A][S], \tag{A10}$$

$$[B\text{-}S] = K_B[P_B][S] \tag{A11}$$

and

$$[A] = 1/\{1 + K_A[P_A] + K_B[P_B]\}. \tag{A12}$$

Assuming reaction (A9) is rate limiting, the rate law is:

$$\text{Rate}_{AB} = \frac{kK_AK_B[P_A][P_B]}{\{1 + K_A[P_A] + K_B[P_B]\}^2} \tag{A13}$$

At lower pressures of either reactant A or B, the order is +1; as the partial pressure is increased, the order decreases to zero and at high pressures of A or B becomes -1. The negative reactant order is a manifestation of the surface site competition between reactants.

For both mechanisms it can be seen that at least one of the reactant orders is going to be pressure dependent as long as the surface sites are conserved:

$$\theta_S + \theta_{A-S} + \theta_{B-S} = 1 \tag{A14}$$

where θ is the fraction coverage of the denoted species. Only in the situation where θ_{A-S} and $\theta_{B-S} << \theta_S$ is valid over a wide pressure range will the orders be independent of pressure and then the reactant order will be one for each reactant.